ELECTRONIC EMISSION SPECTRA OF
$^{12}C\ ^{16}O,\ ^{13}C\ ^{18}O,\ ^{13}C\ ^{18}O^+,$ AND $^{15}N_2^+$

CHINTALAPATI V.V. PRASAD

ELECTRONIC EMISSION SPECTRA OF

$^{12}C\,^{16}O$, $^{13}C\,^{18}O$, $^{13}C\,^{18}O^+$, AND $^{15}N_2^+$

BY

Ⓒ Chintalapati V. V. Prasad

A thesis submitted to the School of Graduate

Studies in partial fulfillment of the

requirements for the degree of

Doctor of Philosophy

Department of Physics

Memorial University of Newfoundland

September 1987

St. John's   Newfoundland

DEDICATED TO MY PARENTS

ABSTRACT

A hollow-cathode discharge tube of special design with physical separation of the anode and cathode columns was used to excite the neutral molecules $^{12}C^{16}O$ and $^{13}C^{18}O$ and the molecular ions $^{13}C^{18}O^+$ and $^{15}N_2^+$. The initial experiments have demonstrated that the cathode glow is an excellent source of molecular ions as well as neutral molecules in their high-lying excited states while the anode glow contains almost exclusively the neutral molecules. The excited spectra were recorded on medium and high resolution optical spectrographs.

Six bands of the Herzberg $(C^1\Sigma^+ - A^1\Pi)$ system of $^{13}C^{18}O$ in the spectral region 3660 - 4190 Å were observed for the first time and the rotational structure of five of them was analyzed. Perturbations observed in the $v = 3$ and 5 levels of state A were analyzed and information concerning the perturbing states was obtained.

In a reinvestigation of the third positive $(b^3\Sigma^+ - a^3\Pi_r)$ system and the three Kaplan bands (which have not been understood since their first observation in 1930) of $^{12}C^{16}O$ in the region 2500 - 3830 Å, five new bands of this molecule were observed in the present work. The Kaplan bands and the five new bands are now assigned to a v''- progression with $v' = 2$ of the third positive system. The new vibrational assignments are confirmed from the calculated Franck-Condon factors and from the experimental data of the corresponding

bands of $^{13}C^{18}O$, observed for the first time. With the identification of the $v = 2$ level in state b of CO, the controversy regarding the dissociation limit of CO existing in the literature is now satisfactorily resolved.

Three bands of the Baldet-Johnson ($B^2\Sigma^+ - A^2\Pi_i$) system in the region 3700 - 4225 Å and seven bands of the comet-tail ($A^2\Pi_i - X^2\Sigma^+$) system in the region 3620 - 6165 Å, of $^{13}C^{18}O^+$, were rotationally analyzed for the first time.

Of the fifteen bands observed in the first negative ($B^2\Sigma_u^+ - X^2\Sigma_g^+$) system of $^{15}N_2^+$, in the region 3570-5170 Å, twelve bands were rotationally analyzed. Perturbations observed in the $v = 0$ level of state B were analyzed and was found to be perturbed by the $v = 25$ level of the $A^2\Pi_{i,u}$ state of $^{15}N_2^+$. In all these investigations, with the exception of third positive system of CO (for which only the vibrational analysis was performed), final molecular constants of various electronic states involved were obtained by the method of "merging."

CONTENTS

CHAPTER 1

INTRODUCTION

1.1 Significance of Molecular Spectra

Even though the experimental investigation and empirical interpretation of molecular spectra began more than a century ago, it is only after the development of quantum mechanics in 1926, that great progress has been made in the spectroscopic studies of molecular structure. Many features of molecular spectra can be understood on the basis of quantum mechanics. Conversely, in many instances, molecular spectroscopy, just as atomic spectroscopy, provided excellent confirmations of the predictions of quantum theory and thus established its importance in understanding many atomic and molecular phenomena.

From an investigation of the electronic spectrum of a molecule, information about its electronic structure and the vibration and rotation of its nuclei can be obtained. Properties such as chemical valence can be understood from the electronic structure. The forces between the atoms of a molecule and its dissociation energy can be calculated from the vibrational frequencies and the corresponding anharmonicities. A detailed rotational analysis of the bands of an electronic spectrum provides very precise values

for the electronic, vibrational and rotational levels of a molecule. Such a study also enables one to obtain information about its moments of inertia and internuclear separations in various energy states, nature of the coupling between electronic (both orbital and spin) and rotational motions, and the perturbations which may occur between the energy levels of different electronic states. The presence of the perturbing electronic states which may not be observed directly in some instances can be inferred from the analysis of the observed perturbations in a band system. From a knowledge of the vibrational and rotational partition functions (Q_v and Q_r), the thermodynamic quantities such as heat content (H^0), heat capacity (C_p or C_v), entropy (S^0) and free energy (F^0) can be estimated. From the observation of intensity alternation (whether the even or odd J (or N) lines are strong) in the rotational structure of a homonuclear diatomic molecule, the nuclear spin and the nature of nuclear statistics (whether Bose-Einstein or Fermi-Dirac) can be determined. If the hyperfine structure of a molecule is observed, quantities such as the nuclear magnetic moment and nuclear quadrupole moment can be obtained. Properties of free radicals and molecular ions which have short life times and are difficult to synthesize chemically can be inferred by the observation and analysis of their spectra. From a knowledge of the vibrational and rotational constants of the electronic states of a band system, quantities such as

Franck-Condon factors which are proportional to the intensities of the bands can be calculated. The information thus obtained for a molecule/free radical/ion by spectroscopic methods enables one to understand its various physical and chemical properties.

The spectra of several diatomic and polyatomic molecules are very important in the investigation of astrophysical problems. In addition to the absorption bands occurring in the solar spectrum, the emission spectra of bands occurring in the aurora, light of the night sky, and twilight, which are produced in the upper layers of the atmosphere, are observed. These spectra provide useful information about the physical conditions and the compositions of the atmospheric layers. The temperature and height of various atmospheric layers, in which auroral or night sky emissions take place, can be estimated from the intensity distribution of a band. The spectra of comets contain many emission band systems of various molecules and a weak continuum with Fraunhofer lines. The band spectra emitted in the head of a comet, called coma, and its nucleus are different from those occurring in the tail. From the total intensity of the radiations emitted by a molecule in a comet, its partial density can be estimated. From a study of the spectra emitted by stars, the temperature of the stars can be estimated and they are classified according to their temperatures. The study of molecular spectra of celestial sources gives the

information regarding the abundance ratios of isotopes. Such investigations are necessary to understand the nuclear processes through which the energy is generated in these objects.

1.2 Importance of the Electronic Spectra of CO, CO^+, N_2, and N_2^+

The neutral carbon monoxide and nitrogen molecules and their ions used in the present work, are interesting for a variety of reasons, including for their astrophysical importance. Carbon monoxide is a constituent of the solar chromosphere, stellar atmospheres, and tails of comets. The comet-tail $(A^2\Pi_i - X^2\Sigma^+)$ band system of CO^+ molecule was first observed in the tail of the comet, Morehouse-1908c, by Pluvinel and Baldet (1909,1911), and was later observed in the laboratory by Fowler (1909, 1910). Nitrogen, being the primary constituent in the earth's atmosphere, has a significant role in atmospheric phenomena such as aurorae and air glows. The Meinel band system $(A^2\Pi_{i,u} - X^2\Sigma_g^+)$ of N_2^+, was first observed in the aurora. The first negative $(B^2\Sigma_u^+ - X^2\Sigma_g^+)$ system of N_2^+ and several other band systems of N_2 were also observed in the auroral emissions. The main features of the auroral spectrum are very similar to those of a hollow-cathode discharge in nitrogen. The first negative system of N_2^+ was also observed in the tails of comets. The carbon monoxide and diatomic nitrogen are isoelectronic and so are

their ions. Hence, the electronic states and also some band systems of these molecules, as well as those of their ions, bear a clear resemblance. These molecules are available in a very pure form and can be readily handled in the laboratory. Recently, from radio astronomical measurements, the abundance ratios of isotopes such as $^{12}C/^{13}C$, $^{14}N/^{15}N$, $^{16}O/^{18}O$, and $^{17}O/^{18}O$ were estimated for meteorites, stars, planetary nebulae, novae, and interstellar space (see Audouze, 1977). At present these ratios are not in their final form and they should be revised and updated. It is essential to have the accurate laboratory data on the $^{13}C^{18}O$ and $^{15}N_2$ molecules and their ions so that these molecules can be identified in the celestial objects and very precise estimates for the abundance ratios of isotopes can be obtained. At present, the laboratory data on the electronic spectra of the $^{13}C^{18}O$ and $^{15}N_2$ molecules and their ions is either fragmentary or nonexistent. Moreover, it is customary to study the spectra of isotopically substituted molecules in order to unambiguously identify the emitter of a particular band system, or confirm the vibrational numbering in an electronic state, etc. The principal objective of the present investigation is to obtain as much laboratory data as possible on the spectra of these molecules and their ions. Several electronic states of these molecules, for example, $A^1\Pi$ of $^{12}C^{16}O$, $A^2\Pi_i$ of $^{12}C^{16}O^+$, and $B^2\Sigma_u^+$ of $^{14}N_2^+$ are known to be severely perturbed. The situation in the corresponding

electronic states of $^{13}C^{18}O$, $^{13}C^{18}O^+$, and $^{15}N_2^+$ is not known. It is also the objective of this work to understand the nature of these electronic states of isotopically substituted molecular species.

1.3 Electronic States of CO and CO$^+$

The nature of the electronic states of a molecule and their binding character (bound state or repulsive state) are determined to a large extent by the electrons in the outermost shells of the constituent atoms. The electronic configurations of carbon and oxygen atoms are:

$$_6C : K \ 2s^2 \ 2p^2$$
$$_8O : K \ 2s^2 \ 2p^4$$

[1.1]

The electronic configuration which gives rise to the ground state $(X^1\Sigma^+)$ of the CO molecule is written as (Mulliken, 1932)

$$K \ K \ (z\sigma)^2 \ (y\sigma)^2 \ (w\pi)^4 \ (x\sigma)^2 \ : \ X^1\Sigma^+.$$

[1.2]
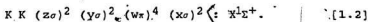
The electronic configurations of the low-lying excited states of CO can be obtained by promoting (i) one of the $x\sigma$ electrons into the $v\pi$ orbital and (ii) one of the $w\pi$ electrons into the $v\pi$ orbital. The resulting electronic configurations and states are written as

$$- - (w\pi)^4 \ (x\sigma) \ (v\pi) \ : \ a^3\Pi_r, \ A^1\Pi.$$

[1.3]
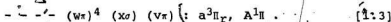
$$- - - - (w\pi)^3 (x\sigma)^2 (v\pi) : a'^3\Sigma^+, e^3\Sigma^-,$$
$$d^3\Delta_i, {}^1\Sigma^+, I^1\Sigma^-, D^1\Delta . \qquad [1.4]$$

The $^1\Sigma^+$ state of Configuration [1.4] has not yet been observed. Further excited states of CO are obtained by promoting one of the $x\sigma$ electrons to the Rydberg orbitals $3s\sigma$, $3p\sigma$, and $3p\pi$. The electronic configurations of the resulting states are written as

$$- - - - (w\pi)^4 (x\sigma)(3s\sigma) : b^3\Sigma^+, B^1\Sigma^+ .$$
$$- - - - (w\pi)^4 (x\sigma)(3p\sigma) : j^3\Sigma^+, C^1\Sigma^+ .$$
$$- - - - (w\pi)^4 (x\sigma)(3p\pi) : c^3\Pi_i, E^1\Pi . \qquad [1.5]$$

According to Lefebvre-Brion et al. (1964) these Rydberg states converge to the ground state $(X^2\Sigma^+)$ of CO^+. The Rydberg-Klein-Rees (RKR) potential energy curves of all these observed states of $^{12}C^{16}O$ below 95000 cm^{-1} given by Tilford and Symmons (1972) are shown in a modified form in Figure 1. It may be noted that states X, a, a', d, e, A, I, and D dissociate into C(^{3}p) and O(^{3}p) atoms.

Extensive experimental studies have been made both in emission and absorption on the electronic spectrum of the $^{12}C^{16}O$ molecule which spans the region 600-8600 Å. In addition to the fourteen electronic states listed above and shown in Figure 1, several other Rydberg states lying above 95000 cm^{-1} are also known for this molecule. More than thirty electronic transitions, taking place among these electronic states, are identified. Of all these transitions, the prominent
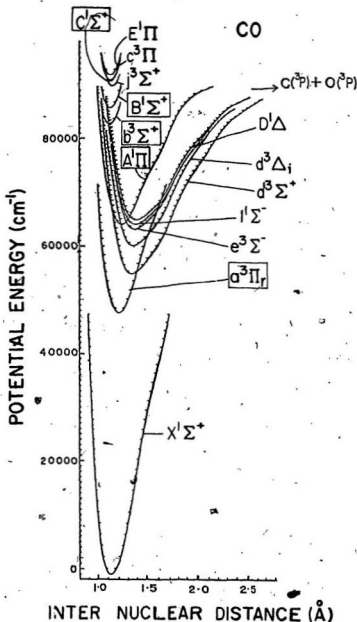
Figure 1. RKR potential energy curves for the electronic states of $^{12}C^{16}O$ below 95000 cm^{-1}. The electronic states, which are of interest in the present work, are shown in boxes.

band systems are (i) the Ångström ($B^1\Sigma^+ - A^1\Pi$) system (4100 - 6600 Å), (ii) the Herzberg ($C^1\Sigma^+ - A^1\Pi$) system (3680 - 5705 Å), (iii) the third positive ($b^3\Sigma^+ - a^3\Pi_r$) system (2600 - 3800 Å), and (iv) the fourth positive ($A^1\Pi - X^1\Sigma^+$) system (1140 - 2800 Å).

Removal of one electron from the CO molecule results in the CO$^+$ ion. Even though the electronic states of CO$^+$ dissociate into C$^+$ + O atoms, traditionally this molecule is identified as CO$^+$. The electronic configuration of the ground state of CO is given by the configuration [1.1]. Removal of an electron from xσ orbital results in the ground state of the CO$^+$ molecule and hence its configuration is written as

$$K\ K\ (z\sigma)^2\ (y\sigma)^2\ (w\pi)^4\ (x\sigma)\ :\ X^2\Sigma^+\ . \qquad [1.6]$$

The electronic configurations of the higher electronic states of CO$^+$ are written as:

$$K\ K\ (z\sigma)^2\ (y\sigma)^2\ (w\pi)^3\ (x\sigma)^2\ :\ A^2\Pi_i\ . \qquad [1.7]$$

$$K\ K\ (z\sigma)^2\ (y\sigma)\ (w\pi)^4\ (x\sigma)^2\ :\ B^2\Sigma^+\ . \qquad [1.8]$$

$$K\ K\ (z\sigma)^2\ (y\sigma)^2\ (w\pi)^3\ (x\sigma)(v\pi)\ :\ C^2\Delta_r\ . \qquad [1.9]$$

The electronic states $X^2\Sigma^+$ and $A^2\Pi_i$ dissociate into C$^+$(^{2}p) and O(^{3}p) atoms whereas the B$^2\Sigma^+$ state dissociates into C$^+$(^{2}p) and O(^{1}D) atoms. The RKR potential energy curves of the X$^2\Sigma^+$, A$^2\Pi_i$, and B$^2\Sigma^+$ states (which are of interest in

the present work), along with that of the ground state of
CO are shown in Figure 2 (modified from Krupenie , 1966).

In the $^{12}C^{16}O^+$ molecule, only three electronic states
$X^2\Sigma^+$, $A^2\Pi_i$, and $B^2\Sigma^+$ are clearly identified and three band
systems arising from these states, i.e., (i) the comet-tail
($A^2\Pi_i$ - $X^2\Sigma^+$) system (3080 - 8500 Å) (ii) the Baldet-
Johnson ($B^2\Sigma^+$ - $A^2\Pi_i$) system (3315 - 4236 Å), and (iii)
the first negative ($B^2\Sigma^+$ - $X^2\Sigma^+$) system (1800 - 3152 Å) are
thoroughly investigated. Recently, Marchand et al. (1969)
identified a new transition $C^2\Delta_r$ - $A^2\Pi_i$ in CO^+, but its
vibrational numbering is uncertain and the rotational
structure is not fully resolved. For more details of all the
electronic states and other spectroscopic details of the CO
and CO^+ molecules, the reader is referred to Krupenie
(1966) and Huber and Herzberg (1979).

1.4 Electronic States of N_2^+

The electronic configuration of the nitrogen atom is

$$_7N : K \; 2S^2 \; 2P^3 \; . \qquad [1.10]$$

The electronic configuration of the ground state ($X^1\Sigma_g^+$) of
N_2 is written as

$$K \; K \; (z\sigma_g)^2 \; (y\sigma_u)^2 \; (w\pi_u)^4 \; (x\sigma_g)^2 : X^1\Sigma_g^+. \qquad [1.11]$$

Removal of an electron from the $x\sigma_g$ orbital results in the
ground state of N_2^+ whose configuration is written as
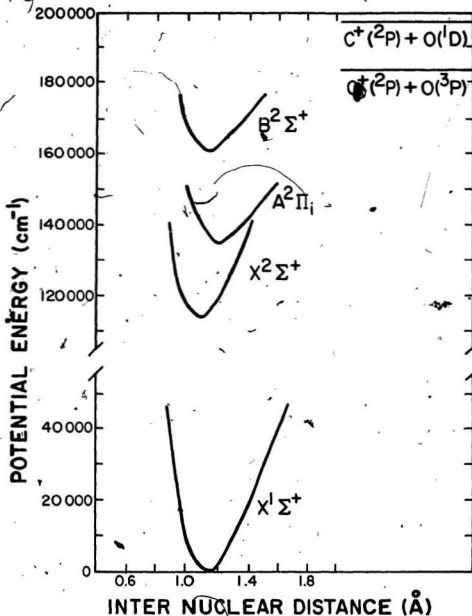
Figure 2.. RKR potential energy curves for the ground electronic state of $^{12}C^{16}O$ and the electronic states of $^{12}C^{16}O^+$.

$$K \ K \ (z\sigma_g)^2 \ (y\sigma_u)^2 \ (w\pi_u)^4 \ (x\sigma_g) \ : \ X^2\Sigma_g{}^+. \qquad [1.12]$$

The configuration of the first excited state of $N_2{}^+$ is

$$K \ K \ (z\sigma_g)^2 \ (y\sigma_u)^2 \ (w\pi_u)^3 \ (x\sigma_g)^2 \ : \ A^2\Pi_{i,u} \ . \qquad [1.13]$$

The $B^2\Sigma_u{}^+$ and $C^2\Sigma_u{}^+$ states arise from the mixture of the following configurations:

$$K \ K \ (z\sigma_g)^2 \ (y\sigma_u) \ (w\pi_u)^4 \ (x\sigma_g)^2, \qquad [1.14a]$$

and

$$K \ K \ (z\sigma_g)^2 \ (y\sigma_u)^2 \ (w\pi_u)^3 \ (x\sigma_g)(v\pi_g) \ . \qquad [1.14b]$$

The Configuration [1.14a] is obtained by removing an electron from the $y\sigma_u$ orbital of the ground state of N_2 whereas the Configuration [1.14b] is obtained by promoting one of the $w\pi_u$ electrons into the $v\pi_g$ orbital from the ground state of $N_2{}^+$. The Configuration [1.14a] is dominant in state B, whereas the Configuration [1.14b] is dominant in state C. Theoretically, several other electronic states (quartet and doublet Σ and Δ states) are possible from the Configuration [1.14b] but none of them have been observed in $N_2{}^+$. There is some controversy regarding the existence of the $a^4\Sigma_u{}^+$ state. Similarly, the $D^2\Pi_{i,g}$ state also arises from the mixture of configurations

$$K \ K \ (z\sigma_g)^2 \ (y\sigma_u)^2 \ (w\pi_u)^2 \ (x\sigma_g)^2 \ (v\pi_g), \qquad [1.15a]$$

and

$$K \ K \ (z\sigma_g)^2 \ (y\sigma_u)^2 \ (w\pi_u)^4 \ (v\pi_g) \ . \qquad [1.15b]$$

Even though the theoretical calculations predict many more electronic states for this molecule, only states X, A, B, D, and C are correctly identified. The RKR potential energy curves for these five states and that of the ground state of N_2 given by Lofthus and Krupenie (1977) is shown in modified form in Figure 3. It should be noted that the $X^1\Sigma_g^+$ state of N_2 dissociates into two ground state $N(^4S^0)$ atoms while the $X^2\Sigma_g^+$, $A^2\Pi_{i,u}$, $B^2\Sigma_u^+$, and $D^2\Pi_{i,g}$ states of N_2^+ dissociate into $N(^4S^0) + N_+(^3P)$ atoms and its $C^2\Sigma_u^+$ state dissociates into $N(^2D^0) + N^+(^3P)$ atoms.

The four prominent electronic band systems of this molecule are (i) Meinel ($A^2\Pi_{i,u} - X^2\Sigma_g^+$) band system (5515-17706 Å), (ii) first negative ($B^2\Sigma_u^+ - X^2\Sigma_g^+$) band system (2860 -5865 Å), (iii) Janin-d'Incan ($D^2\Pi_{i,g} - A^2\Pi_{i,u}$) band system (2057 - 3074 Å), and (iv) second negative ($C^2\Sigma_u^+ - X^2\Sigma_g^+$) system (1276 - 2223 Å). For more details of the electronic states and transitions of N_2^+ and other spectroscopic details of this molecule, the reader is referred to Tyte and Nicholls (1965), Lofthus and Krupenie (1977), and Huber and Herzberg (1979).

1.5 Present Investigations

The neutral molecules, $^{12}C^{16}O$ and $^{13}C^{18}O$, and the molecular ions, $^{13}C^{18}O^+$ and $^{15}N_2^+$, studied in the present investigations were excited in a hollow-cathode discharge tube and their emission spectra were photographed under medium and high
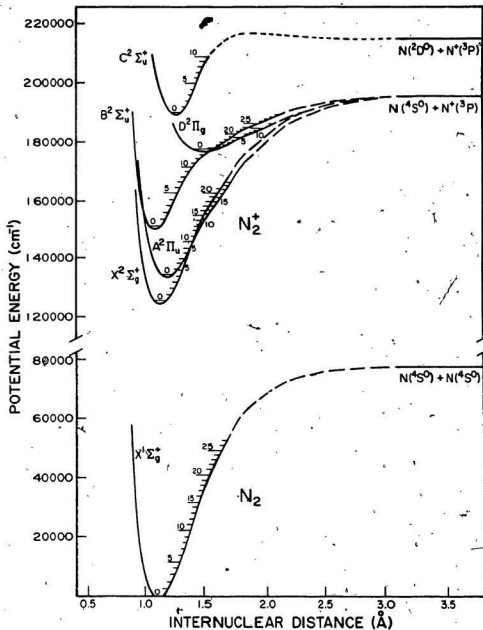
Figure 3. RKR potential energy curves for the ground electronic state of $^{14}N_2$ and the electronic states of $^{14}N_2^+$.

resolutions. The design of this hollow-cathode discharge tube is such that the anode and cathode columns are physically separated so that the characteristic anode and cathode glows can be separately photographed. Details of the hollow-cathode discharge tube, the spectrographs used, and the experimental procedure followed are presented in Chapter 2. The theory of molecular spectra pertinent to the present investigations is reviewed in Chapter 3.

The Herzberg ($C^1\Sigma^+ - A^1\Pi$) band system of the $^{13}C^{18}O$ molecule, consisting of six bands degraded to shorter wavelengths, occurring in the region 3660 - 4190 Å, were observed for the first time and photographed under high resolution. Their rotational structure, except that of the apparently complex 0-0 band, was analyzed. The molecular constants obtained from the analysis of the individual bands were merged with those obtained from the earlier study of the Ångström ($B^1\Sigma^+ - A^1\Pi$) band system of $^{13}C^{18}O$ (see Prasad et al., 1984) and a unique set of molecular constants for the A, B, and C states of this molecule was obtained. The perturbations observed in the v = 3 and 5 levels of state A are in good agreement with those observed earlier by Prasad et al. (1984). The details of all these results are presented in Chapter 4. The preliminary results of this study have already appeared in a publication (see Prasad et al., 1985).

The third positive ($b^3\Sigma^+ - a^3\Pi_r$) system and the three Kaplan bands of $^{12}C^{16}O$, all degraded to shorter wavelengths, occurring in the region 2500 - 3830 Å, were reinvestigated, and in addition to the previously known bands, five new bands were observed for the first time. The three Kaplan bands and the five new bands are now assigned to a v"- progression with v' = 2 of the third positive system. The new vibrational assignments are confirmed from the calculated Franck-Condon factors and also the experimental data obtained for the corresponding bands of $^{13}C^{18}O$, observed for the first time in our laboratory. The identification of the v = 2 level of the $b^3\Sigma^+$ state favors the "higher" value of 89460 cm^{-1} for the dissociation limit, rather than the "lower" value ≤88262 cm^{-1}, existing in the literature. The Kaplan bands of CO observed in 1930 are now interpreted as a part of the third positive system. The results of this investigation are presented in Chapter 5 and have recently appeared in a publication (see Prasad et al., 1987).

The Baldet-Johnson ($B^2\Sigma^+ - A^2\Pi_i$) and the comet-tail ($A^2\Pi_i - X^2\Sigma^+$) band systems of $^{13}C^{18}O^+$, occurring in the regions, 3700 - 4225 Å and 3620 - 6165 Å, respectively, were observed for the first time. The bands of the Baldet-Johnson system are degraded to shorter wavelengths and those of the comet-tail system are degraded to longer wavelengths. The rotational structure of the bands of these systems were analyzed. The molecular constants obtained from the analysis

of the individual bands of both systems were merged together and a unique set of constants for the X, A, and B states of $^{13}C^{18}O^+$ is obtained. The results obtained for the Baldet-Johnson system are discussed in Chapter 6 and those for the comet-tail system are presented in Chapter 7.

Fifteen bands of the first negative $(B^2\Sigma_u^+ - X^2\Sigma_g^+)$ system of the $^{15}N_2^+$ ion, all degraded to shorter wavelengths, occurring in the region 3570 - 5170 Å, were observed and the rotational structure of twelve of them, with $v' = 0$ to 2 and $v'' = 0$ to 5, were analyzed in the present work. The final constants of states B and X are obtained by the method of merging. The spin splitting of the rotational levels was observed in several bands of this system. The $v = 0$ level of state B is found to be perturbed and the information regarding the perturbing state is also obtained from this analysis. The details of all these results are outlined in Chapter 8. Finally, the conclusions drawn from the present investigations are summarized in Chapter 9.

CHAPTER 2

EXPERIMENTAL TECHNIQUES

The spectra of the neutral molecules $^{12}C^{16}O$ and $^{13}C^{18}O$ and of the molecular ions $^{13}C^{18}O^+$ and $^{15}N_2^+$ were excited in a specially designed hollow-cathode discharge tube. Several band systems of these molecular species resulting from this excitation were photographed with medium and high resolution optical spectrographs. A concise description of the hollow-cathode discharge tube and the spectrographs, and the experimental procedure are presented in this chapter. Also discussed briefly here is the mechanism of the hollow-cathode discharges.

2.1 Hollow-Cathode Discharge Tube

The design of the hollow-cathode discharge tube is schematically shown in Figure 4. The hollow cathode (G) made from a copper cylinder is 9.0 cm long, 1.8 cm in outer diameter and 0.3 cm in wall thickness and was silver soldered (I) to a 1.9 cm inner diameter Kovar tube, which is the lower section of a Kovar-pyrex seal (H). The upper end of this seal was joined to the main pyrex glass body (E), 14 cm long and 4.6 cm in outer diameter, of the discharge tube. The side arm (F), 1.7 cm in outer diameter, branches out from the main body. A tungsten anode (B) was fused into
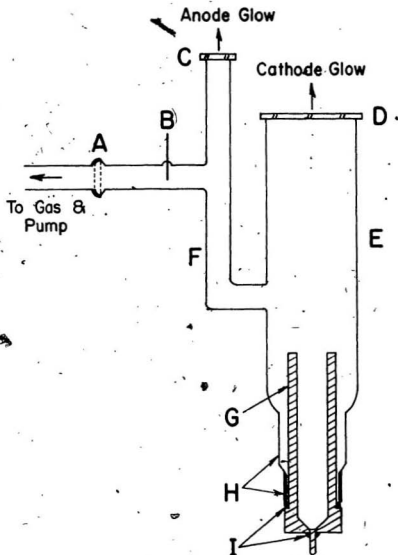
Figure 4. A schematic diagram of the hollow-cathode discharge tube. A: ball and socket joint; B: tungsten anode; C: anode window; D: cathode window; E: pyrex glass body; F: anode column; G: copper cathode; H: Kovar-pyrex seal; and I: silver solderings.

the branch of the side arm. A ball and socket arrangement (A) facilitates the connection or disconnection of the discharge tube to or from the pumping system. Two S1-UV quartz windows (C and D) (supplied by Esco Products Inc.), 0.3 cm thick, were attached to the grounded end surfaces of the anode and cathode branches of the discharge tube with Torr Seal, a low vapor pressure resin.

The main advantage of the present design of the hollow-cathode discharge tube is the physical separation of the anode and cathode glows which can thereby be photographed independently. The presence of a carrier gas, such as helium or neon, is sometimes necessary to produce the spectra of molecular ions and/or suppress the spectra of neutral molecules. In the present work, no carrier gas was found necessary to produce the spectra of $^{13}C^{18}O^+$ and $^{15}N_2^+$. In certain excitations, it may be necessary to cool the cathode portion of the discharge tube with an appropriate coolant. For example, Herzberg et al. (1981) produced the emission spectra of the triatomic molecular species H_3 and D_3 in a hollow-cathode discharge tube of a somewhat similar design in a flow of H_2 and D_2 gas, respectively, and immersing the cathode portion in liquid nitrogen.

Preliminary experiments with the present discharge tube proved that the cathode glow is an excellent source to record the spectra of the molecular ions and the anode glow is convenient for the study of the spectra of the neutral

molecules. As an illustration, the spectra of the anode and cathode glows of molecular nitrogen-14 in the region 3345-5227 Å obtained with the present hollow-cathode discharge tube under identical conditions are shown in juxtaposition in Figure 5. It is noted from this figure that the two spectra are remarkably different; the anode glow spectrum [see Figure 5(a)] contains exclusively the bands of the second positive system ($C^3\Pi_u - B^3\Pi_g$) of the neutral $^{14}N_2$ molecule (with the exception of the weak appearance of the normally very strong 0-0 band of the first negative system of $^{14}N_2^+$) and the cathode glow spectrum [see Figure 5(b)] consists of the first negative system ($B^2\Sigma_u^+ - X^2\Sigma_g^+$) of the molecular ion $^{14}N_2^+$. Also seen in Figure 5(b) is the occurrence of some strong bands of the second positive system of $^{14}N_2$ in the cathode glow. The spectra illustrated in Figure 5 were photographed without any carrier gas. Perhaps the presence of a carrier gas, such as helium, could have further suppressed the intensity of the bands of the second positive system in the cathode glow. From this illustration, it is amply clear that in the hollow-cathode discharge tube of the design used in the present work, the anode glow almost exclusively consists of the spectra of the neutral molecules and the cathode glow is a very rich source of molecular ions.

It should be noted that, in place of the present design of the hollow-cathode tube, if one uses a discharge

Figure 5. Spectrum of molecular nitrogen - 14 excited in a hollow-cathode
discharge tube ● the spectral region 3345 - 5230 Å. (a) Anode
glow spectrum consisting of the second positive ($C^3\Pi_u - B^3\Pi_g$)
system of the neutral $^{14}N_2$ molecule and (b) Cathode glow
spectrum consisting of the first negative system ($B^2\Sigma_u^+ - X^2\Sigma_g^+$)
of the molecular ion $^{14}N_2^+$ and some bands of the second positive
system of $^{14}N_2$. For both (a) and (b) the excitation conditions
are identical and are recorded on a 2 m Bausch and Lomb spectro-
graph in the first order of a 600 grooves/mm grating.
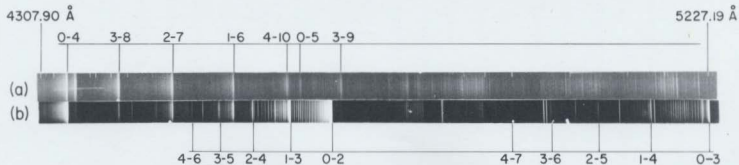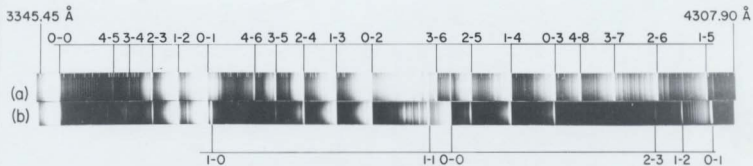
tube in which the cathode glow and the anode glow are in the same column, the spectra of a neutral molecule and of its ion cannot be separated. The spectral broadenings, such as Doppler broadening, pressure broadening, and Stark broadening are greatly minimized in the hollow-cathode discharges compared to the excitation in a straight d.c. arc or in a conventional electrodeless discharge. The mechanism of the electrical discharge in a hollow-cathode tube is discussed in Section 2.2.

A d.c. power supply unit rated at 2000 V and 250 mA was used to maintain the discharge. The details of this unit were described earlier by the author (Prasad, 1983) and a circuit diagram of this unit is shown in Figure 6. Its main components are a powerstat (P), a step-up transformer T (1750 V-0-1750 V), a bridge rectifier made up of four high voltage diffused silicon rectifiers, D_1 to D_4 (VARO VC40), an oil-filled condenser (15 μF, 2000 V) and several DALE HL100 type resistors R_1 to R_7 (R_1: 100 Ω, 100 W; R_2: 1 to 20 KΩ, 100 W; R_3 to R_6: 20 KΩ, 100 W; and R_7: 390 KΩ, 9 W). The desired voltage is applied between the anode and the cathode of the discharge tube by adjusting the primary voltage of the transformer. At normal operating conditions of the discharge tube, an applied voltage of 1100 V gave a current of 65 mA.
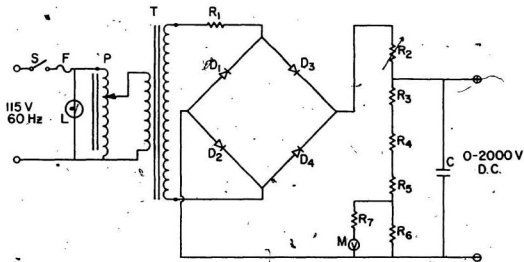
Figure 6. Circuit diagram for the 2000 v d.c. power supply unit. P: powerstat; T: step-up transformer; D_1 to D_4: high voltage rectifiers; R_1 to R_7: resistors; M: voltmeter and C: oil-filled condenser.

2.2 Mechanism of Hollow-Cathode Discharges

The mechanism of an electrical discharge in a hollow-cathode discharge tube can be understood in the following manner. A d.c. voltage applied between the two electrodes of an evacuated discharge tube releases free electrons from the cathode which are then accelerated by the electric field. The accelerated electrons collide with the atoms and molecules of the gas admitted into the discharge tube. In this collision process, the translational kinetic energy of free electrons is transferred to the atoms and molecules of the gas in the discharge tube, thus enabling the atoms to be excited to upper electronic states and the molecules to be excited to different upper rotational, vibrational, and electronic states. As the excited states of the atoms and molecules are highly unstable, they decay to their lower energy states by giving up the excess energy by emitting electromagnetic radiation of energy $h\nu'$, where h is the Planck's constant and ν' is the frequency (in s^{-1}) of the emitted photon. As long as the power supply is maintained between the electrodes, collisions between the accelerated free electrons and the atoms and molecules continue to take place and the emission of the radiation is maintained.

If the free electrons released from the cathode acquire sufficient kinetic energy, they ionize the molecules of the gas during the collisions. These molecular ions, because

of their positive charge, concentrate around the cathode. The cathode region also contains some excited neutral molecules, but most of them spread towards the anode. This explains the spectra shown in Figure 5, where the cathode glow spectrum consists of the N_2^+ spectrum and some normally strong bands of N_2, and the anode glow spectrum almost exclusively consists of the spectrum of neutral N_2. At times, it is also found that certain band systems of the neutral molecules, arising from high-lying states, are preferentially excited in the cathode glow rather than in the anode glow, probably because of the collisions between the neutral molecules and the corresponding molecular ions, present abundantly in the cathode glow (see, for example, Chapter 4).

2.3 Spectrographs and Experimental Procedure

The electronic spectra of the molecules studied in the present investigations were photographed on a 2 m Bausch and Lomb dual grating spectrograph and a 3.4 m Jarrell-Ash Ebert grating spectrograph. A brief description of these spectrographs and the experimental procedure that was followed are presented in this section.

(i) The 2 m Bausch and Lomb Dual Grating Spectrograph

The optical layout of this spectrograph for an incident monochromatic light beam is schematically shown in Figure 7. The light beam entering the spectrograph through a variable
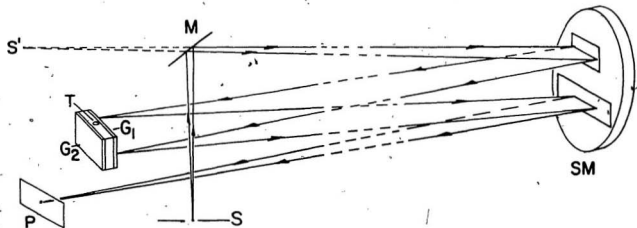
Figure 7. Optical path of a monochromatic light beam in the 2 m Bausch and Lomb dual grating spectrograph. S: slit; M: plane mirror; SM: spherical mirror; T: rotatable turret; G_1 and G_2: gratings; and P: photographic plate.

slit (S) is reflected by the plane mirror (M) onto the upper portion of a spherical mirror (SM). The mirror has a focal length of 2 m and a numerical aperture of f/15.5. The light reflected from the spherical mirror is then dispersed by one of the gratings G_1 or G_2. These plane gratings, one with 600 grooves/mm and blazed at 2.5 μm and the other with 1200 grooves/mm and blazed at 1.0 μm have a ruled area of 128 mm (width) x 102 mm (groove length) and are mounted back to back on a rotatable turret T. The desired grating can be brought into the required position by rotating the turret. The light dispersed by the grating reaches the lower portion of the spherical mirror (SM) which focusses it onto the photographic plate (P). The plate holder is designed to accommodate one 10.16 cm x 25.40 cm or two 5.08 cm x 25.40 cm photographic plates. The measured reciprocal dispersions of the spectra vary from 8.2 Å/mm at 5500 Å in the first order of the 600 grooves/mm grating to 0.69 Å/mm at 4880 Å in the third order of the 1200 grooves/mm grating.

(ii) The 3.4 m Jarrell-Ash Ebert Grating Spectrograph

A schematic diagram of the optical layout of this spectrograph is shown in Figure 8. Light from a source is collimated by two quartz cylindrical lenses L_1 (collimating lens, focal length 10.0 cm and diameter 3.0 cm) and L_2 (condensing lens, focal length 45.0 cm and diameter 3.0 cm) onto the slit (S) and then to the upper section of the
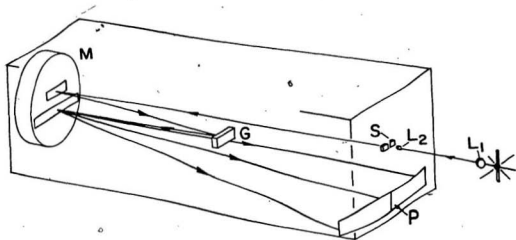
Figure 8. Optical layout of the 3.4 m Jarrell-Ash Ebert grating spectrograph.
L₁: quartz cylindrical source lens; L₂: quartz cylindrical slit lens;
S: slit; M: collimating mirror; G: grating; and, P: photographic plate.

concave mirror (M), whose diameter is 40.6 cm, radius of curvature is 6.655 m and numerical aperture is f/35. The mirror (M) collimates the light onto the grating (G). The light dispersed by the grating consists of a parallel group of rays for each wavelength and is condensed by the lower section of M onto the photographic plates (P). The camera which holds the plates can be tilted about a vertical axis. For a fixed slit position obtained for the best focus condition, the tilt of the camera is found to have a linear dependence on the grating angle. A typical plot of the camera tilt versus grating angle is given in Figure 9. The plate holder is designed to accommodate one 5.08 cm x 50.80 cm or two 5.08 cm x 25.40 cm photographic plates.

The Jarrell-Ash spectrograph can be equipped with either an MIT echelle grating blazed at 5.7 μm and having 300 grooves/mm or a Bausch and Lomb grating blazed at 1.4 μm and having 1200 grooves/mm. Both these gratings have a ruled width of 186 mm and a groove length of 63 mm. In the present work, the Bausch and Lomb grating was used in second and third orders. The measured reciprocal dispersions of the spectra are 0.9 Å/mm at 5200 Å in the second order and 0.6 Å/mm at 3700 Å in the third order.

(iii) Experimental Procedure

The $^{12}C^{16}O$ and $^{14}N_2$ gases used in the present work were supplied by Matheson Gas Products and their purities were
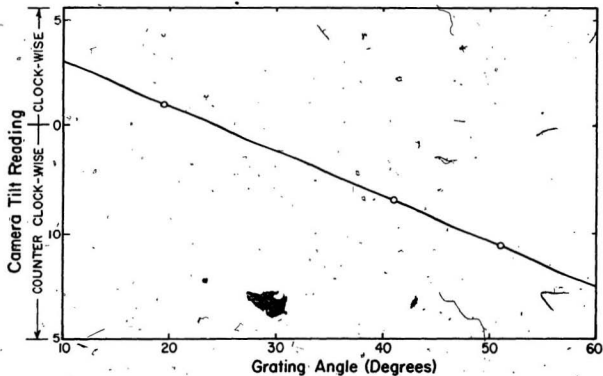
Figure 9. A plot of the camera tilt reading versus grating angle for a fixed slit position obtained for the best focus condition on the 3.4 m Jarrell-Ash spectrograph.

rated as 99.99%. The $^{13}C^{18}O$ and $^{15}N_2$ gases were supplied by Merck Sharpe and Dohme Canada Limited. The purity of the $^{13}C^{18}O$ gas was rated as 99% of ^{13}C and 95% of ^{18}O, and that of the $^{15}N_2$ gas was rated as 99.9% of ^{15}N. The gas-handling system made of pyrex glass which was attached to the hollow cathode discharge tube is shown in Figure 10. In this figure, R_1 and R_2 are the primary and secondary reservoirs, respectively, and S_1, S_2, S_3, and S_4 are the stop-cocks. B_1 and B_2 are ball and socket arrangements; B_1 is used to connect or disconnect the experimental gas to or from the system and B_2 is used to connect or disconnect the discharge tube. Either the anode branch or the cathode branch was first aligned with the optical axis of the spectrograph. Then the discharge tube was thoroughly evacuated and a small quantity of one of the experimental gases from the reservoir was slowly admitted into the discharge tube in stages. In the present investigations, the experiments were done under the stagnant (not continuous flow) conditions of the gas. A d.c. power supply of 1100 V was applied between the electrodes of the discharge tube and the discharge was initiated with a tesla coil. The pressure of the gas inside the tube was regulated until a bright and steady characteristic discharge was obtained. A fresh supply of the experimental gas had to be re-admitted into the discharge tube to maintain the discharge for times longer than an hour. The emitted radiations were photographed under medium

Figure 10. Gas-handling system. T: liquid nitrogen trap; S_1 to S_4 stop-cocks; B_1 and B_2: ball and socket joints; R_1 and R_2: primary and secondary reservoirs; H: hollow-cathode discharge tube.
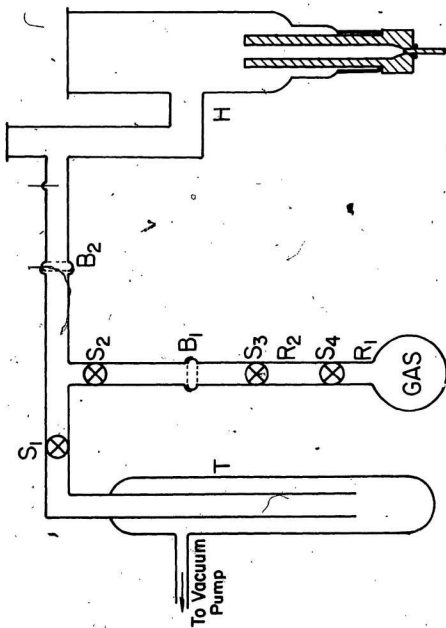
and high resolutions as the Bausch and Lomb spectrograph and under high resolution on the Jarrell-Ash spectrograph. The slit width was maintained at 20 μm on the Bausch and Lomb spectrograph and 30 μm on the Jarrell-Ash spectrograph. An Fe-Ne hollow-cathode lamp was used as a source for the standard spectrum.

Kodak Spectrum Analysis No. 1, 103 a-O, and 103-F type plates were used to photograph various band systems. Corning glass filters and Hoya glass filters were used to eliminate the overlapping orders. Depending on the intensity of the band, sensitivity of the photographic plate, and the transmittance of the filter, the exposure times varied from 5 seconds to 8.5 hours. In general, longer exposure times were required on the Jarrell-Ash spectrograph. The details of photographing various systems will be discussed in their respective chapters.

All the photographic plates were developed in Kodak developer D-19, kept at a temperature of 20°C for about 4 minutes. After finsing them in cold water, they were fixed in Kodak fixer for about 15 minutes. Then the plates were washed in the running water for at least 30 minutes before they were dried.

2.4 Measurement of Spectra

The photographic plates were measured on a linear comparator model M1205C, supplied by the Gaertner Optical

Company, Chicago, Illinois, U.S.A. The least count of the instrument is 0.001 mm but the readings can be estimated accurately up to 0.0005 mm. The positions of all the spectral lines, including the standard Fe-Ne lines were measured and the comparator readings (d) were recorded. The comparator readings of the standard Fe-Ne lines and their air wavelengths (λ_{air}) were fitted to a polynomial

$$\lambda_{air} = \sum_{i=0}^{h} a_i (d-d_0)^i, \qquad [2.1]$$

by the method of least squares to obtain the coefficients a_0, a_1, a_2, ... etc. Here, d_0 is the comparator reading of the first standard line. The wavelengths of the standard Fe-Ne lines were taken from Crosswhite (1958 and 1975). The standard deviation of a typical least-squares fit was generally about 0.003 Å. After obtaining the coefficients a_0, a_1, a_2, ... etc., the air wavelengths of the band heads and the rotational lines were calculated from Eq. [2.1]. The air wavelengths were then converted into vacuum wavenumbers ν (in cm^{-1}) by using the Edlen's formula (1953) for the refractive index, n,

$$n = 1 + 6432.8 \times 10^{-8} + \frac{2949810}{146 \times 10^8 - \nu^2} + \frac{25540}{41 \times 10^8 - \nu^2}, \qquad [2.2]$$

where $\nu = \dfrac{10^8}{n \times \lambda_{air}}$, ($\lambda_{air}$ in the units of Ångström).

An iterative method was employed to calculate the vacuum wavenumbers and the iteration was continued until the absolute value of the difference between the successive values of the wavenumbers was less than or equal to 10^{-10} cm^{-1}. The mathematical calculations involved here and also in the subsequent analysis of the spectra were performed on a VAX 11/785 computer.

CHAPTER 3

THEORETICAL ASPECTS OF ELECTRONIC SPECTRA

The theory of electronic spectra of diatomic molecules which is mainly relevant to the present investigations is briefly discussed in this chapter. The theoretical aspects pertinent to the calculation of Franck-Condon factors and to the merging procedure to obtain a unique set of molecular constants from those of the individual bands are outlined. Finally, the theory of perturbations in electronic spectra is also briefly presented. A detailed theory of electronic band spectra can be found in Mulliken (1930, 1931, 1932) and Herzberg (1950, 1971).

3.1 Energy Levels of a Diatomic Molecule

Within the Born-Oppenheimer approximation (1927), the total energy E (usually expressed in ergs) of a diatomic molecule, neglecting its translational and nuclear spin energies, is represented as

$$E = E_e + E_v + E_r, \qquad [3.1]$$

where E_e is the electronic energy, E_v is the vibrational energy, and E_r is the rotational energy. The term values (in cm^{-1} units) of the molecule are given by

$$T = E/hc = T_e + G(v) + F_v(J), \qquad [3.2]$$

where v and J are vibrational and rotational quantum numbers, respectively, and T_e, $G(v)$, and $F_v(J)$ are the electronic, vibrational, and rotational term values, respectively. The wavenumber (in. cm^{-1}) of a spectral line arising from a transition between the rotational levels of an upper (') and a lower (") electronic state is given by

$$\nu = T' - T''$$

$$= (T_e' - T_e'') + [G'(v') - G''(v'')] + [F_v'(J') - F_v''(J'')]$$

$$= \nu_e + \nu_v + \nu_r. \qquad [3.3]$$

For a given electronic transition, $\nu_e (= T_e' - T_e'')$ is the system origin and $\nu_e + \nu_v = \nu_0$ is the band origin. The three terms of Eqs. [3.2] and [3.3] will be discussed in the following paragraphs.

(i) **Electronic Terms and States**

The term T_e in Eq. [3.2] is generally expressed as

$$T_e = T_0 + A\Lambda\Sigma_S, \qquad [3.4]$$

where T_0 is the electronic term value when the net electronic spin angular momentum $\vec{S}$ of the molecule is neglected, A is the spin-orbit coupling constant, and Λ and Σ_S are the quantized projections, along the internuclear axis, of the electronic orbital and spin angular momenta $\vec{L}$ and $\vec{S}$,

respectively. Electronic states with $\Lambda = 0, 1, 2, \ldots$ are labelled $\Sigma, \Pi, \Delta, \ldots$ respectively. For all the singlet $(S, \Sigma_S = 0)$ and $\Sigma(\Lambda = 0)$ states, T_0 is identical with T_e. The constant A in Eq. [3.4] is either positive or negative; in the former case, the electronic state is termed a regular state, whereas in the latter case, it is known as an inverted state. The Σ electronic states are designated as Σ^+ or Σ^-, depending on whether the electronic wavefunction ψ_e remains unchanged or changes sign, respectively, upon reflection at a plane passing through the internuclear axis. The multiplicity of an electronic state is given by $2S+1$, which is the number of Σ_S components along the internuclear axis. If the two nuclei of a diatomic molecule have the same charge, for example, $^{14}N_2$, $^{14}N^{15}N$, and $^{15}N_2$ (or H_2, HD, and D_2), the electric field of the nuclei in which the electrons move, has a center of symmetry. For such molecules, if ψ_e remains unchanged or changes sign when reflected at the center, in the first case the electronic state is called an even (gerade, g) state and in the second case, it is called an odd (ungerade, u) state. These states are represented as Σ_g^+, Σ_g^-, Σ_u^+, Σ_u^-, Π_g, Π_u, $\ldots$ etc.

(ii) Vibrational Terms and Vibrational Structure of Electronic Spectra

The vibrational term values $G(v)$ of an electronic state are written as

$$G(v) = \omega_e(v+\tfrac{1}{2}) - \omega_e x_e(v+\tfrac{1}{2})^2 + \omega_e y_e(v+\tfrac{1}{2})^3 + \ldots, \qquad [3.5]$$

where ω_e is the vibrational frequency and $\omega_e x_e$, $\omega_e y_e$, etc. are the anharmonic constants. In instances where the experimental data are not obtained for sufficiently high values of v, $\omega_e y_e$ and other higher anharmonic constants in Eq. [3.5] will be neglected. For a vibrational transition to take place between two electronic states, there are no strict selection rules to be satisfied. But, the intensities of these transitions are governed by Franck-Condon factors (see Section 3.2). Neglecting the contribution from the rotational levels, the wavenumber $\nu_{v',v''}$ of a vibrational transition is given by

$$\nu_{v',v''} = \nu_e + \omega_e'(v'+\tfrac{1}{2}) - \omega_e' x_e'(v'+\tfrac{1}{2})^2 + \omega_e' y_e'(v'+\tfrac{1}{2})^3 + \ldots$$
$$- \omega_e''(v''+\tfrac{1}{2}) + \omega_e'' x_e''(v''+\tfrac{1}{2})^2 - \omega_e'' y_e''(v''+\tfrac{1}{2})^3 + \ldots [3.6]$$

The origins obtained from the detailed rotational analysis of a band structure or the wavenumbers of the band heads obtained from the measurements can be directly fitted to the above expression to obtain the constants ν_e, ω_e, $\omega_e x_e$, $\omega_e y_e$, etc. In the matrix notation, Eq. [3.6] can be written as

$$\nu = \chi\, B + \Delta, \qquad [3.7]$$

where ν and B are the column vectors; ν contains either band origins or wavenumbers of band heads and B contains

the unknown molecular constants to be estimated. The coefficient matrix χ contains the coefficients of ν_e, ω_e', $\omega_e'x_e'$, ... etc., and Δ is the column vector containing the unknown measurement errors. Using the method of least-squares, the molecular constants $\hat{B}$ (quantity with $\wedge$ indicates that it is an estimate obtained from the least-squares fitting) can be estimated from the expression,

$$\hat{B} = (\chi^T \chi)^{-1} \chi^T \nu \qquad [3.8]$$

The estimated variance of this least-squares fit is given by

$$\hat{\sigma}^2 = (\nu - \chi \hat{B})^T (\nu - \chi \hat{B})/f, \qquad [3.9]$$

where f is the degrees of freedom. The uncertainties in the estimates of the molecular constants are the square roots of the diagonal elements of the variance-covariance matrix ($\hat{\theta}$) associated with $\hat{B}$. This variance-covariance matrix is given by

$$\hat{\theta} = \hat{\sigma}^2 (\chi^T \chi)^{-1}. \qquad [3.10]$$

The vibrational isotope shift $\Delta\nu$ of a band is given by

$$\begin{aligned}
\Delta\nu &= \nu_{v',v''} - \nu^i_{v',v''} \\
&= (1-\rho)[\omega_e'(v'+\tfrac{1}{2}) - \omega_e''(v''+\tfrac{1}{2})] \\
&\quad - (1-\rho^2)[\omega_e'x_e'(v'+\tfrac{1}{2})^2 - \omega_e''x_e''(v''+\tfrac{1}{2})^2] \\
&\quad + (1-\rho^3)[\omega_e'y_e'(v'+\tfrac{1}{2})^3 - \omega_e''y_e''(v''+\tfrac{1}{2})^3], \ldots \qquad [3.11]
\end{aligned}$$

where $\nu_{v',v''}$ and $\nu^1_{v',v''}$ are the wavenumbers of the band origins (or band heads) with a given v' and v'' of an ordinary molecule and its isotope, respectively, and $\rho = [\mu/\mu^1]^{\frac{1}{2}}$, μ, and μ^1 being the respective reduced masses of these molecules.

(iii) Rotational Terms and Rotational Structure of Electronic Spectra

The rotational structure of an electronic band system is dependent on the nature of the electronic states involved. In this section, only the general features of this structure are discussed but the complex details of the rotational structures of the individual electronic transitions will be presented in subsequent chapters. Each vibrational level of a given electronic state contains a series of rotational levels and the term values of these levels, in case of singlet electronic states, are represented by

$$F_v(J) = B_v[J(J+1)-\Lambda^2] - D_v[J(J+1)-\Lambda^2]^2 + \dots \qquad [3.12]$$

where $B_v = (h/8\Pi^2 c\mu) \overline{[1/r_v^2]}$ is the rotational constant and $D_v = 4B_v^3/\omega^2$ is the centrifugal stretching constant. Here μ is the reduced mass of the molecule and r is the internuclear separation. The constants B_v and D_v can be expressed in terms of vibrational quantum number (v) and the equilibrium molecular constants as

$$B_v = B_e - \alpha_e(v+\frac{1}{2}) + \dots \qquad [3.13a]$$

and

$$D_v = D_e - \beta_e(v + \tfrac{1}{2}) + \ldots \qquad [3.13b]$$

The D_v values obtained in the present investigations are so small (of the order of 10^{-6} cm^{-1}) that a reliable estimate of D_e and β_e could not be made, whereas B_e ($=h/8\Pi^2 c \mu r_e{}^2$) and α_e are estimated very accurately. The doublet, triplet, etc., electronic states contain two, three, etc., series of vibrational levels. The spacing of the rotational levels in these multiplet states as a function of the rotational quantum number depends on the type of coupling between various angular momenta of the molecule, such as the electronic orbital angular momentum $\vec{L}$, the electronic spin angular momentum $\vec{S}$, and in the nuclear rotation angular momentum $\vec{R}$. Of all the five different coupling cases distinguished by Hund, the two most important ones known as Hund's case (a) and case (b), will be discussed here.

In Hund's case (a), the electronic orbital and spin angular momenta are strongly coupled individually to the internuclear axis. The sum of the quantized projections Λ and Σ_S of the orbital and spin angular momenta, respectively, along the internuclear axis is given by

$$\Omega = \Lambda + \Sigma_S . \qquad [3.14]$$

For a given electronic state, i.e., for a fixed Λ, the number of values that Ω can take is the same as that of the multiplicity of the state. The nuclear rotation angular

momentum vector $\vec{R}$ combines with Ω to form the total angular momentum vector $\vec{J}$. For a given value of Ω, J has the values

$$J = \Omega, \ \Omega + 1, \ \Omega + 2, \ \ldots \qquad [3.15]$$

Both J and Ω have either integral or half-integral values, depending on whether the multiplicity of the state is odd or even, respectively.

In Hund's case (b), the spin angular momentum vector $\vec{S}$ may be very weakly coupled to the internuclear axis or not coupled at all. In either case, Ω is not defined and the orbital angular momentum vector $\vec{L}$ combines with $\vec{R}$ to form a new vector $\vec{N}$, which is the total angular momentum apart from the spin. The possible values of new quantum number N are

$$N = \Lambda, \ \Lambda + 1, \ \Lambda + 2, \ldots \qquad [3.16]$$

if $\Lambda = 0$, N takes all the integral values from zero onwards. The vector $\vec{N}$ combines with $\vec{S}$ to form the total angular momentum vector $\vec{J}$. Now for a given N, J has the values

$$J = N + S, \ N + S-1, \ \ldots \ |N - S| \ . \qquad [3.17]$$

Thus, for a given N, each rotational level has 2S+1 components which is the multiplicity of the electronic state. In this case also, J can have either integral or half-integral values depending on whether the multiplicity is odd or even,

respectively. In most of the cases, multiplet Σ states, i.e., $^2\Sigma$, $^3\Sigma$, etc., belong to Hund's case (b), whereas the multiplet Π and Δ states can belong to either case (a) or case (b). There are some instances where $^3\Sigma$ state belongs to Hund's case (c) which is not of interest in the present work. There are several rotational selection rules to be satisfied in a specific electronic transition and these will be discussed in the subsequent chapters.

(iv) Parity and Labelling of Rotational Levels

The parity[i] of a rotational level is defined to be either positive or negative depending on whether the total eigenfunction (ψ) remains unchanged or changes sign, respectively, upon reflection at the origin. In case of a Σ^+ state, the rotational levels with even J values are positive and those with odd J values are negative, whereas for a Σ^- state, the rotational levels with even J values are negative and those with odd J are positive. For the electronic states with $\Lambda \neq 0$, i.e., for Π, Δ, ..., etc., states, the rotational levels are doubly degenerate and for each J value, there is a positive and a negative rotational level. This type of splitting of the rotational levels is called Λ-type doubling.

In the case of homonuclear diatomic molecules (e.g., $^{14}N_2$ and $^{15}N_2$) for exchange of nuclei, the total eigenfunction (ψ) either remains unchanged or changes sign; in the first

case, the rotational level is symmetric (s) and in the second case, it is anti-symmetric (a). In a given electronic state either the positive rotational levels are symmetric and the negative levels are anti-symmetric or the positive are anti-symmetric and the negative are symmetric. In the case of gerade electronic states, i.e., Σ_g, Π_g, etc., all the positive rotational levels are symmetric and the negative levels are anti-symmetric and the reverse is true for ungerade states, i.e., for Σ_u, Π_u, etc., states.

Kopp and Hougen (1967) introduced the following convention for labelling the rotational levels with half-integral J values:

levels with parity $[+(-1)^{J-1/2}]$ are e levels,

and those with parity $[-(-1)^{J-1/2}]$ are f levels.

Later, Brown et al. (1975) extended this labelling convention to the rotational levels with integral J values. According to them,

levels with parity $[+(-1)^J]$ are e levels,

and those with parity $[-(-1)^J]$ are f levels.

The advantage of using e and f labelling scheme is that it is independent of the coupling case in question and depends only on J and parity, which are very well defined in field free space. According to this convention, all the rotational levels in a $^1\Sigma^+$ state are e levels and those in a $^1\Sigma^-$ state are f levels. The general rotational selection rules that are applicable for the electric dipole transitions are

$$\Delta J = 0, \pm 1 \text{ and } + \longleftrightarrow - \, .$$

In terms of this labelling scheme (e and f) these selection rules are written as

$$\Delta J = 0, \quad e \longleftrightarrow f$$

$$\Delta J = \pm 1, \quad e \longleftrightarrow e, \text{ and } f \longleftrightarrow f.$$

The rotational levels shown in the energy level diagrams in the following chapters are labelled according to this scheme.

3.2 Franck-Condon Factors

The intensity of an emitted radiation is defined as the energy emitted by the source per second. If $N_{v'}$ is the number of molecules in the upper state and $A_{v',v''}$ is the fraction of molecules participating in the transition, then the intensity is expressed as

$$I_{v',v''} = N_{v'} \, h \, c \, \nu_{v',v''} \, A_{v',v''} \, , \qquad [3.18]$$

where $\nu_{v',v''}$ is the frequency (in cm^{-1}) of the emitted radiation. The Einstein coefficient for spontaneous emission, $A_{v',v''}$, is given by

$$A_{v',v''} = (64\Pi^4/3h)\nu^3_{v',v''} \mid R_{v',v''} \mid^2 \, . \qquad [3.19]$$

For electric dipole transitions, $R_{v',v''}$ represents the matrix elements of the electric dipole moment. These matrix elements are written as

$$| R_{v',v''} |^2 = | M_{el}(\bar{R}) |^2 | \int \psi_v' \psi_v'' dr |^2 , \qquad [3.20]$$

where $| M_{el}(\bar{R}) |$ is the electronic transition dipole moment which depends on the co-ordinates of the electrons only, and ψ_v' and ψ_v'' are the wavefunctions of the upper and lower vibrational states. The integral in Eq. [3.20] is the overlap integral and the square of its modulus is called the Franck-Condon factor (FCF) $q_{v',v''}$. Substitution of Eqs. [3.19] and [3.20] into Eq. [3.18] gives

$$I_{v',v''} = (64/3) \; \pi^4 \; c \; \nu^4_{v',v''} \; N_{v'} \; |M_{el}(\bar{R})|^2 \; |\int \psi_v' \psi_v'' dr |^2. \qquad [3.21]$$

For a given electronic transition, $N_{v'}$, $\nu_{v',v''}$ and $|M_{el}(\bar{R})|^2$ can be generally taken as constants and the intensity of the emitted radiation is proportional to FCF. The wavefunctions ψ_v' and ψ_v'' can be obtained by solving the Schrödinger equation of a diatomic molecule,

$$(h/8\pi^2\mu c)\nabla^2\psi + [(E/hc) - U]\psi = 0 , \qquad [3.22]$$

where μ is the reduced mass of the molecule and U is the effective potential energy (in cm^{-1}). The solution of this equation depends on the mathematical form of U. In the present work, the "Klein-Dunham potential" suggested by Jarmain (1960, 1971) was used to solve the Schrödinger equation and consequently FCFs were calculated. The theory of Klein-Dunham potential is reviewed earlier in one of the Ph.D. theses from our laboratory (Verma, 1977). A computer

program prepared by Jarmain and McCallum (1970), was modified
by the author to operate it on a VAX 11/785 computer and
was then used to calculate the Franck-Condon factors $q_{v', v''}$.

3.3 Merging of Least-Squares Parameters

The molecular constants are generally estimated from
the wavenumbers of spectral lines by the least-squares
method. The importance of the method of least-squares and
the mathematical expressions involved are compiled by
Albritton et al. (1976). There are several approaches to
obtain the molecular constants from the spectroscopic data.
Some of these are the method of combination differences,
discussed widely by Herzberg (1950), traditional term value
method suggested by Åslund (1965), improved term value
approach and the direct approach, both proposed by Albritton
et al. (1973). These methods are critically discussed by
Albritton et al. (1973). The method of direct approach in
which the wavenumbers of all the observed spectral lines of
a band are used to obtain the molecular constants of both the
upper and lower vibrational states simultaneously, provides
a set of molecular constants which are statistically more
meaningful than the ones obtained by the other methods.
Generally, the bands of one system or those of different
systems of a molecule share common lower or upper vibrational
levels. When the individual bands of such systems are
analyzed to obtain molecular constants, the common vibrational

levels will have multiple estimates for their constants. These multiple estimates can be reduced to a single "best possible" estimate in several ways. Albritton et al. (1977) proposed a method of "merging" in which the results of the individual bands obtained by least-squares fits are combined together, giving due consideration to the uncertainties and the correlations of various molecular constants. The theory of this method of merging is briefly discussed in this section.

The molecular constants obtained in the band by band analysis and their variance-covariance matrices are used as the input for this least-squares merging fit in which the multiple estimates are reduced to a single value. The relation between the input parameters and the best possible values of the output parameters in this merging procedure is given by the set of equations in matrix notation,

$$Y = X\beta + \delta, \qquad [3.23]$$

where Y, β, and δ are the column vectors representing the input parameters, the output parameters, and the unknown errors, respectively. Here, the coefficient matrix X relates the input parameters of Y to the corresponding value of β. The least-squares solution of Eq. [3.23] provides molecular constants β such that the squares of the unknown errors δ are minimized subject to the interrelations among δ. These interrelations exist because the variance-covariance matrices associated with the least-squares fits of the

individual bands have generally unequal diagonal elements and non-zero off-diagonal elements. In order to obtain a set of molecular constants $\hat{\beta}$ with due consideration for these unequal variances and non-zero covariances, a correlated least-squares fit (see Albritton et al., 1976) should be used. The expression for β, in matrix notation, from such a correlated least-squares fit is given by

$$\hat{\beta} = (X^T \Phi^{-1} X)^{-1} X^T \Phi^{-1} Y, \qquad [3.24]$$

where Φ is a non-diagonal generalized weight matrix composed of various variance-covariance matrices obtained from the individual band by band fits. The estimated variance of this merged least-squares fit is given by

$$\hat{\sigma}^2 = (Y - X\hat{\beta})^T \Phi^{-1} (Y - X\hat{\beta})/f , \qquad [3.25]$$

where f is the degrees of freedom of the merged fit. The merged dispersion matrix is given by

$$\hat{V} = (X^T \Phi^{-1} X)^{-1}. \qquad [3.26]$$

The uncertainties in the estimates of the merged molecular constants which are the square roots of the diagonal elements of the variance-covariance matrix associated with $\hat{\beta}$ are given by

$$\hat{\theta} = \hat{\sigma}^2 \hat{V}. \qquad [3.27]$$

According to Coxon (1978), it is convenient to combine two or more sets of separately merged parameters into a single set of parameters by least-squares grand merge method (which is similar to the one described above), instead of obtaining the final set of parameters through a one large single merging. The single set of parameters from the final grand merge are identical with those derived from the equivalent single step merge, provided the weight matrix used in the grand merge is composed of the dispersion matrices [Eq. 3.26] of earlier merges but not of the variance-covariance matrices of the input parameters [Eq. 3.27].

3.4 Perturbations

The theory of perturbations in the spectra of diatomic molecules has been dealt with by several authors. The important ones among them are Kronig (1928), Herzberg (1950), Kovács (1969) and Lefebvre-Brion and Field (1986).

In general, the wavenumber ν of a rotational line of a band which is free from perturbations can be represented by an empirical expression

$$\nu = a + bJ + cJ^2 + \dots \qquad [3.28]$$

However, when perturbations occur, a rotational line or a series of successive lines deviate considerably from Eq. [3.28]. For certain types of perturbations, in addition to the deviations, weakening in intensity may also appear.

Dieke and Mauchly (1932, 1933) observed this type of intensity fluctuations in the rotational structures of the bands of third positive system ($b^3\Sigma^+ - a^3\Pi_r$) of $^{12}C^{16}O$ in which both the electronic states are perturbed. In general, these deviations increase to a maximum with increasing J and suddenly change sign and then increase to zero and continue to follow the regular smooth course. The behaviour of these deviations largely depends on the nature of the perturbing electronic state.

If E_1 and E_2 are two nearby unperturbed energy levels of a molecule and E_a and E_b are the corresponding perturbed levels of E_1 and E_2 respectively, then

$$E_{a,b} = \frac{E_1 + E_2}{2} \pm \frac{1}{2}(4|W_{12}|^2 + \delta^2)^{\frac{1}{2}}, \qquad [3.29]$$

where $\delta = E_1 - E_2$, is the separation of the unperturbed levels and W_{12} is the matrix element of the perturbation function W, which is either an additional term in the potential energy or an operator due to the additional term in kinetic energy (Herzberg, 1950, p. 13). The shifts in the levels $E_a - E_1$ and $E_b - E_2$ are equal in magnitude and opposite in sign. Of the levels E_1 and E_2, the one lying at a higher energy will be shifted towards higher energies and the one lying at a lower energy will be shifted towards lower energy, i.e., if $E_1 > E_2$, then $E_a > E_1$ and $E_b < E_2$. Generally, the levels E_1 and E_2 belong to two different electronic states of the molecule.

Based on theoretical considerations, Kronig (1928) derived the following selection rules for the occurrence of perturbations between two energy levels.

(1) The rotational quantum number J must be same for both the levels, i.e.,

$$\Delta J = 0.$$

This is a rigorous rule and must be satisfied in all circumstances. In Hund's case (b) a further selection rule

$$\Delta N = 0, \pm 1$$

also holds.

(2) The selection rule for the resultant spin S of the two states is

$$\Delta S = 0, \pm 1,$$

which suggests that a singlet state can be perturbed by either a singlet or a triplet state. This selection rule is valid for Hund's case (a) as well as case (b). In case (a) additional selection rules

$$\Delta \Sigma = 0, \pm 1 \text{ and } \Delta \Omega = 0, \pm 1$$

apply.

(3) For the components of the orbital angular momentum along the internuclear axis of the two states the selection rule is

$$\Delta \Lambda = 0, \pm 1.$$

This rule is valid in all Hund's cases in which Λ is defined.

(4) Both the rotational levels should have the same parity, i.e., either positive or negative. In case of homonuclear diatomic molecules, both the levels must be either symmetric or anti-symmetric. From this rule, it also follows that, in case of homonuclear diatomic molecules, a gerade state cannot perturb an ungerade state and vice versa; perturbations can occur only between two gerade states or two ungerade states. According to the e and f labelling scheme of Brown et al. (1975) an e level cannot be perturbed by an f level and vice versa. In summary, these rules are represented as

$$+ \longleftrightarrow +, \quad - \longleftrightarrow -, \quad + \nleftrightarrow -,$$

$$s \longleftrightarrow s, \quad a \longleftrightarrow a, \quad s \nleftrightarrow a,$$

$$g \longleftrightarrow g, \quad u \nleftrightarrow u, \quad g \nleftrightarrow u,$$

and $e \longleftrightarrow e, \quad f \longleftrightarrow f, \quad e \nleftrightarrow f.$

These rules are as rigorous as the first one ($\Delta J=0$) and should always be satisfied.

These four are the most important and general selection rules to be fulfilled for perturbations to occur between two states. Lefebvre-Brion and Field (1986, p. 39) tabulated the selection rules for different types of perturbations that can occur between two states of a molecule.

According to Mulliken (1937), if $\Delta\Lambda = 0$, it is called a homogeneous perturbation and if $\Delta\Lambda = \pm 1$, it is a heterogeneous perturbation. In homogeneous perturbations, the matrix element is independent of the rotational quantum number J and the deviations due to perturbations do not become zero when J=0. Hence, it appears as if the entire vibrational level is shifted. For this reason, according to Dieke (1941), sometimes the homogeneous perturbation is called the vibrational perturbation and the other one is called the rotational perturbation.

The general behaviour of the deviations of the rotational lines in the neighborhood of the maximum perturbation as a function of rotational quantum number J is shown in Figure 11. Sometimes a heterogeneous perturbation in the initial rotational levels produces a shift in the vibrational level and appears as if it were a vibrational perturbation. The question whether it is a vibrational or rotational perturbation is decided depending on the points and magnitudes of perturbations in all the branches of a band.

The selection rules discussed above provide the conditions necessary for the occurrence of perturbations. Sometimes, even if all these conditions are fulfilled, still perturbations may not occur, if the overlap integral of the vibrational eigenfunctions is zero. Hence it can be said that an analogue of the Franck-Condon principle governs the occurrence of perturbations in addition to the above selection rules. In
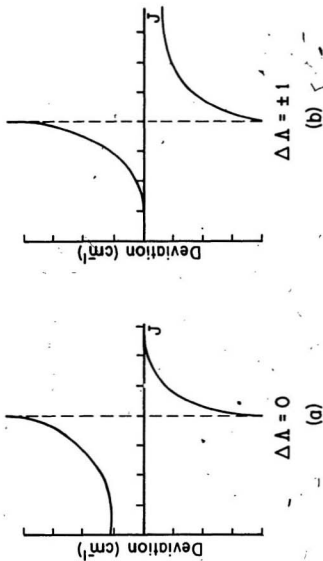
Figure 11. Behavior of the deviation in rotational lines due to perturbations as a function of the rotational quantum number J in case of (a) homogeneous perturbations for which $\Delta \Lambda = 0$ and (b) heterogeneous perturbations for which $\Delta \Lambda = \pm 1$.

other words, two vibrational levels, belonging to two different electronic states and having approximately the same energy, will influence each other strongly only if classically the system could go over from one state to the other without a large alteration of position and momentum. That means two vibrational levels interact with each other if they lie in the neighborhood of the intersections of the potential energy curves of the two electronic states and also all the Kronig's selection rules are fulfilled.

CHAPTER 4

HERZBERG $(C^1\Sigma^+ - A^1\Pi)$ SYSTEM OF $^{13}C^{18}O$

In this chapter, the first observation of the Herzberg band system of the $^{13}C^{18}O$ molecule is reported and its rotational analysis is presented. A review of the previous work on this system in $^{12}C^{16}O$ and other isotopically substituted carbon monoxide molecules, together with the experimental details pertinent to the present, is given in Section 4.1. In Section 4.2, the rotational structure of a $^1\Sigma^+ - ^1\Pi$ system is discussed. The results obtained from the analysis of the Herzberg system of $^{13}C^{18}O$ are presented in Section 4.3. Finally, the perturbations observed in the $A^1\Pi$ state and the information obtained on the perturbing states are discussed in Section 4.4.

4.1 Introduction

Herzberg (1929) observed eight bands of $^{12}C^{16}O$ in the region 3680-5710 Å and assigned them to the transition $^1\Delta - A^1\Pi$. Prior to this, Duffendack and Fox (1927) observed three of these bands and incorrectly assigned them to the Ångström $(B^1\Sigma^+ - A^1\Pi)$ band system because of the similarity in appearance. However, Asundi (1929) and Johnson and Asundi (1929) photographed the 0-1, 0-2, and 0-3 bands of the

Herzberg system under high resolution and correctly identified the transition as $C^1\Sigma^+ - A^1\Pi$ from their rotational analysis. Schmid and Gerö (1935 a,b) performed the rotational analysis of the 0-0, 0-1, 0-2, 0-3 and 0-4 bands and found evidence for the pre-dissociation in the upper state. No bands of this system with v' > 0 have ever been observed, but the existence of the level v = 1 of the $C^1\Sigma^+$ state was confirmed with the observation of the 1-0 band of the $C^1\Sigma^+ - X^1\Sigma^+$ system in absorption by Damany et al. (1966) and in electron scattering by Skerbele et al. (1966), both under low resolution. This was later reaffirmed by Tilford and Vanderslice (1968) with a high resolution study. Most of the details of the C-A system of CO are reviewed by Krupenie (1966).

Asundi et al. (1970) studied the isotope shifts of four band heads of the $^{13}C^{16}O$ molecule of the Herzberg system from the corresponding band heads of $^{12}C^{16}O$. Kepa (1969) did some preliminary work on the Herzberg bands of $^{12}C^{18}O$ and $^{13}C^{16}O$ and later did rotational analysis of seven 0-v" bands of $^{13}C^{16}O$ with v" = 0 to 6 and found perturbations in the 0-0, 0-1, and 0-6 bands (Kepa, 1978). Janjić et al. (1978) performed the rotational analysis of the corresponding seven bands in $^{12}C^{16}O$. Kepa (1982) analyzed the rotational structure of six 0-v" bands with v" = 0 to 5 in $^{14}C^{16}O$. The main results presented in this chapter on the Herzberg system of $^{13}C^{18}O$ have appeared already in a publication (Prasad et al., 1985).

The Herzberg band system of $^{13}C^{18}O$ was produced in the cathode glow of the discharge but not in the anode glow. The reason for this appears to be that neutral $^{13}C^{18}O$ molecules are excited to the high-lying $c^1\Sigma^+$ state when they collide with molecular ions $^{13}C^{18}O^+$ which are abundant in the cathode glow. In our initial experiments with $^{12}C^{16}O$ similar observations were also made. The bands of this system were photographed under medium dispersion in the first order of a 600 grooves/mm grating and also under high resolution in the third order of a 1200 grooves/mm grating on the Bausch and Lomb spectrograph. The reciprocal dispersions of the high resolution spectra vary from 0.99 Å/mm at 3860 Å to 0.69 Å/mm at 4880 Å. Kodak Spectrum Analysis No. 1 and 103a-O plates were used to photograph the spectra, and the exposure times were in the range of 10 to 60 minutes, depending on the intensity of the band. In general, the measurements of the spectral lines are accurate up to ~0.003 Å.

4.2 Rotational Structure of a $^1\Sigma^+ - ^1\Pi$ System

The rotational structure of a band belonging to a $^1\Sigma^+ - ^1\Pi$ system contains three branches, known as P, Q, and R, in accordance with the rotational selection rules,

$$\Delta J = -1 \quad (e \longrightarrow e)$$
$$\Delta J = 0 \quad (e \longrightarrow f)$$
$$\text{and} \quad \Delta J = +1 \quad (e \longrightarrow e), \text{ respectively.}$$

A schematic energy level diagram showing the P, Q, and R

branches of this transition is shown in Figure 12. The parity selection rule to be satisfied in this transition is

$$+ \longleftrightarrow -, \quad + \dashleftarrow \dashrightarrow +, \quad - \dashleftarrow \dashrightarrow - \; .$$

The term values of the rotational levels of the $^1\Sigma^+$ and $^1\Pi$ state are expressed, respectively, as

$$F_v(J) = B_v J(J+1) - D_v J^2(J+1)^2 + \ldots, \qquad [4.1]$$

and

$$F_v(J) = B_v[J(J+1) - 1] - D_v[J(J+1) - 1]^2 + \ldots, \qquad [4.2]$$

according to Eq. [3.8]. From the above equations, the expressions for the wavenumbers of the P(J), Q(J), and R(J) lines can be written, respectively, as

$$P(J) = \nu_0 + B_v' J(J-1) - D_v' J^2(J-1)^2$$
$$- B_v''[J(J+1) - 1] + D_v''[J(J+1) - 1]^2, \qquad [4.3]$$

$$Q(J) = \nu_0 + B_v' J(J+1) - D_v' J^2(J+1)^2$$
$$- B_v''[J(J+1) - 1] + D_v''[J(J+1) - 1]^2, \qquad [4.4]$$

$$R(J) = \nu_0 + B_v'(J+1)(J+2) - D_v'(J+1)^2(J+2)^2$$
$$- B_v''[J(J+1) - 1] + D_v''[J(J+1) - 1]^2, \qquad [4.5]$$

where ν_0 is the band origin. The wavenumbers of the rotational lines of the P, Q, and R branches were simultaneously fitted to the above expressions and the constants ν_0, B_v', D_v', B_v'', and D_v'' were obtained by the method of least-squares.
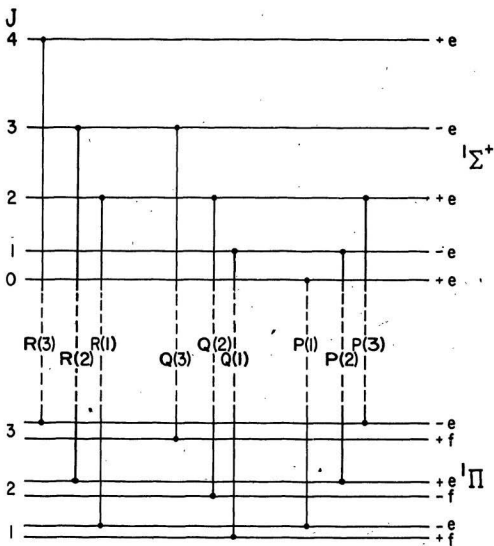
Figure 12. A schematic energy level diagram showing the first few rotational transitions in a band of a $^1\Sigma^+$ - $^1\Pi$ system.

4.3 Analysis of the Spectra

The assignment of vibrational quantum numbers to the Herzberg bands of $^{13}C^{18}O$ is straightforward. A photograph of these bands obtained under medium resolution is shown in Figure 13. When the cathode glow of the discharge was photographed in the region 3618-6165 Å, in addition to the Herzberg system, the Baldet-Johnson ($B^2\Sigma^+$ - $A^2\Pi_i$) system and the comet-tail ($A^2\Pi_i$ - $X^2\Sigma^+$) system of $^{13}C^{18}O^+$ were also observed on the photographic plates. The bands of all these three systems can be seen in Figure 13. Also seen in this figure are the Herzberg band system of $^{13}C^{16}O$ and the Ångström ($B^1\Sigma^+$ - $A^1\Pi$) band systems of the $^{13}C^{16}O$ and $^{13}C^{18}O$ molecules. The vacuum wavenumbers of the band heads of the Herzberg system, their relative intensities, and vibrational quantum numbers are listed in Table 4.1.

(i) Rotational Analysis

The rotational structures of the 0-2 and 0-3 bands of this system photographed under high resolution are shown as examples in Figures 14 and 15, respectively. The quantum numbers J and the vacuum wavenumbers of the spectral lines of the 0-1, 0-2, 0-3, 0-4, and 0-5 bands are listed in Tables 4.2 to 4.6, respectively. For every spectral line the $(\nu_{obs} - \nu_{calc})$ value is also given in parentheses, next to the ν_{obs} value, except for the perturbed lines and a very few unperturbed lines which are excluded from the analysis.

Figure 13. The emission band systems produced in the cathode glow of the hollow-cathode discharge tube by the excitation of the $^{13}C^{18}O$ molecules in the region 3615 - 6165 Å. (a) Baldet-Johnson ($B^2\Sigma^+ - A^2\Pi_i$) system of $^{13}C^{18}O^+$; (b) Herzberg ($C^1\Sigma^+ - A^1\Pi$) system of $^{13}C^{16}O$; (c) Herzberg ($C^1\Sigma^+ - A^1\Pi$) system of $^{13}C^{18}O$; (d) comet-tail ($A^2\Pi_i - X^2\Sigma^+$) system of $^{13}C^{18}O^+$; (e) Ångström ($B^1\Sigma^+ - A^1\Pi$) system of $^{13}C^{16}O$; and (f) Ångström ($B^1\Sigma^+ - A^1\Pi$) system of $^{13}C^{18}O$. This spectrum is photographed on Bausch and Lomb spectrograph in the first order of a 600 grooves/mm grating.
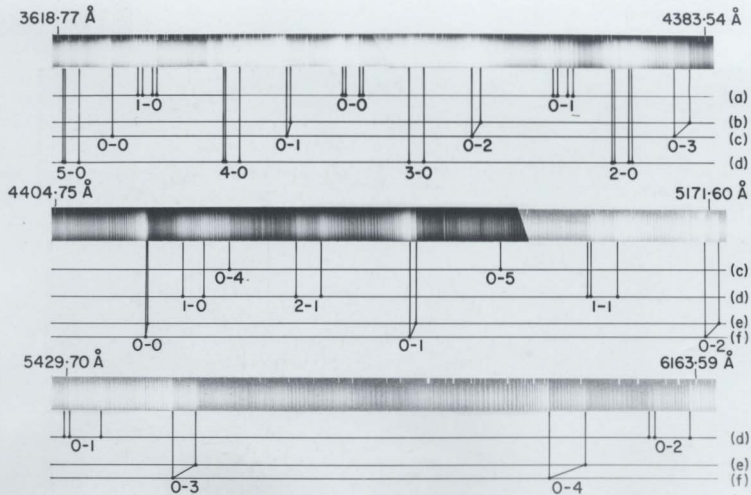
TABLE 4.1 Herzberg $(C^1\Sigma^+ - A^1\Pi)$ band system of the $^{13}C^{18}O$ molecule

Band Head (cm^{-1})	Band Origin[a] (cm^{-1})	Relative Intensity[b]	Assignment $v'-v''$
27147.8	27154.77 [c]	m	0-0
25735.0	25741.437(7)	s	0-1
24354.0	24359.716(8)	s	0-2
23002.8	23007.58(5)	m	0-3
21684.6	21689.555(6)	w	0-4
20397.8	20402.394(7)	vw	0-5

[a]Numbers in parentheses are the uncertainties in the last digit and correspond to one standard deviation.

[b]Abbreviations for relative intensities, s, m, w, and vw denote strong, medium, weak, and very weak respectively.

[c]Extrapolated from the origin of the 0-1 band and the value of the $\Delta G(1/2)$ of the $A^1\Pi$ state.

Figure 14. Rotational structure of the 0-2 band of the Herzberg
($C^1\Sigma^+$ – $A^1\Pi$) system of $^{13}C^{18}O$ photographed on the 2 m
Bausch and Lomb spectrograph in the third order of a
1200 grooves/mm grating.
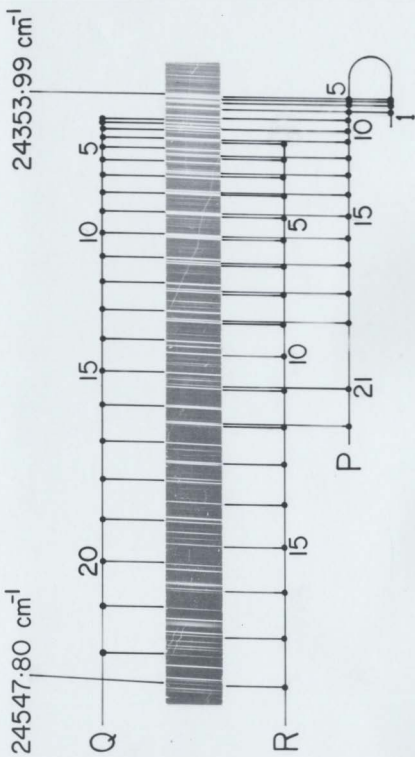
Figure 15. Rotational structure of the 0-3 band of the Herzberg $(C^1\Sigma^+ - A^1\Pi)$ system of $^{13}C^{18}O$ photographed on the 2 m Bausch and Lomb spectrograph in the third order of a 1200 grooves/mm grating.
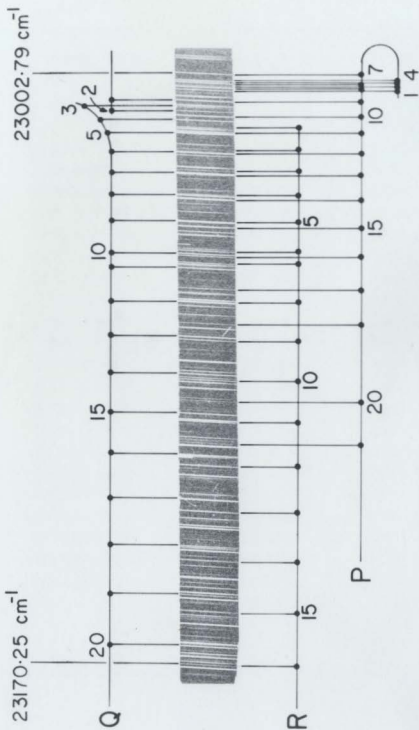
TABLE 4.2   Vacuum wavenumbers (in cm^{-1}) of the rotational lines of the 0-1 band

J	R(J)	Q(J)	P(J)
1	-	25743.60(0.07)	25739.99(0.00)
2	25755.45(0.00)	25744.87(0.02)	25737.79(0.01)
3	25761.06(0.10)	25746.85(0.02)	25736.26(0.04)
4	25767.11(-0.03)	25749.46(-0.01)	25735.27(-0.06)
5	25773.95(-0.02)	25752.74(-0.03)	25734.99(-0.11)
6	25781.48(0.02)	25756.72(0.00)	25735.50(-0.01)
7	25789.59(-0.02)	25761.34(0.00)	25736.59(-0.02)
8	25798.39(-0.02)	25766.62(0.00)	25738.35(-0.01)
9	25807.89(0.01)	25772.55(-0.01)	25740.78(0.01)
10	25817.97(-0.03)	25779.13(-0.03)	25743.85(0.01)
11	25828.78(0.00)	25786.41(-0.01)	25747.56(-0.01)
12	25840.23(0.01)	25794.34(0.00)	25751.97(0.00)
13	25852.31(-0.01)	25802.90(-0.01)	25757.01(-0.02)
14	25865.05(-0.03)	25812.19(0.04)	25762.74(-0.01)
15	25878.46(-0.03)	25822.02(-0.03)	25769.14(0.01)
16	25892.64(0.08)	25832.58(-0.03)	25776.17(0.00)
17	25907.22(-0.07)	25843.78(-0.05)	25783.89(0.01)
18	25922.70(0.03)	25855.68(-0.03)	25792.26(0.01)
19	25938.78(0.07)	25868.20(-0.05)	25801.33(0.05)
20	25955.39(-0.02)	25881.42(-0.03)	25810.96(-0.02)
21	25972.80(0.03)	25895.38(0.07)	25821.43(0.09)
22	25990.82(0.04)	25909.83(0.00)	25832.26(-0.10)
23		25924.96(-0.05)	25844.02(-0.03)
24		25940.89(0.04)	25856.38(-0.02)
25		25957.34(-0.01)	25869.42(0.00)

TABLE 4.3 Vacuum wavenumbers (in cm^{-1}) of the rotational lines of the 0-2 band

J	R(J)	Q(J)	P(J)
1	24368.88(-0.03)	24361.87(0.03)	24358.05[a]
2	24373.78(-0.06)	24363.26(0.02)	24356.13(-0.04)
3	24379.50(0.03)	24365.35(0.01)	24354.66(-0.07)
4	24385.85(0.05)	24368.14(0.01)	24353.99(-0.01)
5	24392.81(-0.01)	24371.65(0.03)	24353.99(0.03)
6	24400.59(0.05)	24375.84(0.02)	24354.66(0.04)
7	24408.98(0.01)	24380.62(-0.09)	24356.03(0.05)
8	24418.09(0.00)	24386.27(-0.03)	24358.05(0.01)
9	24427.93(0.03)	24392.54(-0.05)	24360.82(0.02)
10	24438.43(0.01)	24399.51(-0.07)	24364.28(0.01)
11	24449.65(0.01)	24407.26(-0.02)	24368.43(-0.01)
12	24461.57(0.02)	24415.63(-0.04)	24373.32(0.01)
13	24474.15(-0.02)	24424.74(-0.03)	24378.91(0.03)
14	24487.47(-0.02)	24434.55(-0.02)	24385.16(0.00)
15	24501.60(0.09)	24445.03(-0.04)	24392.15(0.00)
16	24516.25(0.02)	24456.25(-0.03)	24399.85(0.01)
17	24531.65(0.00)	24468.15(-0.04)	24408.27(0.03)
18	24547.80(0.03)	24480.74(-0.07)	24417.38(0.03)
19		24494.11(-0.02)	24427.24(0.08)
20		24508.16(0.00)	24437.69(0.00)
21		24522.88(-0.02)	24448.90(-0.03)
22		24538.37(0.02)	24461.03[a]

[a]Not used in the analysis.

TABLE 4.4　　Vacuum wavenumbers[a] (in cm^{-1}) of the rotational lines of the 0-3 band

J	R(J)	Q(J)	P(J)
1	23017.90	23010.39	23007.40
2	23023.87	23013.37	23006.29
3	23029.79	23011.93	23005.07
4	23036.57	23015.88	23004.75
5	23044.35	23019.57	23005.43
6	23052.39	23024.87	23006.61
7	23055.81	23030.61	23002.79
8	23066.67	23036.91	23006.61
9	23077.48	23044.13	23010.39
10	23088.72	23053.30	23014.59
11	23100.57	23057.31	23019.42
12	23113.13	23066.85	23024.87
13	23126.15	23076.62	23030.91
14	23140.19(-0.01)	23087.17	23037.87(-0.01)
15	23154.86(0.03)	23098.36(-0.05)	23045.53(0.04)
16	23170.25(0.06)	23110.24(-0.03)	23053.84(0.00)
17		23122.82(-0.04)	23062.94(0.01)
18		23136.20(0.02)	23072.76(0.00)
19		23150.25(0.02)	
20		23165.00(0.00)	23094.61(0.00)
21			23106.63(0.00)

[a]The $(\nu_{obs} - \nu_{calc})$ values are given in parentheses only for the unperturbed lines which are used in the analysis.

TABLE 4.5   Vacuum wavenumbers (in cm^{-1}) of the rotational lines of the 0-4 band

J	R(J)	Q(J)	P(J)
1	21698.71(-0.06)	21691.73(0.03)	
2	21703.90(0.04)	21693.29(0.03)	21686.14(-0.06)
3	21709.67(-0.06)	21695.54(-0.06)	21684.95(-0.05)
4	21716.36(-0.01)	21698.71(0.00)	21684.60(0.02)
5	21723.82(0.03)	21702.61(0.01)	21684.95(0.00)
6	21732.01(0.01)	21707.29(0.01)	21686.14(0.05)
7	21740.98(0.00)	21712.74(0.01)	21688.01(0.00)
8	21750.73(0.00)	21718.99(0.03)	21690.72(0.01)
9	21761.28(0.01)	21725.97(0.00)	21694.21(0.02)
10	21772.66(0.08)	21733.77(0.01)	21698.48(0.02)
11	21784.67(-0.01)	21742.33(0.00)	21703.50(0.00)
12	21797.55(0.00)	21751.67(-0.01)	21709.31(-0.02)
13	21811.21(0.01)	21761.79(-0.02)	21715.93(-0.01)
14	21825.61(-0.02)	21772.66(-0.06)	21723.34(0.01)
15	21840.95(0.12)	21784.41(0.00)	21732.51(0.00)
16	21856.81(-0.01)	21796.90(0.01)	21740.46(-0.01)
17	21873.58(-0.01)	21810.14(-0.01)	21750.21(0.00)
18	21891.12(-0.02)	21824.17(-0.01)	21760.74(0.00)
19	21909.45(-0.01)	21838.99(-0.02)	21772.10(0.04)
20	21928.59(0.02)	21854.60(-0.01)	21784.15(-0.01)
21	21948.51(0.05)	21870.98(-0.02)	21796.90(-0.14)
22		21888.17(-0.01)	21810.73(0.01)
23		21906.16(0.02)	21825.15(-0.03)
24			21840.49(0.05)
25		21944.39(-0.02)	21856.46(-0.02)
26			21873.32(0.01)

TABLE 4.6 Vacuum wavenumbers[a] (in cm^{-1}) of the rotational lines of the 0-5 band

J	R(J)	Q(J)	P(J)
1		20404.60(0.03)	
2	20416.78(-0.03)	20406.20(-0.02)	20399.15(0.00)
3	20422.84(0.03)	20408.69(0.01)	20398.08(0.00)
4	20429.59(-0.03)	20411.96(0.00)	20397.84(0.01)
5	20437.23(-0.03)	20416.07(0.01)	20398.40(0.00)
6	20445.73(0.02)	20421.00(0.01)	20399.79(-0.01)
7	20455.01(0.02)	20426.76(0.02)	20402.01(-0.01)
8	20465.08(-0.01)	20433.31(0.00)	20405.06(0.00)
9	20476.02(0.00)	20440.72(0.01)	20408.93(0.00)
10	20487.75(-0.02)	20448.93(-0.01)	20413.65(0.02)
11	20500.39(0.04)	20457.99(0.00)	20419.15(-0.01)
12	20513.76(0.00)	20467.88(0.01)	20425.51(0.00)
13	20527.92	20478.67	20432.66
14	20543.08	20490.42	20440.72
15	20559.06	20504.12	20449.67
16	20576.02	20514.43	20459.62
17	20594.69	20528.92	20471.25
18		20543.95	20478.67
19		20559.82	20491.47
20		20577.03	20505.02
21		20592.17	20518.90
22			20533.64

[a]The ($\nu_{obs} - \nu_{calc}$) values are given in parentheses only for the unperturbed lines which are used in the analysis.

These differences were obtained from the least-squares fits of the individual bands. In general, the standard deviation of such least-squares fits was found to be ~0.03 cm^{-1}.

The molecular constants obtained by merging those from the Ångström and Herzberg systems are presented in various tables of this chapter. The origins of the Herzberg bands are listed in Table 4.1. The rotational constants B_v and D_v for different vibrational levels of $A^1\Pi$, $B^1\Sigma^+$ and $C^1\Sigma^+$ are listed in Table 4.7. The D_0 value of the $A^1\Pi$ state could not be estimated because the wavenumber data of the 1-0 band of Ångström system, which are free from perturbations in the v" = 0 state are very limited. For the same reason, the 0-0 bands of the Ångström and Herzberg systems could not be rotationally analyzed. Table 4.8 contains the equilibrium molecular constants of the $A^1\Pi$ and $B^1\Sigma^+$ states. The values of B_e and α_e of states A and B derived from those of B_v listed in Table 4.7 are also given in Table 4.8. Using the B_e value, the equilibrium internuclear distance (r_e) and the moment of inertia (I_e) of these states were calculated and are listed in the same table. As only one vibrational level (v = 0) was observed in the $C^1\Sigma^+$ state, B_e and α_e could not be estimated for it. From the B_0 value, I_0 and r_0 were obtained and these values are also listed in Table 4.8.

TABLE 4.7   Rotational constants[a] (in cm^{-1}) for the A $^1\Pi$, B $^1\Sigma^+$, and C $^1\Sigma^+$ states of ^{13}C ^{18}O

Vibrational Level	A $^1\Pi$		B $^1\Sigma^+$		C $^1\Sigma^+$	
	B_v	$D_v \times 10^6$	B_v	$D_v \times 10^6$	B_v	$D_v \times 10^6$
0	1.4574(3)	_____[b]	1.7697(1)	5.8(2)	1.7665(1)	5.6(2)
1	1.4366(1)	5.8(2)	1.7473(2)	6.2(4)		
2	1.4173(2)	7.9(3)				
3	1.3931(3)	1.6(5)				
4	1.3772(1)	6.7(2)				
5	1.3561(2)	10.2(7)				

[a]Numbers in the parentheses are the uncertainties in the last digit and correspond to one standard deviation.

[b]Could not be estimated from the observed data.

TABLE 4.8 · Equilibrium molecular constants [a] (in cm^{-1}, unless stated otherwise) of A $^1\Pi$, B $^1\Sigma^+$, and C $^1\Sigma^+$ states of ^{13}C ^{18}O

Molecular Constant	A $^1\Pi$	B $^1\Sigma^+$	C $^1\Sigma^+$
T_e [b]	65075.7$_7$	86926.$_9$	
ω_e	1444.7$_1$(9)	2058.9$_0$	
$\omega_e x_e$	15.6$_0$(1)	35.9$_4$	
B_e	1.4667(2)	1.7811(2)	
α_e	0.01992(2)	0.0226(1)	
r_e (Å)	1.2339	1.1197	1.1243[c]
I_e (g.cm^2)	1.9086 x 10^{-39}	1.5717 x 10^{-39}	1.5847 x 10^{-39}[c]

[a] Numbers in the brackets are the uncertainties in the last digits and correspond to one standard deviation.

[b] Assumed to be same as that of the ^{12}C ^{16}O molecule.

[c] This value is for the v=0 level of the C $^1\Sigma^+$ state and is obtained from the B_0 value.

(ii) **Vibrational Analysis and Isotope Shifts**

The origins of the Herzberg bands listed in Table 4.1, and those of the Ångström bands of $^{13}C^{18}O$ (modified values taken from Prasad et al. (1984), using method of merging) were combined together in the vibrational analysis. The origins of the 0-1, 0-2, 0-4, and 0-5 bands of both systems and that of the 1-1 band of the Ångström system were simultaneously fitted to Eq. [3.6] to obtain a unique set of vibrational constants ω_e and $\omega_e x_e$ for the $A^1\Pi$ state which are given in Table 4.8. The origins of the 0-0 and 0-3 bands of both systems and also that of the 1-0 band of Ångström system were not included in the analysis because of perturbations in the v = 0 and 3 levels of the $A^1\Pi$ state.

The vibrational constants of states B and C could not be obtained directly from Eq. [3.6] because only two levels (v = 0 and 1) of B and one level (v = 0) of C were observed. For the C state, no vibrational constants could be obtained. However, the following indirect method was used to obtain values of ω_e and $\omega_e x_e$ for state B. The term values (T_e) of the A and B of $^{13}C^{18}O$ are assumed to be the same as those of $^{12}C^{16}O$ (which are given by Tilford and Simmons (1972) and Eidelsberg et al. (1987) for the A and B states, respectively) and are listed in Table 4.8. These term values, the vibrational constants of $A^1\Pi$, and the origins of the 0-1 and 1-1 bands of the Ångström (B - A) system of $^{13}C^{18}O$, were used in Eq. [3.6] to obtain the vibrational

constants ω_e and $\omega_e x_e$ of state B. The values thus derived are also listed in Table 4.8.

The band origins listed in Table 4.1 and those of the Ångström band system were used together to obtain the vibrational term values for all the observed levels with respect to the v = 0 level of the A state. These term values are listed in Table 4.9. Using the ω_e and $\omega_e x_e$ values of state A, listed in Table 4.8, the actual position of the v = 0 level from the minimum of its potential energy curve is calculated to be 718.43 cm^{-1}.

In order to obtain the isotope shifts ($\Delta\nu$) of the Herzberg bands of $^{13}C^{18}O$ from the corresponding bands of $^{12}C^{16}O$, the band origins of $^{12}C^{16}O$ were calculated from Eq. [3.6] using the vibrational constants of the C and A states, reported by Tilford and Vanderslice (1968) and Simmons et al. (1969), respectively. This was done because recent values for these origins are not readily available. The observed isotope shifts which correspond to the differences between the calculated band origins of $^{12}C^{16}O$ and those of the corresponding bands of $^{13}C^{18}O$, obtained in the present work and given in Table 4.1, are listed in Table 4.10. These isotope shifts were also calculated from Eq. [3.11] using vibrational constants of C and A states of $^{12}C^{16}O$ and the value of $\rho [=\mu^{\frac{1}{2}} (^{12}C^{16}O)/\mu^{\frac{1}{2}} (^{13}C^{18}O) = 0.9530]$ and are listed in the same table. The agreement between these and the observed values is very satisfactory.

TABLE 4.9   Vibrational term values[a] (in cm^{-1}) of the A $^1\Pi$, B $^1\Sigma^+$, and C $^1\Sigma^+$ states of $^{13}C\ ^{18}O$

Vibrational Level	A $^1\Pi$	B $^1\Sigma^+$	C $^1\Sigma^+$
0	0.0	22146.43(4)	27147.9(4)
1	1406.51(4)	24133.52(5)	
2	2788.17(4)		
3	4139.71(4)		
4	5458.41(4)		
5	6745.52(4)		

[a] The term values are expressed relative to the v=0 level of the A $^1\Pi$ state, which is at a height of 718.43 cm^{-1} from the minimum of its potential energy curve.

TABLE 4.10 Isotope shifts (in cm^{-1}) of the Herzberg bands of $^{13}C\ ^{18}O$

Band	Isotope Shift $\Delta\nu$ ($^{12}C\ ^{16}O - {}^{13}C\ ^{18}O$)	
	Observed	Calculated
0-0	+15.84	+15.56
0-1	-52.15	-52.49
0-2	-116.77	-117.40
0-3	-176.66	-179.18
0-4	-236.43	-237.82
0-5	-292.85	-293.35

4.4 Perturbations in the $A^1\Pi$ State of $^{13}C^{18}O$

According to Kronig's selection rules (see Section 3.4), a $^1\Pi$ state can be perturbed by either singlet or triplet Σ, Π, or Δ states. In this chapter, the perturbations caused by $^3\Sigma^+$ and $^3\Sigma^-$ states in a $^1\Pi$ state are of interest. Since a Σ state does not have Λ-type doubling, a given rotational level of a Σ state perturbs only one of the Λ-doublet components of the Π state, depending on its parity. Thus, the perturbations caused by a Σ^+ state are different from those caused by a Σ^- state. In general, if a singlet state is perturbed by a triplet state, maximum perturbation is expected at three different J values. In a $^1\Sigma^+ - ^1\Pi$ transition, the P and R lines occur between e levels only, whereas the Q lines arise between e and f levels (see Figure 12). Hence the perturbations in the P and R lines are similar, but different from those in the Q lines. Hence if a' $^1\Pi$ state is perturbed by a $^3\Sigma$ state, the three perturbations in the P and R branches on one hand and in the Q branch on the other, will be at different J values. Based on the parity considerations, it is established that any of the following two types of perturbations can occur in the increasing order of J in a band:

(i) Perturbations, first in the Q branch, then in the P and R branches, and finally in the Q branch again.

(ii) Perturbations, first in the P and R branches, then in the Q branch, and finally in the P and R branches again.

If the $^3\Sigma^+$ state causes one of these two types of perturbations, the $^3\Sigma^-$ state causes the other type of perturbation.

Among the five rotationally analyzed bands of the Herzberg system of $^{13}C^{18}O$, some irregularities in the rotational structure of the 0-3 and 0-5 bands are observed unlike in the structure of the 0-1, 0-2, and 0-4 bands. This indicates that there are no perturbations in the $C^1\Sigma^+$, $v = 0$ level and in the $A^1\Pi$, $v = 1$, 2, and 4 levels. From this, it is clear that the levels $A^1\Pi$, $v = 3$ and 5 are perturbed. The fact that no rotational analysis was possible for the 0-0 band because of its complexity indicates that the $v = 0$ level of $A^1\Pi$ is strongly perturbed. A recent study by LeFloch et al. (1987) indicates that the $v = 0$ level of this state in $^{12}C^{16}O$ was strongly perturbed by more than one electronic state. Similarly, the $v = 0$ level of state A in $^{13}C^{18}O$ might be perturbed by more than one electronic state.

Using the appropriate molecular constants listed in Tables 4.1 and 4.7 and Eqs. [4.3 to 4.5], the wavenumbers of P(J), Q(J), and R(J) of the 0-3 and 0-5 bands were calculated. The deviations of the observed wavenumbers of these spectral lines from the calculated ones are plotted against J, as shown in Figure 16. As explained above, the deviations in the P and R branches are found to be similar but different from those in the Q branch. In the 0-3 band, the perturbations are observed in the Q, P and R, and Q
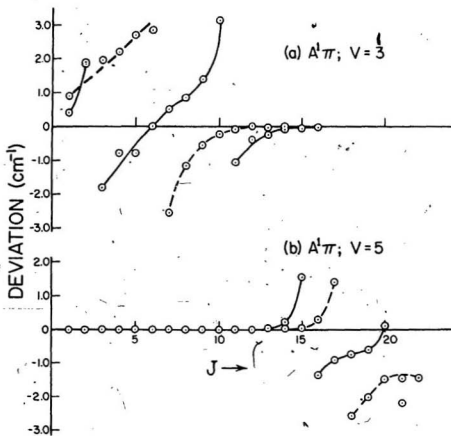
Figure 16. Plots of deviations ($\nu_{obs} - \nu_{calc}$) of the rotational lines versus the rotational quantum number J in (a) 0-3 and (b) 0-5 bands. The solid curves represent the deviations in the Q branch and the dashed curves represent those in the P and R branches.

branches at J=2, 6, and 10 respectively. As the P and Q branches are perturbed at different J values, this is not a $\Pi - \Pi$ or $\Pi - \Delta$ perturbation and is clearly a $\Pi-\Sigma$ perturbation. Finally, on the considerations of parity and proximity of the electronic states, it is concluded that the v = 3 level of $A^1\Pi$ state is perturbed by $a'^3\Sigma^+$ state. But, although the difference, $\Delta\Lambda$, between the perturbed and the perturbing states is +1, the perturbation curves are similar to those of the $\Delta\Lambda = 0$ perturbation (see Figure 11). This is due to a shift in the band origin. If the origin is shifted by approximately +1.0 cm^{-1}, the calculated wavenumbers increase by +1.0 cm^{-1} and hence the differences between the observed and calculated wavenumbers decrease by the same amount uniformly in all the branches. Then these curves look similar to the perturbation curves of $\Delta\Lambda = \pm 1$ (see Figure 11). Hence it is clear that the origin of the 0-3 band is shifted due to the perturbations in the initial rotational levels.

From the perturbation curves drawn for the 0-5 band (see Figure 16), it is seen that the maximum perturbations occur at J=15, 18, and 21 in Q, P and R, and Q branches, respectively. Hence, as in the case of the vibrational level v=3, the y=5 level of $A^1\Pi$ state is also found to be perturbed by the $a'^3\Sigma^+$ state. In this case, the perturbation curves are similar to those shown in Figure 11 for the case of $\Delta\Lambda = \pm 1$. As the initial rotational levels are not perturbed

in the v=5 level, no significant shift in the origin of the 0-5 band is observed. The perturbations observed in the 0-3 and 0-5 bands of this system are in excellent agreement with those observed in the corresponding bands of the Ångström system (Prasad et al., 1984). This agreement confirms the correctness of the assignments of the rotational quantum numbers in the 0-3 and 0-5 bands of both the systems.

The rotational constants B_v of the perturbing levels are obtained through a procedure described earlier by Coster and Brons (1934) and Herzberg (1950, P. 289). To obtain these B_v values, the rotational term values $F(J)$ of the perturbed levels v=3 and 5 of the $A^1\Pi$ state are plotted against J. The plot drawn for the v=5 level is shown in Figure 17. In this figure the points of maximum perturbation shown on the solid curve are indicated at J=15, 18, and 21. At these points, according to Kronig's selection rule (1), the perturbing state will also have the same J values. For a $^3\Sigma$ state, there are three levels with same J having N values equal to J-1, J, and J+1. The dashed curves in Figure 17 represent the energy curves for the components N = J-1, J, and J+1 of the $^3\Sigma$ state. From the energy curve of N=J in Figure 17, the rotational term values $F(J)$ for different J and hence the corresponding B_v value of the perturbing state are obtained. The accuracy of the B_v value thus obtained for the perturbing state is somewhat less than that of the corresponding B_v value of the $A^1\Pi$
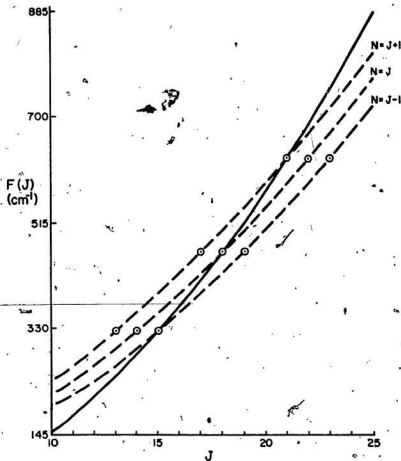
Figure 17. Crossing of the v=5 level of the $A^1\Pi$ state by the $a'^3\Sigma^+$ state causing perturbations at J = 15, 18, and 21.

state. The B_v values obtained for the levels perturbing
the v=3 and 5 levels of state A are listed in Table 4.11,
which are in good agreement with those obtained from the
Angstrom band system by Prasad et al (1984). The B_v values
obtained for the perturbing levels are smaller than those
of the perturbed levels in the $A^1\Pi$ state and hence only
those vibrational levels which are slightly above the
vibrational levels of the $A^1\Pi$ state can perturb the latter.

From B_v values of the perturbing states and the energy
values $(T_e + G(v) + F_v(J))$ of the perturbed levels at the
points of maximum perturbation, the positions of the perturbing
vibrational levels $(T_e + G(v))$ are calculated. These
$T_e + G(v)$ values of the perturbing levels belonging to the
$a'^3\Sigma^+$ and $e^3\Sigma^-$ states of the $^{13}C^{18}O$ molecule are also
calculated from the constants of $^{12}C^{16}O$ (Tilford and Simmons
1972), using the usual isotope relations. All these values
are listed in Table 4.11 and the agreement between them is
very satisfactory. It is found that the levels v=3 and 5
of $A^1\Pi$ are perturbed by the levels v=13 and 16 of $a'^3\Sigma^+$,
respectively. For the sake of completeness, the values of
B_v and $T_e + G(v)$ of the level (v = 1 of $e^3\Sigma^-$) perturbing
the $A^1\Pi$, v = 0 level, given by Prasad et al. (1984), are also
given in the same table. The vibrational levels of the
$a'^3\Sigma^+$, $A^1\Pi$, and $e^3\Sigma^-$ states indicating the perturbed regions
are shown in Figure 18.

TABLE 4.11 B_v and $(T_e + G(v))$ values of the perturbing levels of $e^3\Sigma^-$ and $a'^3\Sigma^+$ states of $^{13}C^{18}O$

Perturbed level of A $^1\Pi$	Perturbing level	$B_v{}^a$ (cm^{-1})	$T_e + G(v)$	
			Calculated from observed perturbations (cm^{-1})	Calculated from known constants[b] (cm^{-1})
v = 0	v = 1 of $e^3\Sigma^-$	1.074(7)	65816.58	65806.48
v = 3	v = 13 of $a'^3\Sigma^+$	1.009(9)	69956.05	69958.36
v = 5	v = 16 of $a'^3\Sigma^+$	0.996(3)	72669.85	72667.46

[a] Uncertainty in the last digit is indicated in parentheses and corresponds to one standard deviation.

[b] Taken from Tilford and Simmons (1972).
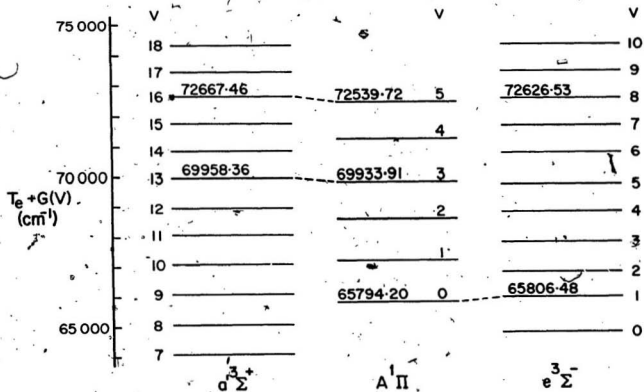
Figure 18. Relative positions of the vibrational levels of the $a'^3\Sigma^+$, $A^1\Pi$, and $e^3\Sigma^-$ states of $^{13}C^{18}O$.

From Figure 18, it is seen that the levels v=1, 2, and
4 of $A^1\Pi$ are not very close to the levels v=11, 12, and
15 of $a'^3\Sigma^+$ and also v=3, 4, and 7 of $e^3\Sigma^-$, respectively.
But these vibrational levels of the a' and e states may cause
perturbations in the v=1, 2, and 4 levels of state A at higher
rotational levels. As the hollow-cathode discharge tube used
in the present study was generally operated at low currents,
the rotational levels with J > 25 are not excited. Hence,
the perturbations are not observed in the v=1, 2, and 4
levels of $A^1\Pi$ state for J < 25. Though level v=8 of $e^3\Sigma^-$
is closer to v=5 of $A^1\Pi$ than v=16 of $a'^3\Sigma^+$, only the latter
is causing perturbations in the v=5 level. The reason for
this is that though the vibrational levels are closer, the
potential energy curve of the $e^3\Sigma^-$ state might not be
crossing the curve of $A^1\Pi$ in the proximity of the v=5 level
(see Herzberg 1950, p. 286). In the case of the $A^1\Pi$, v=0
level, as the perturbing level v=1 of $e^3\Sigma^-$ is very close
(the difference between them is only 12.28 cm^{-1}), the initial
rotational levels are strongly interacting, which could be
the reason for the complicated structure of the 0-0 bands
of the Herzberg and Ångström systems of $^{13}C^{18}O$.

CHAPTER 5

THIRD POSITIVE ($b^3\Sigma^+ - a^3\Pi_r$) SYSTEM OF CO: OBSERVATION OF THE v = 2 LEVEL OF $b^3\Sigma^+$ STATE

The third positive system ($b^3\Sigma^+ - a^3\Pi_r$) and three Kaplan bands (represented in the literature as $K - a^3\Pi_r$) of $^{12}C^{16}O$ are reinvestigated in the present work. In a reanalysis, the Kaplan bands and five newly observed bands are now assigned to the v" progressions with v'=2 and v"=0 to 3 and 5 to 8 of the third positive system. Also, the corresponding bands of $^{13}C^{18}O$ are observed and analyzed for the first time. The new vibrational assignments of the bands of $^{12}C^{16}O$ are confirmed from the calculated Franck-Condon factors and isotope data obtained from the bands of $^{13}C^{18}O$. The present work interprets the Kaplan bands of CO as a part of the third positive system, after their first observation in 1930. All these results which have appeared in a recent publication (Prasad et al., 1987) are presented in this chapter. The contributions made by earlier researchers to the third positive system and the Kaplan bands of CO are discussed in Section 5.1. The experimental details pertinent to this system are also briefly outlined in the same Section. The results obtained from the vibrational analysis of this system in the $^{12}C^{16}O$ and $^{13}C^{18}O$ molecules and also the

- 96 -

Franck-Condon factors of these bands in $^{12}C^{16}O$ are presented in Section 5.2. Finally, Section 5.3 is devoted to the discussion of the results presented in Section 5.2.

5.1 Introduction

The third positive system of $^{12}C^{16}O$ was first observed by Deslandres in 1888 (as quoted by Birge, 1926) and the vibrational quantum numbers were first assigned to these bands by Johnson (1926) who identified the lower state of these bands with the upper state of the Cameron bands, observed for the first time by Cameron (1926). Later, some controversy prevailed over the correct identification of the upper and lower states of the bands of the third positive system. Finally, Dieke and Mauchly (1932 and 1933) correctly identified the transition as $b^3\Sigma^+ - a^3\Pi_r$. Both the electronic states a and b are severely perturbed and these perturbations cause intensity fluctuations in the rotational lines and clustering of lines toward the tails. For a detailed review of the previous work on this system, the reader is referred to the review article by Krupenie (1966). Only the v" progressions with v'=0 and 1 were known for this system. Barrow et al. (1956) studied the intensities of the bands of this system and reported that the 2-0 band could not be observed even though it has sufficient intensity to appear according to the calculated Franck-Condon factors (FCFs). Kaplan (1930) reported three new bands of $^{12}C^{16}O$.

The rough measurements of these three bands photographed under low dispersion were 2518, 2630, and 2750 Å. Kaplan assigned them to a new system K-$a^3\Pi_r$ (see Krupenie, 1966) and suggested that the K state could be a metastable quintet state. The third positive system and the Kaplan bands were never observed in any of the isotopically substituted carbon monoxide molecules, prior to the present work on $^{13}C^{18}O$.

The emission spectra of $^{12}C^{16}O$ and $^{13}C^{18}O$ were excited separately in the hollow-cathode discharge tube described earlier (see Section 2.1). The Kaplan bands and the third positive system were excited better in the anode glow of the discharge. The spectra were photographed under medium dispersion on the 2 m Bausch and Lomb spectrograph in the first order of a 1200 grooves/mm grating. In the spectral region 2500-3830 Å, the reciprocal dispersion of the spectra is about 4.1 Å/mm. Maintaining the slit width at 20 μm, the spectra were photographed on Kodak Spectrum Analysis No. 1 plates with exposure times up to 30 minutes. The accuracy of the measurements is ~0.05 Å.

5.2 Analysis of the Spectra

The bands of the third positive system degraded to shorter wavelengths have multi-headed structure and in the present work for each band, only the sharp head formed at the longest wavelength is measured. The three Kaplan bands and the five new bands of $^{12}C^{16}O$ and $^{13}C^{18}O$ observed in the

spectral region 2500-3830 Å are now considered as a v'' progression with $v'=2$ of the third positive system. The spectrograms of the emission spectra of $^{12}C^{16}O$ and $^{13}C^{18}O$ photographed under medium dispersion in the region 2500-3360 Å are presented in Figure 19. The vacuum wavenumbers of the band heads of $^{12}C^{16}O$ and $^{13}C^{18}O$, their relative intensities, and the vibrational quantum numbers are listed in Table 5.1. The vibrational analyses for the bands of $^{12}C^{16}O$ and $^{13}C^{18}O$ listed in this table were carried out separately and the results are summarized in this Section.

(i) Third Positive System of $^{12}C^{16}O$

The three Kaplan bands of $^{12}C^{16}O$ are now assigned as 2-0, 2-1, and 2-2 bands of this system. The present measurements of the heads of these three bands at the longest wavelengths are 2524.49, 2638.07, and 2760.71 Å. The 2-3 band is the weakest of all the eight bands observed in this progression and the 2-4 band is too weak to be observed. The positions of the heads of the 2-5 and 2-8 bands do not fit well in the Deslandres scheme, probably due to the perturbations in the initial rotational lines. In their study of the Cameron ($a^3\Pi_r - X^1\Sigma^+$) band system of $^{12}C^{16}O$, Field et al. (1972) found that the vibrational levels v=5 and 8 of the $a^3\Pi_r$ state were perturbed at the initial rotational levels, which is in agreement with our observation.

Figure 19. A part of the third positive ($b^3\Sigma^+ - a^3\Pi_r$) system of the $^{12}C^{16}O$ and $^{13}C^{18}O$ molecules, in the region 2500 - 3360 Å, photographed on Bausch and Lomb spectrograph in the first order of a 1200 grooves/mm grating.
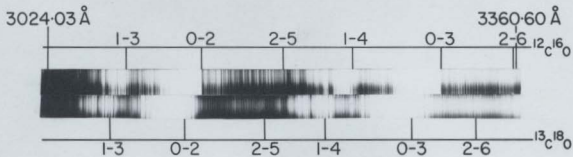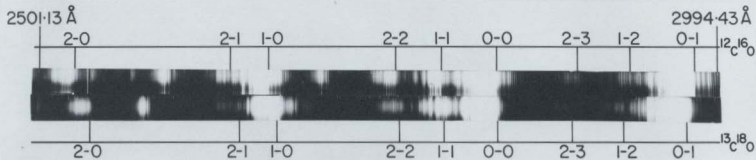
TABLE 5.1 Third positive system of the ^{12}C ^{16}O and ^{13}C ^{18}O molecules

Band Heads (cm^{-1})		Relative Intensity[a]	Assignment $v' - v''$
^{12}C ^{16}O	^{13}C ^{18}O		
39600.0	39400.1	s	2-0
37895.3	37768.0	w	2-1
37503.3	37386.1	vs	1-0
36211.9	36169.8	m	2-2
35792.8	35759.9	m	1-1
35287.3	35273.3	s	0-0
34560.9	34588.0	vw	2-3
34111.3	34156.7	vw	1-2
33576.7	33645.2	vs	0-1
32459.0	32576.3	m	1-3
31895.2	32037.8	vs	0-2
31308.6	31441.0	w	2-5
30834.9	31022.9	m	1-4
30242.6	30460.8	s	0-3
29769.3	30006.4	w	2-6
29238.1	29494.9	m	1-5
28618.0	28908.9	m	0-4
28231.8	28530.0	w	2-7
27672.6	27996.0	m	1-6
27022.8	27379.5	w	0-5
26700.9	27103.7	w	2-8
26135.6	26522.1	w	1-7

[a] Abbreviations for relative intensities vs, s, m, w, and vw denote very strong, strong, medium, weak, and very weak respectively.

Excluding the wavenumbers of the band heads of the 2-5 and 2-8 bands, the band head data of all the remaining twenty bands were used to obtain the vibrational constants of the $b^3\Sigma^+$ and $a^3\Pi_r$ states and the system origin simultaneously. The vacuum wavenumbers of these band heads were fitted to Eq. [3.6] and the derived molecular constants are listed in Table 5.2. The values obtained for ω_e and $\omega_e x_e$ of the $a^3\Pi_r$ state of $^{12}C^{16}O$ in the present work are very close to the deperturbed vibrational constants obtained from the analysis of the Cameron band system by Field et al. (1972). The value of $\omega_e x_e$ for the $b^3\Sigma^+$ state (see Table 5.2) obtained in this analysis may appear rather large. This can be understood from the fact that $b^3\Sigma^+$ is a high-lying state and its vibrational levels are close to the dissociation limit (see Section 5.3). In view of this, it is believed that the potential energy curve of $b^3\Sigma^+$ state may show large anharmonicity.

(ii) Franck-Condon Factors

In an attempt to study the intensities of the bands belonging to the third positive system of $^{12}C^{16}O$, the FCFs' for all the bands of this system are calculated according to the theory discussed in Section 3.2. A computer program prepared by Jarmain and McCallum (1970) was modified to operate on a VAX 11/785 computer and then used to calculate the FCFs. The vibrational constants ω_e and $\omega_e x_e$ listed in

TABLE 5.2   Vibrational constants for the $a^3\Pi_r$ and $b^3\Sigma^+$ states of the $^{12}C\ ^{16}O$ and $^{13}C\ ^{18}O$ molecules

Vibrational Constant (cm^{-1})	$^{12}C\ ^{16}O$		$^{13}C\ ^{18}O$	
	$a^3\Pi_r$	$b^3\Sigma^+$	$a^3\Pi_r$	$b^3\Sigma^+$
ν_e (system origin)	$34999.7_9 \pm 1.6$		$35000.3_1 \pm 2.0$	
ω_e	$1738.2_6 \pm 0.6$	$2333.9_0 \pm 2.1$	$1655.2_9 \pm 0.7$	$2220.0_9 \pm 2.6$
			1656.5^a	2224.2^a
$\omega_e x_e$	$14.2_5 \pm 0.1$	$58.6_4 \pm 0.7$	$12.8_2 \pm 0.1$	$52.1_0 \pm 0.8$
			12.9^a	53.3^a

[a] These are the vibrational constants of the electronic states of $^{13}C\ ^{18}O$ calculated from the corresponding values of the $^{12}C\ ^{16}O$ molecule using the isotope relations.

Table 5.2 and the rotational constants B_e and α_e listed by
Huber and Herzberg (1979) for the $b^3\Sigma^+$ state of $^{12}C^{16}O$ and
the deperturbed molecular constants reported by Field et
al. (1972) for the $a^3\Pi_r$ state of $^{12}C^{16}O$ were used to calculate
the FCFs. The values of FCFs for all the bands relative to
that of the 0-0 band are listed in Table 5.3. In general,
the relative intensities quoted in Table 5.1 are qualitatively
in good agreement with the FCFs listed in Table 5.3. Very
small values obtained for the FCFs of the 2-3 and 2-4 bands
provide the explanation for the weakness of the 2-3 band
and the absence of the 2-4 band. Thus the agreement between
the relative intensities of the bands and their FCFs confirms
not only the correctness of the vibrational quantum numbers
assigned to the bands but also the existence of the v=2
level in the $b^3\Sigma^+$ state. The FCFs calculated in the present
work are more accurate than the ones reported earlier by
Barrow et al. (1956) and Ortenberg (1964), who used the
molecular constants available at that time in their
calculations.

(iii) Third Positive System of $^{13}C^{18}O$

In view of the similarity of the spectra of $^{12}C^{16}O$ and
$^{13}C^{18}O$, the assignment of the vibrational quantum numbers
to the bands of $^{13}C^{18}O$ is straightforward. As the commercial
sample of $^{13}C^{18}O$ contains some traces of ^{12}C and ^{16}O, some
of the band heads of $^{13}C^{18}O$ are slightly overlapped by those

TABLE 5.3 Franck-Condon factors for the third positive system of $^{12}C\,^{16}O$

v' \ v''	0	1	2	3	4	5	6	7	8
0	1.00[a]	1.42	1.19	0.76	0.40	0.19			
1	2.04	0.33	0.07	0.53	0.74	0.62	0.40	0.21	
2	1.53	0.50	0.79	0.11	0.07	0.40	0.56	0.49	0.33

[a]The FCFs listed here are relative to that of the 0-0 band. The actual value of FCF obtained for the 0-0 band is 0.20.

of $^{13}C^{16}O$, $^{12}C^{18}O$, and $^{12}C^{16}O$, and hence, in general, the accuracy of the measurements is slightly less for the bands of $^{13}C^{18}O$. The vacuum wavenumbers of the band heads are listed in Table 5.1. Just as for the case of $^{12}C^{16}O$, the positions of the 2-5 and 2-8 bands of $^{13}C^{18}O$ were not used in obtaining the vibrational constants. The vacuum wavenumbers of heads of all the remaining 20 bands were fitted to Eq. [3.6] and the derived constants are listed in Table 5.2. The vibrational constants ω_e and $\omega_e x_e$ for the b and a states of $^{13}C^{18}O$ are also calculated from those of $^{12}C^{16}O$ using the standard isotopic relations $\omega_e^i = \rho \omega_e$, $\omega_e^i x_e^i = \rho^2 \omega_e x_e$, and ρ as quoted in Chapter 4 [Section 4.3(ii)] and are listed in the same table. These calculated values are in good agreement with those obtained directly.

(iv) Isotope Shifts

The observed isotope shifts ($\Delta \nu$) of the bands of the third positive system of $^{13}C^{18}O$ from the corresponding bands of $^{12}C^{16}O$ are obtained as the differences between the wavenumbers of the measured band heads, i.e., $[\nu(^{12}C^{16}O) - \nu(^{13}C^{18}O)]$ (Table 5.1) and listed in Table 5.4. The calculated isotope shifts, using the molecular constants of $^{12}C^{16}O$ (Table 5.2), ρ as quoted in Section 4.3(ii) and Eq. [3.11] are also listed in the same table. The agreement between them is good except for the perturbed 2-5 and 2-8 bands.

TABLE 5.4 Isotope shifts (in cm^{-1}) in the third positive system of ^{13}C ^{18}O

Band	Isotope Shift $\Delta\nu$ (^{12}C ^{16}O – ^{13}C ^{18}O)	
	Observed	Calculated
2-0	+199.9	+200.1
2-1	+127.3	+121.0
1-0	+117.2	+111.9
2-2	+42.1	+44.5
1-1	+32.9	+32.8
0-0	+14.0	+13.0
2-3	-27.1	-29.3
1-2	-45.4	-43.7
0-1	-68.5	-66.1
1-3	-117.3	-117.5
0-2	-142.6	-142.6
2-5[a]	-132.4	-169.2
1-4	-188.0	-188.8
0-3	-218.2	-216.5
2-6	-237.1	-235.3
1-5	-256.8	-257.4
0-4	-290.9	-287.7
2-7	-298.2	-298.7
1-6	-323.4	-323.4
0-5	-356.7	-356.4
2-8[a]	-402.8	-359.5
1-7	-386.5	-389.9

[a]The large discrepancy between the observed and calculated isotope shifts may be due to perturbations in the initial rotational levels.

5.3 Discussion

The results presented in the previous section clearly show the occurrence of the v=2 level of the $b^3\Sigma^+$ state in both $^{12}C^{16}O$ and $^{13}C^{18}O$. The term value T_e of $b^3\Sigma^+$ of $^{12}C^{16}O$ is obtained as 83686.5 cm^{-1} from the sum of the system origin, ν_e = 34999.8 cm^{-1} (see Table 5.2) and the term value T_e = 48686.7 cm^{-1} of $a^3\Pi_r$ (Huber and Herzberg, 1979). The vibrational levels v=0, 1, and 2 of the $b^3\Sigma^+$ state of $^{12}C^{16}O$ are found to be situated at 84838.8, 87055.4, and 89154.8 cm^{-1}, respectively, with respect to the minimum of the potential energy curve of $X^1\Sigma^+$. This indicates that the v=2 level of the b state is clearly lying below the dissociation limit $D_0^0 \approx 89460$ cm^{-1} (i.e., $D^e = 90542$ cm^{-1}), reported by Brewer and Searcy (1956).

The dissociation energy of the CO molecule has a long controversial history with a variety of values ranging from 55822 to 89608 cm^{-1} and the earlier work is reviewed by Gaydon (1968). The values for the dissociation energy $D_0^0(CO)$ below 88262 cm^{-1} ($\approx$10.94 eV) are generally considered as "low" and those above this value as "high" in the literature. Douglas and Møller (1955) reported a value of 89595 ± 30 cm^{-1} for the dissociation limit from a study of the predissociation in the $B^1\Sigma^+$ state of $^{12}C^{16}O$ and $^{13}C^{16}O$. Recently, Eidelsberg et al. (1987) reported a value of D_0^0 = 89592 cm^{-1} (D^e = 90674 ± 15 cm^{-1}) for the dissociation limit from a study of the predissociation in state B of $^{12}C^{16}O$, $^{13}C^{16}O$, and

$^{13}C^{18}O$ from a study of the B-X system. Brewer and Searcy (1956) reported a value of 89460 ± 150 cm^{-1} from the experiments on effusion from a Knudsen cell. The works reported, Douglas and Møller (1955), Brewer and Searcy (1956), and Gaydon (1968) resolved this question in favor of the "high" value with some minor inconsistencies. Krupenie (1966) considers the value reported by Brewer and Searcy, (1956) as the best value for the dissociation limit, but Huber and Herzberg (1979) listed the value reported by Douglas and Møller (1955). The only spectroscopic evidence supporting a "lower" value for the dissociation limit, ≤88262 cm^{-1} (see Barrow et al., 1956) was the absence of bands with v'=2 in the third positive system ($b^3\Sigma^+ - a^3\Pi_r$). But the present work firmly establishes the existence of the v=2 level of $b^3\Sigma^+$ and hence provides strong evidence in favor of the "high" value for the dissociation limit, and the arguments in favor of the "lower" value are no longer valid. Since the first observation of Kaplan bands in 1930, no further work has ever been reported on these bands and the nature of the so-called K state is unresolved. In the present investigation with the observation of new bands of $^{12}C^{16}O$ and $^{13}C^{18}O$, calculation of Franck-Condon factors and identifying satisfactory isotope shifts, it is firmly established that the Kaplan bands form a part of the third positive system of CO. Thus, the problem which remained unsolved for nearly 60 years is solved in the present work.

CHAPTER 6

BALDET–JOHNSON ($B^2\Sigma^+ - A^2\Pi_i$) SYSTEM OF $^{13}C^{18}O^+$

The results of the rotational analysis of the 1-0, 0-0, and 0-1 bands of the Baldet–Johnson ($B^2\Sigma^+ - A^2\Pi_i$) system of $^{13}C^{18}O^+$, observed for the first time in the present work, are presented in this chapter. The previous work done on the corresponding band systems of $^{12}C^{16}O^+$ and other isotopically substituted CO^+ molecules is reviewed in Section 6.1. A brief description of the experimental details pertinent to the present work is included in the same section. The general appearance of the rotational structure of a band of a $^2\Sigma^+ - ^2\Pi_i$ transition is discussed in Section 6.2. Finally, the rotational analysis of the three bands of the Baldet-Johnson system of $^{13}C^{18}O^+$ and the molecular constants obtained from it are presented in Section 6.3.

6.1 Introduction

Three bands of the $B^2\Sigma^+ - A^2\Pi$ system of $^{12}C^{16}O^+$ were first observed by Baldet (1924, 1925a) and these bands plus three additional bands of this system were also observed by Johnson (1925). Bulthuis (1934) reported the rotational analysis of two bands of Baldet-Johnson system. In these

- 111 -

earlier studies, state A was considered to be a regular Π state. However, Rao (1950a) who performed a detailed rotational analysis of the comet-tail ($A^2\Pi - X^2\Sigma^+$) system of $^{12}C^{16}O^+$ and Rao and Sarma (1953) who did rotational analysis of the Baldet-Johnson system of the same ion concluded that state A is an inverted doublet Π (i.e., Π_i) state and revised the earlier vibrational numbering by lowering the v values of state A by three units. It should be noted that Rao (1950b) also did the rotational analysis of the first negative ($B^2\Sigma^+ - X^2\Sigma^+$) system of $^{12}C^{16}O^+$. The new vibrational numbering in state A was confirmed by Asundi et al. (1970) and Dhumwad et al. (1979) from the isotope shifts of the bands of the comet-tail system and the Baldet-Johnson system of $^{13}C^{16}O^+$ and $^{12}C^{18}O^+$, respectively, from the corresponding bands of $^{12}C^{16}O^+$. Recently, Jakubek et al. (1987) reinvestigated the rotational structure of the 1-0, 0-0, and 0-1 bands of the Baldet-Johnson system of $^{12}C^{16}O^+$ and reported the rotational constants for states A and B. Čonkić et al. (1978) analyzed some bands of this system in $^{12}C^{18}O^+$ and $^{13}C^{16}O^+$ but Brown et al. (1983) consider that the results of Čonkić et al. (1978) are questionable. Jakubek et al. (1986) performed the rotational analysis of the 1-0, 0-0, and 0-1 bands of this system in the $^{14}C^{16}O^+$ molecule.

In the present work the 1-0, 0-0, and 0-1 bands of the Baldet-Johnson system of $^{13}C^{18}O^+$ were observed and their rotational structures were analyzed for the first time.

These bands were excited in the cathode glow of a hollow-cathode discharge (see Section 2.1) and photographed under medium dispersion in the first order of a 600 grooves/mm grating on the Bausch and Lomb spectrograph and under high resolution in the third order of a 1200 grooves/mm grating on the Jarrell-Ash spectrograph. The exposure times for the high resolution spectra were 1 hour for the strong 1-0 and 0-0 bands and 2 hours for the 0-1 band. Kodak Spectrum Analysis No. 1 plates were used and the slit width was maintained at 30 μm on the Jarrell-Ash spectrograph. The reciprocal dispersion of the spectra is about 0.58 Å/mm at 3960 Å. In general, the measurements of the spectral lines are accurate up to ~0.003 Å.

6.2 Rotational Structure of a $^2\Sigma^+ - ^2\Pi_i$ System

If the spin-orbit coupling constant A (see Section 3.1(i)) of a $^2\Pi$ state is negative and large in magnitude, then the state is called an inverted state and belongs to Hund's case (a). Normally a $^2\Sigma$ state belongs to Hund's case (b) and hence $^2\Sigma^+ - ^2\Pi_i$ represents a mixed case transition. The rotational structure of such a system contains twelve different branches. A schematic energy level diagram showing all the twelve branches is given in Figure 20. The selection rules to be satisfied in this transition are
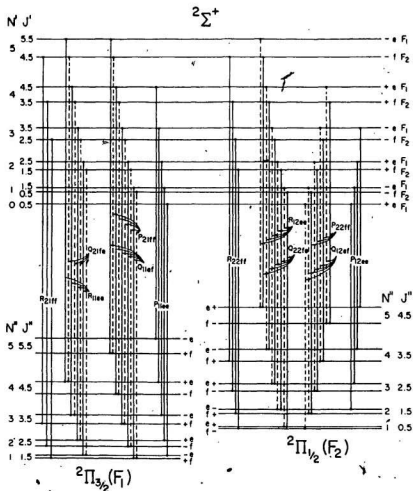
Figure 20. A schematic energy level diagram showing the first few rotational transitions of all the twelve branches of a band of a $^2\Sigma^+ - {}^2\Pi_i$ system.

$$\Delta J = 0, \quad e \longleftrightarrow f,$$

$$\Delta J = \pm 1, \quad e \longleftrightarrow e, \quad f \longleftrightarrow f$$

$$+ \longleftrightarrow -, \quad + \;/\!\!/\!\!+\; +, \quad - \;/\!\!/\; -$$

The twelve different branches of this system are identified as P_{12ee}, P_{22ff}, Q_{12ef}, Q_{22fe}, R_{12ee}, R_{22ff}, P_{11ee}, P_{21ff}, Q_{11ef}, Q_{21fe}, R_{11ee} and R_{21ff}. If the bands of this system degrade to shorter wavelengths, as in the Baldet-Johnson system, then the P_{12ee}, Q_{12ef}, P_{11ee} and Q_{11ef} branches form four different heads in the rotational structure of a band. In some instances, all these four heads can be clearly seen even under medium resolution (for example, see Baldet-Johnson bands of $^{13}C^{18}O^{+}$ in figure 13).

The rotational levels of a $^2\Sigma^+$ state in Hund's case (b) are given by

$$F_{1e}(N) = B_v N(N+1) - D_v N^2 (N+1)^2 + \tfrac{1}{2}\gamma_v N, \qquad [6.1]$$

and

$$F_{2f}(N) = B_v N(N+1) - D_v N^2 (N+1)^2 - \tfrac{1}{2}\gamma_v (N+1), \qquad [6.2]$$

where $F_{1e}(N)$ and $F_{2f}(N)$ refer to the components with $J = N+1/2$ and $N-1/2$, respectively, and γ_v is the spin-splitting constant. In terms of J, $F_{1e}(N)$ and $F_{2f}(N)$ can be written as

$$F_{1e}(J) = B_v (J-\tfrac{1}{2})(J+\tfrac{1}{2}) - D_v (J-\tfrac{1}{2})^2 (J+\tfrac{1}{2})^2 + \tfrac{1}{2}\gamma_v (J-\tfrac{1}{2}), \qquad [6.3]$$

and

$$F_{2f}(J) = B_v (J+\tfrac{1}{2})(J+\tfrac{3}{2}) - D_v (J+\tfrac{1}{2})^2 (J+\tfrac{3}{2})^2 - \tfrac{1}{2}\gamma_v (J+\tfrac{3}{2}). \qquad [6.4]$$

In a $^2\Pi_i$ state, a series of rotational levels exists for each of the sub-states $^2\Pi_{1/2}$ (J=0.5, 1.5,...) and $^2\Pi_{3/2}$ (J=1.5, 2.5,...) with the levels of $^2\Pi_{3/2}$ having lower energy than the corresponding levels of $^2\Pi_{1/2}$. Hence the $^2\Pi_{3/2}$ levels are called the F_1 levels and the other ones are called the F_2 levels. In both $^2\Pi_{1/2}$ and $^2\Pi_{3/2}$, the rotational levels are doubly degenerate due to the Λ-doubling which is larger in $^2\Pi_{1/2}$ than in $^2\Pi_{3/2}$. All these four types of rotational levels can be represented by the following expressions:

$$^2\Pi_{3/2} : F_{1e}(J) = B_V[J(J+1)-1.75] - D_V[J(J+1)-1.75]^2$$
$$+ \tfrac{1}{2}\left[\frac{p_V B_V^2}{A_V^2} + \frac{2q_V B_V}{A_V}\right](J-\tfrac{1}{2})(J+\tfrac{1}{2})(J+\tfrac{3}{2})$$
$$+ \tfrac{1}{2} A_V + \tfrac{1}{2} A_{DV}[J(J+1) - 1.75], \qquad [6.5]$$

$$F_{1f}(J) = B_V[J(J+1)-1.75] - D_V[J(J+1)-1.75]^2$$
$$- \tfrac{1}{2}\left[\frac{p_V B_V^2}{A_V^2} + \frac{2q_V B_V}{A_V}\right](J-\tfrac{1}{2})(J+\tfrac{1}{2})(J+\tfrac{3}{2})$$
$$+ \tfrac{1}{2} A_V + \tfrac{1}{2} A_{DV}[J(J+1)-1.75], \qquad [6.6]$$

$$^2\Pi_{1/2} : F_{2e}(J) = B_V[J(J+1)+0.25] - D_V[J(J+1)+0.25]^2$$
$$+ \tfrac{1}{2}p_V(J+0.5)-\tfrac{1}{2}A_V-\tfrac{1}{2}A_{DV}[J(J+1)+0.25], \qquad [6.7]$$

$$F_{2f}(J) = B_V[J(J+1)+0.25] - D_V[J(J+1)+0.25]^2$$
$$- \tfrac{1}{2}p_V(J+0.5)-\tfrac{1}{2}A_V-\tfrac{1}{2}A_{DV}[J(J+1)+0.25]. \qquad [6.8]$$

In the above equations p_V and q_V are the Λ-doubling parameters (see Mulliken and Christy, 1931), A_V is the spin-orbit coupling constant (see Section 3.1(i)) and is the

centrifugal distortion parameter of the spin-orbit coupling constant. The expressions for the twelve branches of the $^2\Sigma^+ - ^2\Pi_i$ system can be obtained from Eqs. [6.3] to [6.8] according to the general expression

$$\nu = (T'_{v\Sigma} - T''_{v\Pi}) + F_\Sigma{}'(J') - F_\Pi{}''(J''), \qquad [6.9]$$

with $J'' = J$. In this equation $T_{v\Sigma}$ is the term value of the vibrational level of the $^2\Sigma^+$ state and $T_{v\Pi}$ is the average term value of the vibrational levels $T_{v\Pi(3/2)}$ and $T_{v\Pi(1/2)}$ of the $^2\Pi$ state (all with respect to the minimum of the ground state potential energy curve). A band of this system has two origins, one for each of the $^2\Sigma^+ - ^2\Pi_{1/2}$ and $^2\Sigma^+ - ^2\Pi_{3/2}$ sub-bands. In the present work, instead of the two origins only the $(T_v{}'-T_v{}'')$ value is determined. If necessary, the two origins can be calculated from $(T_v{}'-T_v{}'') \pm (1/2)A_v$.

6.3 Analysis of the Spectra

The 1-0, 0-0, and 0-1 bands of Baldet-Johnson system of $^{13}C^{18}O^+$, photographed under medium dispersion are shown in Figure 13 in which all the four possible heads (P_{12ee}, Q_{12ef}, P_{11ee} and Q_{11ef}) are clearly seen for all the bands. The vacuum wavenumbers of the band heads, relative intensities, and vibrational quantum numbers are listed in Table 6.1 for all the three bands.

TABLE 6.1   Baldet-Johnson ($B^2\Sigma^+ - A^2\Pi_i$) band system of the ^{13}C $^{18}O^+$ molecule

Band Head[a] (cm^{-1})	$T_v{}' - T_v{}''$[b] (cm^{-1})	Relative[c] Intensity	Assignment $v' - v''$
26728.11	26825.265(6)	w	1-0
26759.84		s	
26860.09		m	
26885.61		s	
25130.32	25222.567(4)	m	0-0
25157.65		s	
25260.60		s	
25283.18		s	
23669.41	23758.512(5)	w	0-1
23694.06		m	
23798.70		m	
23819.36		s	

[a]The four heads identified for each band are formed by P_{12ee}, Q_{12ef}, P_{11ee}, and Q_{11ef} branches in the order of increasing wavenumber.

[b]The number in the parentheses indicates the uncertainty in the last digit and corresponds to one standard deviation.

[c]Abbreviations for relative intensities, s, m, and w represent strong, medium, and weak, respectively.

(i) Rotational Analysis

The rotational structure of the 0-1 band of this system photographed under high resolution on the Jarrell-Ash spectrograph is shown in Figure 21. In this figure, all the twelve branches that are expected in the rotational structure of a band of this system can be clearly seen. The rotational quantum numbers and the vacuum wavenumbers of the spectral lines of the 1-0, 0-0, and 0-1 bands are listed in Tables 6.2, 6.3, and 6.4, respectively. The vacuum wavenumbers of the spectral lines of all the branches were simultaneously fitted to the expressions of their respective branches [Eq. 6.9] and the molecular constants were estimated by the method of least-squares. For every spectral line, except for the ones not included in the analysis, the $(\nu_{obs} - \nu_{calc})$ value is given in parentheses. These differences were obtained from the least-squares fits of the individual bands. In general, the standard deviation of such a least-squares fit is found to be ~0.04 cm^{-1}.

The molecular constants obtained from the analysis of the individual bands were merged together. The $T_v' - T_v''$ values obtained from the merging are listed in Table 6.1. The rotational constants B_v, D_v, A_v, A_{Dv}, p_v and q_v of state A and B_v, D_v, and τ_v of state B for different vibrational levels are listed in Table 6.5. The values of B_e and α_e of states A and B were not calculated from the B_v values listed in this table. As the lower state of this system,

Figure 21. Rotational structure of the 0-1 band of the Baldet-Johnson $(B^2\Sigma^+ - A^2\Pi_i)$ system of $^{13}C^{18}O^+$ photographed on the Jarrell-Ash spectrograph in the third order of a 1200 grooves/mm grating.
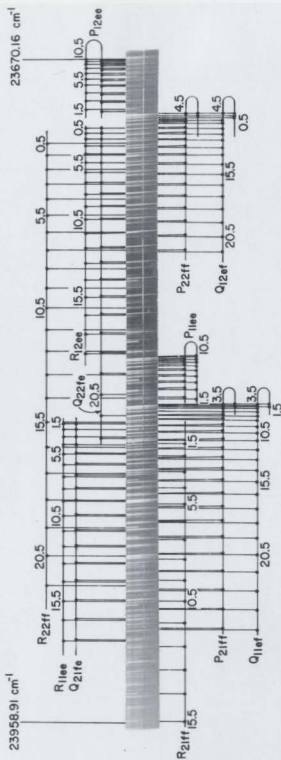
TABLE 6.2   Vacuum wavenumbers (in cm^{-1}) of the rotational lines of the 1-0 band

$$^2\Sigma^+ - \,^2\Pi_{1/2}$$

J	$P_{12ee}(J)$	$P_{22ff}(J)$	$Q_{12ef}(J)$
0.5			26762.70(-0.02)
1.5	26758.37(-0.02)	26761.55(0.01)	26761.55(-0.02)
2.5	26754.66[a]	26760.71(0.05)	26760.71(0.01)
3.5	26750.50[a]	26760.10(0.03)	26760.10(-0.02)
4.5	26747.12(-0.01)	26759.84(0.08)	26759.84(0.00)
5.5	26743.98(0.03)	26759.84(0.09)	26759.84(0.00)
6.5	26741.05(-0.02)	26760.10(0.08)	26760.10(-0.03)
7.5	26738.51(0.04)	26760.71[a]	26760.71(0.00)
8.5	26736.14(-0.03)	26761.55[a]	26761.55(-0.03)
9.5	26734.12(-0.03)	26762.64(0.06)	26762.70(-0.04)
10.5	26732.39(-0.04)	26764.07(0.06)	26764.14(-0.05)
11.5	26731.01(0.02)	26765.72(-0.01)	26765.90(-0.03)
12.5	26729.89(0.04)	26767.67[a]	26767.96(0.01)
13.5	26728.97(-0.02)	26769.76[a]	26770.25(-0.02)
14.5	26728.36(-0.07)	26772.54[a]	26772.90(0.03)
15.5	26728.11(-0.04)	26775.47(-0.03)	26775.78(0.02)
16.5	26728.11(-0.05)	26778.60(-0.06)	26778.97(0.03)
17.5	26728.36[a]	26782.04(-0.07)	26782.43(0.02)
18.5	26728.97[a]	26785.81(-0.04)	26786.18(0.02)
19.5	26729.89(-0.05)	26780.88(0.01)	26790.21(0.01)
20.5		26794.18(0.00)	26794.54(0.01)
21.5		26798.82(0.04)	26799.15(0.01)
22.5		26803.73(0.07)	26804.05(0.01)
23.5			26809.24(0.01)
24.5			26814.70(0.00)
25.5			26820.45(-0.01)
26.5			26826.52(0.02)
27.5			26832.85(0.03)
28.5			26839.49(0.06)
29.5			26846.41[a]
30.5			26853.65[a]

TABLE 6.2 (continued)

$$^2\Sigma^+ - {}^2\Pi_{1/2}$$

J	$Q_{22fe}(J)$	$R_{12ee}(J)$	$R_{22ff}(J)$
0.5	26765.90(0.00)	26765.90(-0.03)	-
1.5	26767.96(0.04)	26767.96(-0.01)	-
2.5	26770.25(0.01)	26770.25(-0.05)	26782.97(0.02)
3.5	26772.90(0.06)	26772.90(-0.02)	26788.78(0.05)
4.5	26775.78(0.05)	26775.78(-0.04)	26794.78(-0.02)
5.5	26778.97(0.06)	26778.97(-0.05)	26801.20(0.05)
6.5	26782.43(0.05)	26782.43(-0.08)	26807.83(0.03)
7.5	26786.18(0.04)	26786.18[a]	26814.70(-0.03)
8.5	26790.21(0.03)	26790.21[a]	26821.93(-0.02)
9.5	26794.54(0.03)	26794.78[a]	26829.45(0.00)
10.5	26799.15(0.01)	26799.41(0.08)	26837.24(0.00)
11.5	26804.05(0.01)	26804.50[a]	26845.30(-0.02)
12.5	26809.24(0.00)	26809.43(-0.04)	26853.65(-0.04)
13.5	26814.70(-0.02)	26814.92(-0.05)	26862.24(-0.10)
14.5	26820.45(-0.04)	26820.73(-0.03)	26871.20(-0.07)
15.5	26826.52(-0.03)	26826.80(-0.03)	26880.43(-0.06)
16.5	26832.85(-0.04)	26833.16(-0.03)	26889.94(-0.06)
17.5	26839.49(-0.03)	26839.86(0.02)	26899.73(-0.06)
18.5	26846.41(-0.03)	26846.75(-0.02)	26909.88(0.02)
19.5	26853.65(0.01)	26854.03(0.04)	26920.24(0.03)
20.5	26861.16(0.04)	26861.57(0.08)	
21.5	26868.90(0.01)	26869.25(-0.02)	
22.5	26876.99(0.05)		

TABLE 6.2 (continued)

$$^2\Sigma^+ - {}^2\Pi_{3/2}$$

J	$P_{11ee}(J)$	$P_{21ff}(J)$	$Q_{11ef}(J)$
1.5	26883.47(-0.05)	26886.67(-0.02)	26886.67(-0.04)
2.5	26870.57(-0.05)	26885.95(-0.01)	26885.95(-0.06)
3.5	26876.04(-0.04)	26885.61(0.02)	26885.61(-0.04)
4.5	26872.82(-0.08)	26885.61(0.03)	26885.61(-0.04)
5.5	26870.05(-0.01)	26885.95(0.04)	26885.95(-0.05)
6.5	26867.40[a]		26886.67(-0.04)
7.5	26865.46(0.01)	26886.67(0.08)	
8.5	26863.61(-0.06)	26887.75[a]	26887.75(-0.01)
9.5	26862.24(0.00)	26889.16[a]	26889.16(-0.01)
10.5	26861.16(-0.01)	26890.79(0.03)	26890.94(0.02)
11.5	26860.45(0.01)	26892.94(0.09)	26893.06(0.09)
12.5	26860.09(0.02)	26895.32(0.02)	26895.52(0.03)
13.5	26860.09(0.03)	26898.12(0.03)	26898.32(0.02)
14.5	26860.45(0.06)	26901.29(0.05)	26901.52(0.05)
15.5	26861.16(0.08)	26904.77(0.04)	26905.02(0.04)
16.5	26862.24[a]	26908.63(0.05)	26908.88(0.04)
17.5	26863.61[a]	26912.71(-0.07)	26913.09(0.03)
18.5	26865.29(0.04)	26917.30(-0.03)	26917.63(0.01)
19.5	26867.33(-0.01)	26922.14(-0.08)	26922.55(0.01)
20.5	26869.75(-0.03)	26927.42(-0.05)	26927.71(-0.09)
21.5	26872.48(-0.10)		

TABLE 6.2 (continued)

$$^2\Sigma^+ - {}^2\Pi_{3/2}$$

J	$Q_{21fe}(J)$	$R_{11ee}(J)$	$R_{21ff}(J)$
1.5	26893.06(0.01)	26893.06(-0.04)	
2.5	26895.52(0.00)	26895.52(-0.06)	26908.28(0.02)
3.5	26898.32(-0.01)	26898.32(-0.09)	26914.40[a]
4.5	26901.52(0.02)	26901.52(-0.07)	26920.50[a]
5.5	26905.02(0.00)	26905.02(-0.11)	26927.42[a]
6.5	26908.88(-0.01)	26908.88[a]	26934.33(-0.04)
7.5	26913.09(-0.02)	26913.09[a]	26941.75(-0.02)
8.5	26917.63(-0.05)	26917.90(0.06)	26949.60(0.07)
9.5	26922.55(-0.05)	26922.80(0.02)	26957.69(0.06)
10.5	26927.89(0.02)	26928.11(0.04)	26966.15(0.06)
11.5	26933.52(0.02)	26933.73(0.02)	26974.91(0.02)
12.5	26939.49(0.02)	26939.74(0.04)	26984.10(0.06)
13.5	26945.85(0.06)	26946.16[a]	26993.51(-0.03)
14.5	26952.48(0.02)	26952.81(0.08)	27003.44(0.06)
15.5	26959.52(0.04)	26959.83(0.07)	27013.55(-0.03)
16.5	26966.85(0.00)	26967.21(0.06)	27024.05(-0.07)
17.5	26974.55(-0.01)	26974.91(0.03)	
18.5	26982.60(-0.03)	26982.97(0.01)	
19.5	26991.01(-0.03)	26991.37(-0.02)	
20.5	26999.70(-0.10)	27000.12(-0.04)	

[a]Not used in the analysis.

TABLE 6.3   Vacuum wavenumbers (in cm⁻¹) of the rotational lines of the 0-0 band

$$^2\Sigma^+ - {}^2\Pi_{1/2}$$

J	$P_{12ee}(J)$	$P_{22ff}(J)$	$Q_{12ef}(J)$
0.5	-	25160.08(0.03)	-
1.5	25155.68(-0.04)	25158.95(0.03)	25158.95(0.01)
2.5	25151.72(0.00)	25158.18(0.05)	25158.18(0.00)
3.5	25148.04(-0.03)	25157.73(0.04)	25157.73(-0.02)
4.5	25144.77(0.02)	25157.65(0.06)	25157.65(-0.02)
5.5	25141.76(-0.02)	25157.92(0.10)	25157.92(0.00)
6.5	25130.14(-0.01)	25158.50(0.10)	25158.50(-0.02)
7.5	25136.85(-0.01)	25159.37(0.05)	25159.44(-0.02)
8.5	25134.90(-0.01)	25160.65(0.07)	25160.73(-0.01)
9.5	25133.29(-0.01)	25162.25(0.06)	25162.35(-0.01)
10.5	25132.02(-0.02)	25164.12(-0.01)	25164.32(0.00)
11.5	25131.09(-0.03)	25166.38(-0.03)	25166.60(-0.01)
12.5	25130.48(-0.05)	25169.01(-0.03)	25169.26(-0.01)
13.5	25130.32(0.02)	25171.97(-0.04)	25172.24(-0.01)
14.5	25130.36(-0.04)	25175.27(-0.05)	25175.57(-0.01)
15.5	25130.89(0.04)	25178.93(-0.05)	25179.28(0.02)
16.5	25131.66(0.01)	25182.96(-0.02)	25183.26(-0.01)
17.5	25132.82(0.04)	25187.29(-0.03)	25187.63(-0.01)
18.5	25134.29(0.02)	25191.99(-0.02)	25192.33(-0.01)
19.5	25136.16(0.07)	25197.01(-0.03)	25197.40(0.01)
20.5	25138.33(0.06)	25202.40(-0.02)	25202.84(0.06)
21.5		25208.13(-0.01)	25208.53(0.01)
22.5		25214.25(0.04)	25214.61(0.00)
23.5		25220.59(-0.03)	25221.07(0.03)
24.5		25227.38(0.00)	25227.85(0.03)
25.5		25234.51(0.02)	25234.98(0.03)
26.5		25241.94(-0.01)	25242.43(0.00)
27.5		25249.72(-0.04)	25250.21(-0.04)
28.5		25257.89(-0.02)	25258.48(0.05)

TABLE 6.3 (continued)

$$^2\Sigma^+ - ^2\Pi_{1/2}$$

J	$Q_{22fe}(J)$	$R_{12ef}(J)$	$R_{22ff}(J)$
0.5	25163.34(0.06)	25163.34(0.03)	25169.92[a]
1.5	25165.44(0.03)	25165.44(-0.01)	25175.27[a]
2.5	25167.90(0.03)	25167.90(-0.04)	25180.80(0.01)
3.5	25170.71(0.03)	25170.71(-0.05)	25186.83(0.01)
4.5	25173.86(0.03)	25173.86(-0.07)	25193.20(0.00)
5.5	25177.36(0.05)	25177.36(-0.07)	25199.87(-0.05)
6.5	25181.17(0.03)	25181.17(-0.11)	25207.00(0.03)
7.5	25185.32(0.01)	25185.48(0.02)	25214.38(0.01)
8.5	25189.84(0.02)	25190.00(0.01)	25222.11(0.01)
9.5	25194.67(0.00)	25194.88(0.02)	25230.18(0.00)
10.5	25199.87(0.01)	25200.06(-0.01)	25238.34(-0.06)
11.5	25205.38(-0.01)	25205.62(0.00)	25247.34(-0.01)
12.5	25211.27(0.00)	25211.48(-0.03)	25256.42(-0.03)
13.5	25217.45(-0.03)	25217.73(-0.01)	
14.5	25224.01(-0.03)	25224.28(-0.04)	
15.5	25230.92(-0.03)	25231.17(-0.07)	
16.5	25238.12(-0.06)	25238.54(0.04)	

TABLE 6.3 (continued)

$$^2\Sigma^+ - {}^2\Pi_{3/2}$$

J	$P_{11ee}(J)$	$P_{21ff}(J)$	$Q_{11ef}(J)$
1.5	25280.71(-0.08)	25283.98(-0.03)	25283.98(-0.06)
2.5	25276.89(-0.06)	25283.36(-0.03)	25283.42(-0.02)
3.5	25273.47(-0.04)	25283.18(0.01)	25283.22(-0.02)
4.5	25270.44(-0.04)	25283.36(0.00)	25283.42(-0.02)
5.5	25267.84(-0.01)	25283.98(0.03)	25284.04(-0.01)
6.5	25265.65(0.03)	25284.99(0.05)	25285.09(0.03)
7.5	25263.83(0.03)	-	25286.48(0.01)
8.5	25262.38(0.00)		25288.31(0.02)
9.5	25261.41(0.04)	25290.40(0.06)	25290.47(-0.04)
10.5	25260.77(0.01)	25293.03(0.08)	25293.13(-0.01)
11.5	25260.60(0.04)	25295.70^a	25296.14(-0.03)
12.5	25260.77(0.01)	25299.51^a	25299.62(0.02)
13.5	25261.41(-0.04)	25303.31^a	25303.47(0.03)
14.5	25262.38(-0.01)	25307.55^a	25307.70(0.02)
15.5	25263.83(0.01)	25312.11(-0.06)	25312.33(0.00)
16.5	25265.65(0.00)	25317.17(0.08)	25317.41(0.02)
17.5	25267.84(-0.05)	25322.51(-0.03)	25322.85(0.00)
18.5	25270.44(-0.10)	25328.30(-0.08)	25328.66(-0.06)
19.5		25334.53^a	25334.90(0.09)
20.5		25341.32(0.02)	

TABLE 6.3 (continued)

$$^2\Sigma^+ - {}^2\Pi_{3/2}$$

J	$Q_{21fe}(J)$	$R_{11ee}(J)$	$R_{21ff}(J)$
1.5	25290.47(-0.01)	25290.53(0.00)	
2.5	25293.03(-0.07)	25293.13(-0.03)	25306.06(0.01)
3.5	$^{\mathrm{a}}$25296.14(0.02)	25296.22(0.04)	25312.33(0.02)
4.5	25299.5ll(-0.04)	25299.62(-0.03)	25319.02(0.05)
5/5	25303.31(-0.07)	25303.47(-0.02)	25326.04(0.00)
6.5	25307.55(-0.06)	25307.70(-0.05)	25333.49(-0.02)
7.5	25312.26(0.01)	25312.42(0.02)	25341.32(-0.06)
8.5	25317.34(0.05)	25317.41(-0.05)	25350.68(0.02)
9.5	25322.81(0.08)	25322.93(0.01)	25358.35(0.02)
10.5	25328.61(0.03)	25328.83(0.04)	25367.45(0.04)
11.5	25334.85(0.01)	25335.10(0.04)	25376.95(0.05)
12.5	25341.50(0.01)	25341.78(0.04)	25386.83(0.04)
13.5	25348.59(0.03)	25348.84(0.02)	25397.11(0.03)
14.5	25356.02(-0.01)	25356.31(0.00)	25407.77(0.00)
15.5	25363.87(-0.03)	25364.17(-0.03)	

$^{\mathrm{a}}$Not used in the analysis.

TABLE 6.4   Vacuum wavenumbers (in cm^{-1}) of the rotational lines of the 0-1 band

$$^2\Sigma^+ - {}^2\Pi_{1/2}$$

J	$P_{12ee}(J)$	$P'_{22ff}(J)$	$Q_{12ef}(J)$
0.5	-	-	23696.14[a]
1.5	23691.70[a]	23695.93(0.05)	23695.03(0.02)
2.5	23687.86(0.00)	23694.36[a]	23694.36(0.03)
3.5	23684.35(0.02)	23694.06[a]	23694.06(0.03)
4.5	23681.15(-0.02)	23694.06(0.04)	23694.06(-0.05)
5.5	23678.38(-0.01)	23694.45(0.00)	23694.54(-0.02)
6.5	23676.04(0.05)	23695.35[a]	23695.35(-0.03)
7.5	23673.96(0.00)	23696.48(0.03)	23696.52(-0.07)
8.5	23672.28(-0.03)	23697.97(-0.03)	23698.14(-0.02)
9.5	23671.00(-0.03)	23699.95(0.01)	23700.07(-0.04)
10.5	23670.16(0.03)	23702.19(-0.05)	23702.39(-0.05)
11.5	23669.62(0.02)	23704.86(-0.07)	23705.11(-0.03)
12.5	23669.41(-0.04)	23707.93(-0.05)	23708.18(-0.04)
13.5	23669.67(-0.01)	23711.34(-0.07)	23711.62(-0.05)
14.5	23670.27(-0.01)	23715.18(-0.04)	23715.45(-0.04)
15.5	23671.25(0.00)	23719.35(-0.05)	23719.65(-0.04)
16.5	23672.64(0.04)	23723.91(-0.04)	23724.26(0.00)
17.5	23674.40(0.07)	23728.86(-0.01)	23729.19(-0.01)
18.5	23676.54[a]	23734.20(0.03)	23734.55(0.04)
19.5	23679.12[a]	23739.86(0.02)	23740.25(0.05)
20.5	23681.51[a]	23745.94(0.06)	23746.33(0.07)
21.5	23685.02(0.06)	23752.38(0.09)	23752.87
22.5	23688.51(-0.04)		
23.5	23692.47(-0.05)		

TABLE 6.4 (continued)

$$^2\Sigma^+ - {}^2\Pi_{1/2}$$

J	$Q_{22fe}(J)$	$R_{12ee}(J)$	$R_{22ff}(J)$
0.5	23699.36(0.08)	23699.36(0.05)	23705.82(0.07)
1.5	23701.53(0.07)	23701.53(0.02)	23711.34[a]
2.5	23704.08(0.07)	23704.08(0.00)	23716.96(0.02)
3.5	23707.01(0.07)	23707.01(-0.02)	23723.13(0.03)
4.5	23710.31(0.06)	23710.31(-0.04)	23729.68(0.04)
5.5	23713.97(0.05)	23713.97[a]	23736.57(0.02)
6.5	23718.02(0.04)	23718.02[a]	23743.82(-0.01)
7.5	23722.42(0.02)	23722.42[a]	23751.47(-0.01)
8.5	23727.22(0.02)	23727.38(0.00)	23759.48(-0.03)
9.5	23732.38(0.00)	23732.59(0.01)	23767.89(-0.03)
10.5	23737.90(-0.03)	23738.09(-0.05)	23776.64(-0.05)
11.5	23743.82(-0.03)	23744.10(0.02)	23785.78(-0.06)
12.5	23750.11(-0.04)	23750.37(-0.03)	23795.30(-0.06)
13.5	23756.79(-0.02)	23757.08(0.00)	23805.18(-0.07)
14.5	23763.84(-0.01)	23764.11(-0.03)	23815.46(-0.05)
15.5	23771.26(-0.01)	23771.57(0.00)	23826.09(-0.05)
16.5	23779.07(0.02)	23779.38(0.00)	23837.07(-0.07)
17.5	23787.24(0.03)	23787.60(0.05)	23848.46(-0.05)
18.5	23795.79(0.06)	23796.16(0.07)	23860.26(0.02)
19.5	23804.69(0.07)		23872.35(0.00)
20.5	23814.00[a]		23884.90(0.08)
21.5	23823.46(-0.06)		23897.73(0.07)
22.5	23833.50(-0.02)		

TABLE 6.4 (continued)

$$^2\Sigma^+ - {}^2\Pi_{3/2}$$

J	$P_{11ee}(J)$	$P_{21ff}(J)$	$Q_{11ef}(J)$
1.5	23816.71(-0.02)	23820.00(0.05)	23820.00(0.02)
2.5	23812.94(-0.03)	23819.36(-0.06)	23819.36[a]
3.5	23800.60(-0.05)	23819.36(0.04)	23819.36(-0.02)
4.5	23806.72(-0.05)	23819.69(0.04)	23819.69(-0.05)
5.5	23804.29(-0.04)	23820.50(0.07)	23820.50(-0.03)
6.5	23802.31(-0.01)	23821.70(0.06)	23821.70(-0.06)
7.5	23800.73(-0.03)	23823.34(0.05)	23823.40(-0.02)
8.5	23799.61(-0.02)	23825.43(0.06)	23825.53(0.00)
9.5	23798.91(-0.03)	23827.90(0.01)	23828.09(0.03)
10.5	23798.70(0.02)	23830.89(0.05)	23831.08(0.04)
11.5	23798.91(0.04)	23834.24(0.01)	23834.48(0.03)
12.5	23799.49(0.00)	23838.07(0.01)	23838.34(0.05)
13.5	23800.53(-0.03)	23842.39[a]	23842.61(0.04)
14.5	23802.03(-0.03)	23847.07(0.06)	23847.32(0.04)
15.5	23803.94(-0.06)	23852.20(0.06)	23852.48(0.05)
16.5	23806.33(-0.04)	23857.69(-0.01)	23858.06(0.06)
17.5	23809.11(-0.08)	23863.67(-0.02)	23864.08[a]
18.5	23812.33[a]	23870.66(-0.04)	23870.51(0.05)
19.5	23816.15(0.02)	23876.91(-0.07)	23877.37(0.03)
20.5		23884.27(0.00)	23884.65(0.00)
21.5		23891.98(-0.01)	23892.37(-0.02)
22.5		23900.12(-0.02)	23900.53(-0.03)
23.5		23908.67(-0.05)	23909.07[a]
24.5		23917.67(-0.06)	23918.03[a]

TABLE 6.4 (continued)

$$^2\Sigma - {}^2\Pi_{3/2}$$

J	$Q_{21fe}(J)$	$R_{11ee}(J)$	$R_{21ff}(J)$
1.5	23826.42(0.00)	23826.42(-0.05)	23836.09(-0.04)
2.5	23829.14(0.01)	23829.14(-0.05)	23842.02(-0.06)
3.5	23832.25(-0.02)	23832.25[a]	23848.46(0.01)
4.5	23835.84(-0.01)	23835.84[a]	23855.22(-0.05)
5.5	23839.88(0.02)	23839.95(-0.03)	23862.51(-0.01)
6.5	23844.29(-0.02)	23844.44(-0.01)	23870.20(0.00)
7.5	23849.18(-0.02)	23849.34(-0.02)	23878.34(0.02)
8.5	23854.52(-0.01)	23854.72(0.02)	23886.92(0.04)
9.5	23860.26(-0.03)	23860.53(0.05)	23895.92(0.05)
10.5	23866.49(0.00)	23866.73(0.03)	23905.39[a]
11.5	23873.15(0.03)	23873.38(0.03)	23915.19(0.05)
12.5	23880.20(0.01)	23880.47(0.03)	23925.53[a]
13.5	23887.69(-0.01)	23887.98(0.01)	23936.18(0.03)
14.5	23895.64(0.00)	23895.92(-0.01)	23947.22(-0.08)
15.5	23904.01(0.00)	23904.33(0.01)	23958.91(0.03)
16.5	23912.74[a]	23913.09(-0.06)	
17.5	23921.98[a]	23922.35(-0.06)	

[a]Not used in the analysis.

TABLE 6.5   Rotational Constants[a] (in cm^{-1}) of the A $^2\Pi_i$ and B $^2\Sigma^+$ states of $^{13}C\,^{18}O^+$

Rotational Constant	A $^2\Pi_i$		B $^2\Sigma^+$	
	v=0	v=1	v=0	v=1
B_v	1.4342(1)	1.4160(1)	1.6201(1)	1.5945(1)
$D_v \times 10^{-6}$	5.0(2)	3.3(2)	4.4(2)	5.7(2)
γ_v			-0.0183(3)	0.0173(5)
A_v	-122.150(6)	-122.040(8)		
A_{Dv}	-0.03134(3)	-0.03088(3)		
$p_v \times 10^{+2}$	-0.96(4)	-0.72(5)		
$q_v \times 10^4$	-1.4(8)	-13.2(8)		

[a]The number in the parentheses indicates the uncertainty in the last digit and corresponds to one standard deviation.

i.e., the $A^2\Pi_i$ state is same as the upper state of the comet-tail ($A^2\Pi_i$ - $X^2\Sigma^+$) band system (see Chapter 7), the molecular constants obtained from the analyses of these two systems were merged together to obtain a unique set of constants for the X, A, and B states. In fact, the B_v values obtained from this merging were used to obtain the equilibrium molecular con-stants and all these results will be discussed in Chapter 7.

(ii) Isotope Shifts

In order to obtain the isotope shifts ($\Delta\nu$) of the Baldet-Johnson bands of $^{13}C^{18}O^+$ relative to the corresponding bands of $^{12}C^{16}O^+$, the (T_v' - T_v'') values of $^{12}C^{16}O^+$ were calculated from Eq. [3.6] using the vibrational constants of the B and A states listed by Huber and Herzberg (1979). The isotope shifts, which correspond to the differences between the calculated (T_v' - T_v'') values of $^{12}C^{16}O^+$ and those of the corresponding bands of $^{13}C^{18}O^+$ obtained in the present work (Table 6.1), are listed in Table 6.6. The isotope shifts were also obtained using the (T_v' - T_v'') values of $^{12}C^{16}O^+$ quoted by Jakubek et al. (1987) and are also listed in the same table. The isotope shifts were also calculated from Eq. [3.11] using the vibrational constants of the B and A states of $^{12}C^{16}O^+$ and the value of ρ [$=\mu^{\frac{1}{2}}$ ($^{12}C^{16}O^+$)/$\mu^{\frac{1}{2}}$ ($^{13}C^{18}O^+$) = 0.9530] and are listed in the same table. The observed isotope shifts which were obtained from the calculated

TABLE 6.6 Isotope shifts (in cm^{-1}) in the Baldet-Johnson system of ^{13}C ^{18}O$^+$

	Isotope shift $\Delta\nu$ (^{12}C ^{16}O$^+$ - ^{13}C ^{18}O$^+$)		
Band	Present work[a]	Jakubek et al. (1987)[b]	Calculated
1-0	80.03	81.72	80.27
0-0	3.34	5.05	3.72
0-1	-67.65	-65.96	-67.24

[a]Obtained from the calculated $(T_v' - T_v'')$ values of ^{12}C ^{16}O$^+$ using the constants listed by Huber and Herzberg (1979).

[b]Obtained from the $(T_v' - T_v'')$ values of ^{12}C ^{16}O$^+$ reported by Jakubek et al. (1987).

$(T_v' - T_v'')$ values of $^{12}C^{16}O^+$ are in better agreement with the calculated ones than those obtained from the values of Jakubek et al. (1987).

CHAPTER 7

COMET-TAIL $(A^2\Pi_i - X^2\Sigma^+)$ SYSTEM OF $^{13}C^{18}O^+$

In this chapter, observation of nine bands of the comet-tail $(A^2\Pi_i - X^2\Sigma^+)$ system of $^{13}C^{18}O^+$ and the results of the rotational analysis of seven of them are presented. The previous work done on this system in $^{12}C^{16}O^+$ and other isotopically substituted molecules is reviewed in Section 7.1. The experimental details relevant to this band system are also briefly presented in the same section. The rotational structure of a $^2\Pi_i - ^2\Sigma^+$ system is discussed in Section 7.2. The results obtained from the rotational and vibrational analyses of this system are given in Section 7.3.

7.1 Introduction

The comet-tail band system $(A^2\Pi_i - X^2\Sigma^+)$ of $^{12}C^{16}O^+$ ion has been the subject of numerous spectroscopic studies, since its first observation by Pluvinel and Baldet (1909, 1911) in the tail of the comet Morehouse-1908c and shortly after that by Fowler (1909, 1910) in the laboratory. Several other researchers also observed the bands of this system under low resolution (see Krupenie, 1966). Baldet (1925b,c) observed most of these bands and Birge (1925) identified the transition. Coster et al. (1932), Schmid and Gerö (1933), and Bulthuis

(1935) performed the rotational analysis of several bands. In all these studies the upper state was considered as a regular state. Rao (1950a) identified this state as an inverted state and revised the vibrational numbering of this state which was later confirmed by Asundi et al. (1970) and Dhumwad et al. (1979), as stated in Section 6.1. The work done on this system prior to 1966 was reviewed by Kupenie (1966). Gagnaire and Goure (1976) reinvestigated the system and analyzed the rotational structure of the 2-0 band of $^{12}C^{16}O^+$. Later Katayama and Welsh (1981) analyzed the 0-0 band of this system and found the perturbations in the v=0 level of state A. They observed some extra lines in the structure of the $^2\Pi_{1/2}$ - $^2\Sigma^+$ sub-band. In an erratum published later, Katayama and Welsh (1982) corrected some molecular constants reported earlier by them. Coxon and Foster (1982) performed the deperturbation analysis of the levels $A^2\Pi_i$, v=0, 5, and 10 using all the available spectroscopic data of $A^2\Pi_i \longleftrightarrow X^2\Sigma^+$ pertinent to these levels. Later Brown et al. (1984) reanalyzed the 0-0 band of this system. The work done on this band system in the isotopically substituted CO^+ molecules is very fragmentary. Vujisić et al. (1980) and Brown et al. (1983) investigated the 2-0 and 0-0 bands, respectively, of this system in the $^{13}C^{16}O^+$ molecule. Brown et al. (1983) refitted the data reported by Vujisić et al. (1980) and concluded that the work of the latter was erroneous.

▽

Recently in our laboratory, nine bands of the comet-tail band system $^{13}C^{18}O^+$, excited in the cathode glow of the hollow-cathode discharge, were observed for the first time. They were photographed under medium dispersion in the first order of a 600 grooves/mm grating on the Bausch and Lomb spectrograph. Two of these bands (0-1 and 0-2) were photographed under high resolution in the second order of a 1200 grooves/mm grating on the Bausch and Lomb spectrograph. Of the remaining seven bands (5-0, 4-0, 3-0, 2-0, 1-0, 2-1, and 1-1) which were photographed under high resolution on the Jarrell-Ash spectrograph, the 1-1 band was recorded in the second order and the rest were in the third order of a 1200 grooves/mm grating. The exposure times for the high resolution spectra on the Bausch and Lomb spectrograph were about an hour, whereas on the Jarrell-Ash spectrograph, the times varied from 45 minutes (for the 3-0 band) to 8.5 hours (for the 1-1 band). Kodak Spectrum Analysis No. 1, 103a-O and 103-F plates were used to photograph the spectra. The slit widths were maintained at 20 μm and 30 μm on the Bausch and Lomb and the Jarrell-Ash spectrographs, respectively. The reciprocal dispersions of the spectra are ~0.56 Å/mm at 3950 Å in the third order on the Jarrell-Ash spectrograph and about 1.42 Å/mm at 6200 Å in the second order on the Bausch and Lomb spectrograph. The measurements of the spectral lines are accurate up to ~0.002 Å for the spectra photographed in the

third order and -0.004 Å for those recorded in the second order.

7.2 Rotational Structure of a $^2\Pi_i - ^2\Sigma^+$ System

The rotational structure of a $^2\Pi_i - ^2\Sigma^+$ system contains twelve branches and is somewhat similar to that of the $^2\Sigma^+ - ^2\Pi_i$ system discussed in Section 6.2 A schematic energy level diagram showing the twelve branches of a $^2\Pi_i - ^2\Sigma^+$ system is shown in Figure 22. The selection rules to be satisfied in this transition are

$$\Delta J = 0, \quad e \longleftrightarrow f,$$
$$\Delta J = \pm 1, \quad e \longleftrightarrow e, \quad f \longleftrightarrow f,$$
$$+ \longleftrightarrow -, \quad + \not\longleftrightarrow +, \quad \text{and} \quad - \not\longleftrightarrow -.$$

The twelve different branches of this system are identified as R_{21ee}, R_{22ff}, Q_{21fe}, Q_{22ef}, P_{21ee}, P_{22ff}, R_{11ee}, R_{12ff}, Q_{11fe}, Q_{12ef}, P_{11ee}, and P_{12ff}. If the bands of this system degrade to longer wavelengths, as in the case of comet-tail system, then the R_{21ee}, Q_{21fe}, R_{11ee}, and Q_{11fe} branches form four different heads in the rotational structure of a band. In some instances, all these four heads can be clearly seen even in the spectra photographed under medium resolution (see, for example, the 2-0 band of comet-tail system of $^{13}C^{18}O^+$ shown in Figure 13). The rotational levels of the $^2\Sigma^+$ and $^2\Pi_i$ states involved in this transition can be expressed by Eqs. [6.1 to 6.4] and Eqs. [6.5 to 6.8],
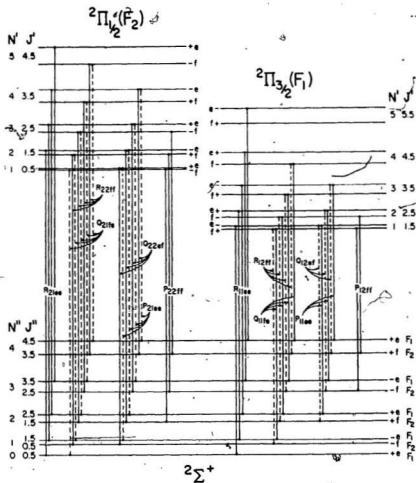
Figure 22.   A schematic energy level diagram showing the
             first few rotational transitions of all the
             twelve branches of a band of a $^2\Pi_i$ - $^2\Sigma^+$
             system.

respectively. The expressions for the twelve branches of a $^2\Pi_i - {}^2\Sigma^+$ system mentioned above can be obtained from Eqs. [6.3 to 6.8] according to a general expression,

$$\nu = (T'_{v\Pi} - T''_{v\Sigma}) + F_\Pi'(J') - F_\Sigma''(J''),\qquad [7.1]$$

with $J'' = J$. In this equation, $T_{v\Pi}$ and $T_{v\Sigma}$ are the same as those explained in Section 6.2 in connection with the Eq. [6.9], and $F_\Pi'(J')$ and $F_\Sigma''(J'')$ refer to the rotational levels of the $^2\Pi_i$ and $^2\Sigma^+$ states, respectively. The rotational quantum number J' takes values J-1, J, and J+1 for various P, Q, and R branches in accordance with the selection rules given above. All the bands of this system have two band origins, one for each of the $^2\Pi_{1/2} - {}^2\Sigma^+$ and $^2\Pi_{3/2} - {}^2\Sigma^+$ sub-bands. For the bands of the comet-tail system, the $(T_{v\Pi} - T_{v\Sigma})$ value is estimated from the analysis. The band origins of the two sub-systems can be calculated from $(T_{v\Pi} - T_{v\Sigma}) \pm (1/2)A_v$.

7.3 Analysis of the Spectra

The comet-tail system of $^{13}C^{18}O^+$ photographed under medium dispersion is shown in Figure 13. All the four possible heads are identified for the 2-0 band only. Three heads are identified for five bands and two heads are identified for each of the weak 1-0 and 2-1 bands. For the 3-0 band only two heads are identified in the medium resolution spectrum while all the four heads are clearly identified in

the high resolution spectrum. The vacuum wavenumbers of the four heads of each band, relative intensity of the band, and the vibrational quantum numbers are listed in Table 7.1. The vacuum wavenumbers listed for the R_{11ee} and Q_{11fe} heads of both 0-1 and 0-2 bands are slightly uncertain because of the diffuse nature of the $^2\Pi_{3/2} - {}^2\Sigma^+$ sub-bands.

(i) Rotational Analysis

The rotational structure of the 4-0 band of the comet-tail system of the $^{13}C^{18}O^+$ molecule photographed under high resolution on the Jarrell-Ash spectrograph is shown in Figure 23. In this figure, all the twelve branches that are expected in its rotational structure are clearly identified. As the spin-splitting of the rotational levels of the $X^2\Sigma^+$, v=0 level is not resolved, the pairs of the branches R_{22ff} and Q_{21fe}, Q_{22ef} and P_{21ee}, Q_{12ef} and P_{11ee} and Q_{11fe} and R_{12ff} are overlapping. This type of overlapping was observed in all the bands of this system. For the 0-1 and 0-2 bands, the rotational structures of only the $^2\Pi_{1/2} - {}^2\Sigma^+$ sub-bands were analyzed and those of the $^2\Pi_{3/2} - {}^2\Sigma^+$ sub-bands could not be analyzed because of their diffused nature. The rotational quantum numbers and the vacuum wavenumbers of the spectral lines of all the seven bands analyzed in the present work are listed in Tables 7.2 to 7.8. The vacuum wavenumbers of the spectral lines of all the branches of a band were simultaneously fitted to the

TABLE 7.1 Comet-tail $(A^2\Pi_i - X^2\Sigma^+)$ band system of the $^{13}C\ ^{18}O^+$ molecule

Band Head[a] (cm^{-1})	$T_{v'} - T_{v''}$[b] (cm^{-1})	Relative[c] Intensity	Assignment $v' - v''$
27572.38	27498.287(5)	w	5-0
27560.99			
27447.17			
27436.64			
26206.66	26131.812(4)	s	4-0
26194.60			
26081.26			
26070.09			
24816.72	24740.998(3)	s	3-0
24803.88			
24690.91			
24679.32			
23402.79	23325.086(4)	s	2-0
23389.10			
23276.60			
23264.31			
19882.21	19803.859(5)	m	1-1
19867.14			
19755.62			
19742.12			

TABLE 7.1 (continued)

Band Head[a] (cm^{-1})	$T_v' - T_v''$[b] (cm^{-1})	Relative[c] Intensity	Assignment $v' - v''$
18419.19	18339.717(9)[d]	vw	0-1
18403.19			
18292.2[e]			
18277.6[e]			
16364.95	16284.709(9)[d]	w	0-2
16348.29			
16253.4[e]			
16236.8[e]			

[a]The four heads identified for each band are formed by R_{21ee}, Q_{21fe}, R_{11ee}, and Q_{11fe} branches in the order of decreasing wavenumber.

[b]The number in the parentheses indicates the uncertainty in the last digit and corresponds to one standard deviation.

[c]Abbreviations for the relative intensities s, m, w, and vw represent strong, medium, weak, and very weak respectively.

[d]Extrapolated from the origin of the $^2\Pi_{1/2} - \,^2\Sigma^+$ band and the A_0 value.

[e]The vacuum wavenumber of this head is slightly uncertain because of its diffuse nature.

Figure 23. Rotational structure of the 4-0 band of the comet-tail $(A^2\Pi_i - X^2\Sigma^+)$ system of $^{13}C^{18}O^+$ photographed on the Jarrell-Ash spectrograph in the third order of a 1200 grooves/mm grating.
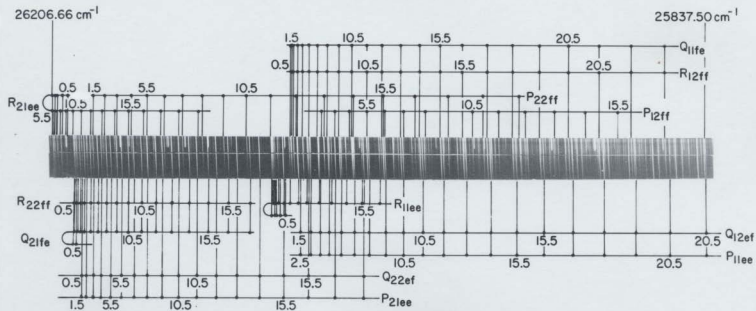
TABLE 7.2   Vacuum wavenumbers (in cm^{-1}) of the rotational lines of the 5-0 band

$$^2\Pi_{1/2} - {}^2\Sigma^+$$

J	R$_{21ee}$(J)	R$_{22ff}$(J)	Q$_{21fe}$(J)
0.5	27564.61(0.06)	27560.99(0.00)	-
1.5	27567.79(0.00)	27560.69(0.02)	27560.99(0.00)
2.5	27570.18(-0.02)	27559.51(0.01)	27560.69(0.02)
3.5	27571.74(-0.02)	27557.51(0.01)	27559.51(0.01)
4.5	27572.38^a	27554.67(0.02)	27557.51(0.01)
5.5	27572.38(0.04)	27550.98(0.03)	27554.67(0.02)
6.5	27571.37(0.01)	27546.41(-0.01)	27550.98(0.03)
7.5	27569.53(0.00)	27541.05(0.02)	27546.41(-0.01)
8.5	27566.80(-0.06)	27534.82(0.02)	27541.05(0.02)
9.5	27563.36(0.03)	27527.75(0.02)	27534.82(0.02)
10.5	27558.98(0.03)	27519.80(-0.01)	27527.75(0.02)
11.5		27511.04(0.00)	27519.80(-0.01)
12.5		27501.41(-0.01)	27511.04(0.00)
13.5		27490.96(0.01)	27501.41(-0.01)
14.5		27479.64(0.00)	27490.96(0.01)
15.5		27467.50(0.03)	27479.64(0.00)
16.5		27454.45(-0.01)	27467.50(0.03)
17.5		27440.62(0.03)	27454.45(-0.01)
18.5		27425.89(0.02)	27440.62(0.03)
19.5		27410.36(0.07)	27425.89(0.02)
20.5		27393.81(-0.05)	27410.36(0.07)
21.5		27376.60(0.02)	27393.81(-0.05)
22.5		27358.35(-0.08)	27376.60(0.02)
23.5			27358.35(-0.08)

TABLE 7.2 (continued)

$$^2\Pi_{1/2} - {}^2\Sigma^+$$

J	$Q_{22ef}(J)$	$P_{21ee}(J)$	$P_{22ff}(J)$
0.5	27556.88(-0.01)	-	-
1.5	27553.81(-0.02)	27556.88(-0.01)	-
2.5	27549.95(0.01)	27553.81(-0.02)	27543.06(-0.07)
3.5	27545.19(-0.01)	27549.95(0.01)	27535.59(-0.08)
4.5	27539.62(0.00)	27545.19(-0.01)	27527.41(0.04)
5.5	27533.15(-0.04)	27539.62(0.00)	27518.22(0.00)
6.5	27525.92(0.00)	27533.15(-0.04)	27508.23(0.00)
7.5	27517.79(-0.02)	27525.92(0.00)	27497.44(0.04)
8.5	27508.82(-0.04)	27517.79(-0.02)	27485.72(-0.01)
9.5	27499.03(-0.03)	27508.82(-0.04)	27473.21(0.00)
10.5	27488.39(-0.02)	27499.03(-0.03)	27459.89(0.04)
11.5	27476.89(-0.03)	27488.39(-0.02)	27445.59(-0.05)
12.5	27464.60(0.02)	27476.89(-0.03)	27430.62(0.02)
13.5	27451.39(-0.01)	27464.60(0.02)	27414.66(-0.04)
14.5	27437.30(-0.02)	27451.39(-0.01)	27397.98(0.01)
15.5	27422.48(-0.01)	27437.39(0.02)	27380.41(0.02)
16.5	27406.77(0.00)	27422.48(-0.01)	27361.97(0.01)
17.5	27390.20(0.01)	27406.77(0.00)	27342.62(-0.06)
18.5	27372.80(0.03)	27390.20(0.01)	27322.58(0.02)
19.5	27354.50(0.01)	27372.80(0.03)	27301.59(0.00)
20.5	27335.35(-0.01)	27354.50(0.01)	27279.76(-0.01)
21.5	27315.39(0.01)	27335.35(-0.01)	27257.11(0.00)
22.5	27294.57(0.02)	27315.39(0.01)	27233.63(0.04)
23.5		27294.57(0.02)	27209.18(-0.04)
24.5			27183.97(-0.03)

TABLE 7.2 (continued)

$$^2\Pi_{3/2} - {}^2\Sigma^+$$

J	$R_{11ee}(J)$	$R_{12ef}(J)$	$Q_{11fe}(J)$
0.5	27440.17(0.02)	27436.64(0.06)	-
1.5	27443.26(0.01)	27436.13(0.02)	27436.64(0.06)
2.5	27445.59	27434.77(0.02)	27436.13(0.02)
3.5	27446.72(-0.04)	27432.50(0.02)	27434.77(0.02)
4.5	27447.17(0.00)	27429.33(0.02)	27432.50(0.02)
5.5	27446.72(0.05)	27425.28(0.03)	27429.33(0.02)
6.5	27445.23(-0.03)	27420.30(0.02)	27425.28(0.03)
7.5	27442.94(-0.02)	27414.33(-0.07)	27420.30(0.02)
8.5	27439.72(-0.03)	27407.55(-0.08)	27414.33(-0.07)
9.5	27435.60(-0.04)	27399.87(-0.08)	27407.55(-0.08)
10.5	27430.62(0.00)	27391.33(-0.04)	27399.87(-0.08)
11.5	27424.70(0.01)	27381.87(0.02)	27391.33(-0.04)
12.5	27417.83(-0.03)	27371.48(-0.02)	27381.87(-0.02)
13.5	27410.14(0.02)	27360.19(-0.01)	27371.48(-0.02)
14.5	27401.51(0.04)	27347.96(-0.04)	27360.19(-0.01)
15.5		27334.94(0.05)	27347.96(-0.04)
16.5		27320.94(0.06)	27334.94(0.05)
17.5			27320.94(0.06)

TABLE 7.2 (continued)

$$^2\Pi_{3/2} - \,^2\Sigma^+$$

J	$Q_{12ef}(J)$	$P_{11ee}(J)$	$P_{12ff}(J)$
1.5	27429.33[a]		
2.5	27425.28[a]	27429.33[a]	
3.5	27420.49(0.03)	27425.28[a]	27411.17(0.06)
4.5	27414.66(0.03)	27420.49(0.03)	27402.65(0.04)
5.5	27407.84(-0.05)	27414.66(0.03)	27393.29(0.09)
6.5	27400.22(-0.03)	27407.84(-0.05)	27382.89(-0.01)
7.5	27391.72(0.01)	27400.22(-0.03)	
8.5	27382.30(0.03)	27391.72(0.01)	27359.64(0.05)
9.5	27371.91(-0.02)	27382.30(0.03)	27346.60(0.02)
10.5	27360.08(0.00)	27371.91(-0.02)	27332.63(-0.05)
11.5	27348.50(-0.03)	27360.08(0.00)	27317.85(-0.02)
12.5	27335.43(-0.05)	27348.50(-0.03)	27302.00[a]
13.5	27321.49(-0.04)	27335.43(-0.05)	27285.50(-0.06)
14.5	27306.67(0.00)	27321.49(-0.04)	27268.08(0.03)
15.5	27290.93(0.03)	27306.67(0.00)	27249.61(-0.02)
16.5	27274.28(0.05)	27290.93(0.03)	27230.37(0.05)
17.5		27274.28(0.05)	27210.14(0.04)

[a]Not used in the analysis.

TABLE 7.3   Vacuum wavenumbers (in cm^{-1}) of the rotational lines of the 4-0 band

$$^2\Pi_{1/2} - {}^2\Sigma^+$$

J		$R_{21ee}(J)$	$R_{22ff}(J)$	$Q_{21fe}(J)$
0.5		26198.27(0.09)	26194.60(-0.03)	26194.02(-0.03)
1.5		26201.52(0.01)	26194.36(-0.03)	26194.60(-0.03)
2.5		26203.97(-0.05)	26193.34(0.00)	26194.36(-0.03)
3.5		26205.68(-0.05)	26191.47(-0.01)	26193.34(0.00)
4.5		26206.66(0.04)	26188.83(0.02)	26191.47(-0.01)
5.5		26206.66(-0.04)	26185.33(0.00)	26188.83(0.02)
6.5		26205.97(0.00)	26181.06(0.02)	26185.33(0.00)
7.5		26204.47(0.04)	26175.97(0.02)	26181.06(0.02)
8.5		26202.13(0.05)	26170.08(0.04)	26175.97(0.02)
9.5		26198.98(0.07)	26163.35(0.03)	26170.08(0.04)
10.5		26194.96(0.02)	26155.81(0.02)	26163.35(0.03)
11.5		26190.20(0.05)	26147.46(0.00)	26155.81(0.02)
12.5		26184.59(0.05)	26138.31(0.00)	26147.46(0.00)
13.5		26178.18(0.05)	26128.36(0.00)	26138.31(0.00)
14.5		26170.93(0.03)	26117.60(0.00)	26128.36(0.00)
15.5		26162.84(-0.01)	26106.00(-0.04)	26117.60(0.00)
16.5		26154.04(0.05)	26093.63(-0.03)	26106.00(-0.04)
17.5		26144.28(-0.04)		26093.63(-0.03)
18.5		26133.81(-0.02)		
19.5		26122.51(-0.01)		

TABLE 7.3 (continued)

$$^2\Pi_{1/2} - {}^2\Sigma^+$$

J	$Q_{22ef}(J)$	$P_{21ee}(J)$	$P_{22ff}(J)$
0.5	26190.44(-0.04)		
1.5	26187.46(-0.01)	26190.44(-0.04)	26183.36(0.02)
2.5	26183.62(-0.04)	26187.46(-0.01)	26176.78(0.01)
3.5	26178.99(-0.04)	26183.62(-0.04)	26169.40(0.00)
4.5	26173.56(-0.03)	26178.99(-0.04)	26161.15(-0.06)
5.5	26167.36(0.01)	26173.56(-0.03)	26152.21(0.00)
6.5	26160.27(-0.02)	26167.36(0.01)	26142.38(-0.02)
7.5	26152.38(-0.05)	26160.27(-0.02)	26131.78(-0.01)
8.5	26143.75(0.00)	26152.38(-0.05)	26120.36(0.00)
9.5	26134.28(0.01)	26143.75(0.00)	26108.16(0.03)
10.5	26123.07(-0.01)	26134.28(0.01)	26095.12(0.03)
11.5	26112.92(0.04)	26123.97(-0.01)	26081.23(0.00)
12.5	26101.00(0.03)	26112.92(0.04)	26066.63(0.05)
13.5	26088.28(0.02)	26101.00(0.03)	26051.16(0.05)
14.5	26074.75(0.02)	26088.28(0.02)	26034.88(0.04)
15.5	26060.39(-0.01)	26074.75(0.02)	26017.78(0.02)
16.5	26045.22(-0.05)	26060.39(-0.01)	25999.89(0.01)
17.5	26029.27(-0.06)	26045.22(-0.05)	25981.23(0.04)
18.5		26029.27(-0.06)	25961.64(-0.06)
19.5			25941.35(-0.05)

TABLE 7.3 (continued)

$$^2\Pi_{3/2} - {}^2\Sigma^+$$

J	$R_{11ee}(J)$	$R_{12ff}(J)$	$Q_{11fe}(J)$
0.5	26073.49(-0.03)	26070.09(0.00)	-
1.5	26076.87(0.03)	26069.71(0.01)	26070.09(0.00)
2.5	26079.16(0.00)	26068.45(0.01)	26069.71(0.01)
3.5	26080.66(0.06)	26066.33(0.01)	26068.45(0.01)
4.5	26081.26(0.08)	26063.33(0.00)	26066.33(0.01)
5.5	26080.93(0.05)	26059.47(0.01)	26063.33(0.00)
6.5	26079.74(0.07)	26054.70(-0.03)	26059.47(0.01)
7.5	26077.72(0.03)	26049.14(0.01)	26054.70(-0.03)
8.5	26074.75(-0.05)	26042.65(-0.02)	26049.14(0.01)
9.5	26071.05(0.02)	26035.32(-0.01)	26042.65(-0.02)
10.5	26066.38(-0.02)	26027.08(-0.05)	26035.32(-0.01)
11.5	26060.92(0.03)	26018.08(0.02)	26027.08(-0.05)
12.5	26054.50(-0.03)	26008.12(0.00)	26018.08(0.02)
13.5	26047.25(-0.04)	25997.33(0.01)	26008.12(0.00)
14.5	26039.15(-0.04)	25985.63(-0.02)	25997.33(0.01)
15.5	26030.17(-0.05)	25973.15(0.04)	25985.63(-0.02)
16.5	26020.34(-0.05)	25959.70(-0.02)	25973.15(0.04)
17.5		25945.45(0.00)	25959.70(-0.02)
18.5		25930.32(0.00)	25945.45(0.00)
19.5		25914.32(-0.01)	25930.32(0.00)
20.5		25897.48(0.01)	25914.32(-0.01)
21.5		25879.75(-0.01)	25897.48(0.01)
22.5		25861.18(0.00)	25879.75(-0.01)
23.5			25861.18(0.00)

TABLE 7.3 (continued)

$$^2\Pi_{3/2} - {}^2\Sigma^+$$

J	$Q_{12ef}(J)$	$P_{11ee}(J)$	$P_{12ff}(J)$
1.5	26062.94(-0.01)	-	-
2.5	26058.99(0.00)	26062.94(-0.01)	26052.23(-0.01)
3.5	26054.18(0.02)	26058.99(0.00)	26044.78(0.07)
4.5	26048.47(0.00)	26054.18(0.02)	26036.24(-0.07)
5.5	26041.87(-0.04)	26048.47(0.00)	26027.08(0.03)
6.5	26034.45(-0.03)	26041.87(-0.04)	26017.01[a]
7.5	26026.18(0.00)	26034.45(-0.03)	26005.94(0.02)
8.5	26017.01(0.00)	26026.18(0.00)	25994.04(-0.01)
9.5	26006.97(-0.01)	26017.01(0.00)	25981.23(-0.09)
10.5	25996.08(0.00)	26006.97(-0.01)	25987.72(0.01)
11.5	25984.29(-0.02)	25996.08(0.00)	25953.24(-0.01)
12.5	25971.68(0.00)	25984.29(-0.02)	25937.96(0.05)
13.5	25958.15(-0.03)	25971.68(0.00)	25921.76(0.05)
14.5	25943.80(-0.01)	25958.15(-0.03)	25904.71(0.06)
15.5	25928.56(-0.03)	25943.80(-0.01)	25886.80(0.08)
16.5	25912.46(-0.03)	25928.56(-0.03)	
17.5	25895.57(0.03)	25912.46(-0.03)	
18.5	25877.68(-0.04)	25895.57(0.03)	
19.5	25859.02(-0.02)	25877.68(-0.04)	
20.5	25839.50(0.01)	25859.02(-0.02)	
21.5		25839.50(0.01)	

[a]Not used in the analysis.

TABLE 7.4   Vacuum wavenumbers (in cm^{-1}) of the rotational lines of the 3-0 band

$$^2\Pi_{1/2} - {}^2\Sigma^+$$

J	$R_{21ee}(J)$	$R_{22ff}(J)$	$Q_{21fe}(J)$
0.5	24807.44(0.01)	24803.88(0.00)	24803.23(-0.02)
1.5	24810.81(-0.04)	24803.70(-0.03)	24803.88(0.00)
2.5	24813.46(-0.02)	24802.82(0.01)	24803.70(-0.03)
3.5	24815.33(-0.01)	24801.12(0.01)	24802.82(0.01)
4.5	24816.38(-0.05)	24798.65(0.02)	24801.12(0.01)
5.5	24816.72(-0.01)	24795.38(0.00)	24798.65(0.02)
6.5	24816.26(0.00)	24791.35(0.00)	24795.38(0.00)
7.5	24815.02(0.01)	24786.59(0.04)	24791.35(0.00)
8.5	24812.99(0.01)	24781.02(0.05)	24786.59(0.04)
9.5	24810.21(0.04)	24774.66(0.04)	24781.02(0.05)
10.5	24806.64(0.07)	24767.53(0.03)	24774.66(0.04)
11.5	24802.27(0.07)	24759.64(0.04)	24767.53(0.03)
12.5	24797.14(0.10)	24750.92(0.00)	24759.64(0.04)
13.5	24790.99(-0.10)	24741.48(0.01)	24750.92(-0.00)
14.5	24784.28(-0.08)	24731.22(-0.03)	24741.48(0.01)
15.5	24777.10^a	24720.26(0.00)	24731.22(-0.03)
16.5	24768.60(0.07)	24708.42(-0.07)	24720.26(0.00)
17.5	24759.58^a		24708.42(-0.07)
18.5	24749.51(-0.01)		

TABLE 7.4 (continued)

$$^2\Pi_{1/2} \cdot {}^2\Sigma^+$$

J	$Q_{22ef}(J)$	$P_{21ee}(J)$	$P_{22ff}(J)$
0.5	24799.65(-0.02)		
1.5	24796.69(-0.03)	24799.65(-0.02)	24792.53(-0.01)
2.5	24792.95(-0.04)	24796.69(-0.03)	24786.00(-0.02)
3.5	24788.46(-0.02)	24792.95(-0.04)	24778.69(-0.04)
4.5	24783.18(-0.02)	24788.46(-0.02)	24770.65(-0.02)
5.5	24777.10(-0.05)	24783.18(-0.02)	24761.81(-0.01)
6.5	24770.30(-0.01)	24777.10(-0.05)	24752.21(0.00)
7.5	24762.71(0.00)	24770.30(-0.01)	24741.85(0.03)
8.5	24754.33(0.00)	24762.71(0.00)	24730.71(0.05)
9.5	24745.21(0.03)	24754.33(0.00)	24718.77(0.05)
10.5	24735.27(0.02)	24745.21(0.03)	24706.04(0.02)
11.5	24724.54(-0.01)	24735.27(0.02)	24692.58(0.04)
12.5	24713.13(0.05)	24724.54(-0.01)	24678.32(0.03)
13.5	24700.82(-0.01)	24713.13(0.05)	24663.29(0.03)
14.5	24687.85(0.03)	24700.82(-0.01)	24647.49(0.02)
15.5	24674.02(-0.01)	24687.85(0.03)	24630.91(0.00)
16.5	24659.50(0.02)	24674.02(-0.01)	24613.53(-0.05)
17.5	24644.10(-0.05)	24659.50(0.02)	24595.40(-0.08)
18.5		24644.10(-0.05)	

TABLE 7.4 (continued)

$$^2\Pi_{3/2} - {}^2\Sigma^+$$

J	$R_{11ee}(J)$	$R_{12ff}(J)$	$Q_{11fe}(J)$
0.5	24682.89(0.00)	24679.32(0.01)	
1.5	24686.16(0.01)	24679.02(0.01)	24679.32(0.01)
2.5	24688.60(0.02)	24677.88(0.01)	24679.02(0.01)
3.5	24690.19(0.01)	24675.90(0.01)	24677.88(0.01)
4.5	24690.91(-0.03)	24673.10(0.02)	24675.90(0.01)
5.5	24690.91(0.05)	24669.44(0.01)	24673.10(0.02)
6.5	24689.94(-0.01)	24664.94(-0.01)	24669.44(0.01)
7.5	24688.19(0.00)	24659.62(-0.01)	24664.94(-0.01)
8.5	24685.59(-0.02)	24653.45(-0.02)	24659.62(-0.01)
9.5	24682.18(0.00)	24646.49(0.00)	24653.45(-0.02)
10.5	24677.94(0.02)	24638.63(-0.03)	24646.49(0.00)
11.5	24672.81(-0.02)	24630.00(0.00)	24638.63(-0.03)
12.5	24666.89(-0.01)	24620.51(0.00)	24630.00(0.00)
13.5	24660.13(0.00)	24610.18(0.00)	24620.51(0.00)
14.5	24652.51(-0.02)	24599.02(0.00)	24610.18(0.00)
15.5	24644.10(0.01)	24587.05(0.02)	24599.02(0.00)
16.5	24634.83(0.01)	24574.19(-0.02)	24587.05(0.02)
17.5	24624.74(0.03)	24560.54(-0.01)	24574.19(-0.02)
18.5	24613.81(0.03)	24546.04(-0.02)	24560.54(-0.01)
19.5	24602.02(0.02)	24530.72(-0.02)	24546.04(-0.02)
20.5	24589.40(0.00)	24514.55(-0.05)	24530.72(-0.02)
21.5	24575.97(0.01)	24497.61(-0.01)	24514.55(-0.05)
22.5	24561.71(0.02)	24479.81(0.00)	24497.61(-0.01)
23.5	24546.59(-0.01)	24461.19(0.01)	24479.81(0.00)
24.5	24530.72(0.05)	24441.74(0.02)	24461.19(0.01)
25.5	24513.92(0.01)	24421.43(0.00)	24441.74(0.02)
26.6	24496.32(0.00)	24400.32(0.00)	24421.43(0.00)
27.5	24477.92(0.02)	24378.39(0.01)	24400.32(0.00)
28.5	24458.64(-0.02)	24355.63(0.01)	24378.39(0.01)
29.5	24438.54(-0.05)		24355.63(0.01)

TABLE 7.4 (continued)

$$^2\Pi_{3/2} - {}^2\Sigma^+$$

J	$Q_{12ef}(J)$	$P_{11ee}(J)$	$P_{12ff}(J)$
1.5	24672.19(0.02)	-	-
2.5	24668.33(0.04)	24672.19(0.02)	24661.40(-0.05)
3.5	24663.60(0.02)	24668.33(0.04)	24654.03(0.02)
4.5	24658.04(0.00)	24663.60(0.02)	24645.73(0.00)
5.5	24651.65(0.00)	24658.04(0.00)	24636.59(-0.02)
6.5	24644.42(-0.02)	24651.65(0.00)	24626.67(0.01)
7.5	24636.37(-0.01)	24644.42(-0.02)	24615.89(0.02)
8.5	24627.49(-0.01)	24636.37(-0.01)	24604.27(0.02)
9.5	24617.78(0.00)	24627.49(-0.01)	24591.81(0.01)
10.5	24607.21(-0.01)	24617.78(0.00)	24578.53(0.01)
11.5	24595.81(-0.03)	24607.21(-0.01)	24564.42(0.02)
12.5	24583.60(-0.02)	24595.81(-0.03)	24549.46(0.01)
13.5	24570.55(-0.02)	24583.60(-0.02)	24533.68(0.01)
14.5	24556.68(0.00)	24570.55(-0.02)	24517.07(0.01)
15.5	24541.94(-0.03)	24556.68(0.00)	24499.63(0.01)
16.5	24526.39(-0.03)	24541.94(-0.03)	24481.39(0.04)
17.5	24510.01(-0.04)	24526.39(-0.03)	24462.29(0.03)
18.5	24492.83(-0.01)	24510.01(-0.04)	24442.36(0.03)
19.5	24474.82(0.01)	24492.83(-0.01)	24421.60(0.02)
20.5	24455.96(0.01)	24474.82(0.01)	24399.98(-0.03)
21.5	24436.29(0.03)	24455.96(0.01)	24377.66(0.05)
22.5	24415.71(-0.04)	24436.29(0.03)	
23.5	24394.43(0.02)	24415.71(-0.04)	
24.5	24372.25(0.01)	24394.43(0.02)	
25.5		24372.25(0.01)	

^{a}Not used in the analysis.

TABLE 7.5   Vacuum wavenumbers (in cm^{-1}) of the rotational lines of the 2-0 band

$$^2\Pi_{1/2} - {}^2\Sigma^+$$

J	$R_{21ee}(J)$	$R_{22ff}(J)$	$Q_{21fe}(J)$
0.5	23392.72(0.01)	23389.10(-0.07)	23388.45(-0.05)
1.5	23396.21(-0.02)	23389.10(-0.01)	23389.10(-0.07)
2.5	23398.97(-0.02)	23388.29(-0.02)	23389.10(-0.01)
3.5	23400.99(-0.02)	23386.75(-0.01)	23388.29(-0.02)
4.5	23402.28(0.00)	23384.48(0.01)	23386.75(-0.01)
5.5	23402.79(-0.02)	23381.44(-0.01)	23384.48(0.01)
6.5	23402.59(-0.01)	23377.70(0.03)	23381.44(-0.01)
7.5	23401.64(0.00)	23373.18(0.02)	23377.70(0.03)
8.5	23399.94(0.00)	23367.93(0.02)	23373.18(0.02)
9.5	23397.50(0.01)	23361.94(0.03)	23367.93(0.02)
10.5	23394.33(0.04)	23355.18(0.01)	23361.94(0.03)
11.5	23390.40(0.06)	23347.72(0.04)	23355.18(0.01)
12.5	23385.74(0.09)	23339.49(0.03)	23347.72(0.04)
13.5	23380.26(0.06)	23330.53(0.04)	23339.49(0.03)
14.5	23373.97(-0.02)	23320.80(0.02)	23330.53(0.04)
15.5	23367.21[a]	23310.29(-0.03)	23320.80(0.02)
16.5	23359.54[b]	23299.09(-0.03)	23310.29(-0.03)
17.5	23350.79(-0.04)	23287.15(-0.02)	23299.09(-0.03)
18.5	23341.56(-0.03)	23274.45(-0.03)	23287.15(-0.02)
19.5		23261.05(0.01)	23274.45(-0.03)
20.5		23246.80(-0.06)	23261.05(0.01)
21.5		23231.87(-0.06)	23246.80(-0.06)
22.5		23216.26(0.01)	23231.87(-0.06)
23.5		23199.91(0.08)	23216.26(0.01)
24.5			23199.91(0.08)
25.5		23164.72(-0.02)	-
26.5			23164.72(-0.02)

TABLE 7.5 (continued)

$$^2\Pi_{1/2} - {}^2\Sigma^+$$

J	$Q_{22ef}(J)$	$P_{21ee}(J)$	$P_{22ff}(J)$
0.5	23384.91(-0.01)	-	-
1.5	23382.01(-0.01)	23384.91(-0.01)	-
2.5	23378.33(-0.04)	23382.01(-0.01)	23371.31(-0.01)
3.5	23373.97(-0.02)	23378.33(-0.04)	23364.09(-0.02)
4.5	23368.85(-0.01)	23373.97(-0.02)	23356.17(0.01)
5.5	23362.98(-0.02)	23368.85(-0.01)	23347.49(0.01)
6.5	23356.30(0.00)	23362.98(-0.02)	23338.08(0.02)
7.5	23349.04(0.00)	23356.30(0.00)	23327.90(0.02)
8.5	23340.95(-0.02)	23349.04(0.00)	23316.99(0.01)
9.5	23332.11(-0.02)	23340.95(-0.01)	23305.36(0.03)
10.5	23322.55(0.00)	23332.11(-0.02)	23292.99(0.05)
11.5	23312.23(-0.01)	23322.55(0.00)	23279.85(-0.04)
12.5	23301.20(0.02)	23312.23(-0.01)	23265.06(0.02)
13.5	23289.39(0.00)	23301.20(0.02)	23251.36(-0.03)
14.5	23276.90(0.05)	23289.39(0.00)	23236.02(0.04)
15.5	23263.58(0.01)	23276.90(0.05)	23219.90(0.01)
16.5	23249.56(0.02)	23263.58(0.01)	23202.99(-0.07)
17.5	23234.79(0.01)	23249.56(0.02)	23185.52(0.03)
18.5	23219.24(-0.03)	23234.79(0.01)	23167.19(0.01)
19.5	23202.99(-0.03)	23219.24(-0.03)	23148.12(0.00)
20.5	23185.98(-0.04)	23202.99(-0.03)	23128.32(-0.01)
21.5	23168.22(-0.06)	23185.98(-0.04)	
22.5	23149.70[a]	23168.22(-0.06)	
23.5	23130.65(0.08)	23149.70[a]	
24.5	23110.64(0.04)	23130.65(0.08)	
25.5		23110.64(0.04)	

TABLE 7.5 (continued)

$$^2\Pi_{3/2} - {}^2\Sigma^+$$

J	$R_{11ee}(J)$	$R_{12ff}(J)$	$Q_{11fe}(J)$
0.5	23267.90(0.03)	23264.31(0.02)	-
1.5	23271.24(0.02)	23264.68(0.01)	23264.31(0.02)
2.5	23273.80(0.03)	23263.07(0.02)	23264.68(0.01)
3.5	23275.54(0.03)	23261.25(0.02)	23263.07(0.02)
4.5	23276.47(0.01)	23258.59(-0.01)	23261.25(0.02)
5.5	23276.60(0.00)	23255.19(0.02)	23258.59(-0.01)
6.5	23275.93(0.00)	23250.91(0.03)	23255.19(0.02)
7.5	23274.45(-0.02)	23245.90(-0.01)	23250.91(-0.03)
8.5	23272.18(-0.01)	23240.05(-0.02)	23245.90(-0.02)
9.5	23269.11(-0.01)	23233.38(-0.07)	23240.05(-0.02)
10.5	23265.21(-0.03)	23225.95(-0.03)	23233.38(-0.07)
11.6	23260.52(-0.03)	23217.72(-0.02)	23225.95(-0.03)
12.5	23255.07(0.01)	23208.65(-0.03)	23217.72(-0.02)
13.5	23248.77(0.01)	23198.80(-0.03)	23208.65(-0.03)
14.5	23241.68(0.03)	23188.17(0.00)	23198.80(-0.03)
15.5	23233.79(0.05)	23176.70(0.00)	23188.17(0.00)
16.5	23225.10(0.08)	23164.40(-0.03)	23176.70(0.00)
17.5		23151.35(-0.01)	23164.40(-0.03)
18.5		23137.50(0.02)	23151.35(-0.01)
19.5		23122.82(0.03)	23137.50(0.02)
20.5		23107.35(0.05)	23122.82(0.03)
21.5			23107.35(0.05)

TABLE 7.5 (continued)

$$^2\Pi_{3/2} - {}^2\Sigma^+$$

J	$Q_{12ef}(J)$	$P_{11ee}(J)$	$P_{12ff}(J)$
1.5	23257.16(0.01)		
2.5	23253.35(-0.01)	23257.16(0.01)	23246.33[a]
3.5	23248.77(0.00)	23253.35(-0.01)	23239.15(0.08)
4.5	23243.38(0.01)	23248.77(0.00)	23230.91(0.00)
5.5	23237.16(-0.01)	23243.38(0.01)	23221.99(0.05)
6.5	23230.17(0.00)	23237.16(-0.01)	23212.19(0.01)
7.5	23222.37(0.00)	23230.17(0.00)	23201.62(0.01)
8.5	23213.74(-0.03)	23222.37(0.00)	23190.25(0.01)
9.5	23204.33(-0.03)	23213.74(-0.03)	23178.09(0.02)
10.5	23194.15(0.00)	23204.33(-0.03)	23165.18(0.08)
11.5	23183.12(-0.02)	23194.15(0.00)	23151.35(0.02)
12.5	23171.31(-0.01)	23183.12(-0.02)	23136.78(0.02)
13.5	23158.70(0 00)	23171.31(-0.01)	23121.40(0.02)
14.5	23145.29(0.01)	23158.70(0.00)	23105.21(0.00)
15.5	23131.08(0.02)	23145.29(0.01)	
16.5	23116.06(0.03)	23131.08(0.02)	23070.40(-0.05)
17.5	23100.13(-0.06)	23116.06(0.03)	23051.89(0.01)
18.5	23083.52(-0.04)	23100.13(-0.06)	
19.5	23066.14(0.03)	23083.52(-0.04)	23012.26(-0.05)
20.5		23066.14(0.03)	

[a]Not used in the analysis.

TABLE 7.6   Vacuum wavenumbers (in, cm^{-1}) of the rotational lines of the 1-1
              band

$$^2\Pi_{1/2} - {}^2\Sigma^+$$

J	R$_{21ee}$(J)	R$_{22ff}$(J)	Q$_{21fe}$(J)
0.5		19867.14(0.06)	19866.34(0.02)
1.5		19867.14(-0.03)	19867.14(0.06)
2.5	19877.13(-0.05)	19866.56(-0.03)	19867.14(-0.03)
3.5	19879.49(0.04)	19865.37(0.04)	19866.56(-0.03)
4.5	19881.07(0.02)	19863.42(0.02)	19865.37(0.04)
5.5	19881.84	19860.82(0.02)	19863.42(0.02)
6.5	19882.21(-0.01)	19857.53(0.01)	19860.82(0.02)
7.5	19881.84(0.05)	19853.57(0.01)	19857.53(0.01)
8.5	19880.68(0.00)	19848.93(0.00)	19853.57(0.01)
9.5	19878.96(0.06)	19843.61(-0.02)	19848.93(0.00)
10.5	19876.40(-0.03)	19837.64(-0.01)	19843.61(-0.02)
11.5	19873.30(0.02)	19831.00(0.01)	19837.64(-0.01)
12.5	19869.49(0.04)	19823.67(0.02)	19831.00(0.01)
13.5	19865.04(0.10)	19815.65(0.02)	19823.67(0.02)
14.5	19859.75(0.02)	19806.96(0.02)	19815.65(0.02)
15.5		19797.54(-0.03)	19806.96(0.02)
16.5		19787.51(0.00)	19797.54(-0.03)
17.5		19776.71(-0.06)	19787.51(0.00)
18.5		19765.40(0.05)	19776.71(-0.06)
19.5		19753.21(-0.04)	19765.40(0.05)
20.5		19740.43(-0.03)	19753.21(-0.04)
21.5		19727.09	19740.43(-0.03)
22.5		19712.83(0.00)	19727.09
23.5		19697.93(-0.05)	19712.83(0.00)
24.5		19682.50(0.00)	19697.93(-0.05)
25.5		19666.11(-0.10)	19682.50(0.06)
26.5		19649.34(0.06)	19666.11(-0.10)
27.5			19649.34(0.06)

TABLE 7.6 (continued)

$$^2\Pi_{1/2} - {}^2\Sigma^+$$

J	$Q_{22e}(J)$	$P_{21ee}(J)$	$P_{22ff}(J)$
0.5	19862.76(-0.02)	-	
1.5	19860.01(0.01)	-	
2.5	19856.52(-0.02)	19860.01(0.01)	19849.40(0.00)
3.5	19852.39(-0.02)	19856.52(-0.02)	19842.43(0.02)
4.5	19847.60(-0.01)	19852.39(-0.02)	19834.72(-0.03)
5.5	19842.09(-0.05)	19847.60(-0.01)	19826.46(0.04)
6.5	19835.96(-0.03)	19842.09(-0.05)	19817.43(0.01)
7.5	19829.16(-0.01)	19835.96(-0.03)	19807.66(-0.08)
8.5	19821.65(-0.02)	19829.16(-0.01)	19797.28(-0.11)
9.5	19813.50(0.00)	19821.65(-0.02)	19786.37(0.01)
10.5	19804.63(-0.02)	19813.50(0.00)	19774.69(0.02)
11.5	19795.13(0.00)	19804.63(-0.02)	19762.33(0.04)
12.5	19784.93(0.00)	19795.13(0.00)	19749.24(-0.01)
13.5	19774.05(-0.01)	19784.93(0.00)	19735.56(0.04)
14.5	19762.42(-0.08)	19774.05(-0.01)	19721.18(0.06)
15.5	19750.29(0.02)	19762.42(-0.08)	19706.08(0.03)
16.5	19737.40(0.04)	19750.29(0.02)	19690.35(0.05)
17.5	19723.78(0.01)	19737.40(0.04)	
18.5	19709.55(0.05)	19723.78(0.01)	19656.78(0.02)
19.5	19694.54(-0.01)	19709.55(0.05)	19639.01(0.04)
20.5	19678.90(-0.02)	19694.54(-0.01)	
21.5	19662.61(0.01)	19678.90(-0.02)	
22.5	19645.59(-0.01)	19662.61(0.01)	
23.5		19645.59(-0.01)	

TABLE 7.6 (continued)

$$^2\Pi_{3/2} - {}^2\Sigma^+$$

J	$R_{11ee}(J)$	$R_{12ff}(J)$	$Q_{11fe}(J)$
0.5	19745.69(0.04)	19742.12(0.01)	
1.5	19749.24	19742.12(0.08)	19742.12(0.01)
2.5	19751.93(0.08)	19741.23(0.00)	19742.12(0.08)
3.5	19753.91(0.07)	19739.71(0.02)	19741.23(0.00)
4.5	19755.14(0.04)	19737.40(-0.01)	19739.71(0.02)
5.5	19755.62(0.00)	19734.40(0.00)	19737.40(-0.01)
6.5	19755.38(-0.03)	19730.64(-0.01)	19734.40(0.00)
7.5	19754.47(0.02)	19726.12(-0.04)	19730.64(-0.01)
8.5	19752.75(-0.01)	19720.87(-0.06)	19726.12(-0.04)
9.5	19750.29(-0.04)	19714.93(-0.03)	19720.87(-0.06)
10.5	19747.13(-0.03)	19708.21(-0.05)	19714.93(-0.03)
11.5	19743.24(-0.01)	19700.78(-0.04)	19708.21(-0.05)
12.5	19738.59(0.00)	19692.61(-0.02)	19700.78(-0.04)
13.5	19733.21(0.01)	19683.71(0.00)	19692.61(-0.02)
14.5	19727.09(0.03)	19674.06(0.02)	19683.71(0.00)
15.5	19720.24(0.06)	19663.70(0.07)	19674.06(0.02)
16.5			19663.70(0.07)

TABLE 7.6 (continued)

$$^2\Pi_{3/2} - {}^2\Sigma^+$$

J	$Q_{12ef}(J)$	$P_{11ee}(J)$	$P_{12ff}(J)$
1.5	19735.05(0.02)		
2.5	19731.43(0.01)	19735.05(0.02)	
3.5	19727.09(0.01)	19731.43(0.01)	19717.37(0.10)
4.5	19722.02(0.02)	19727.09(0.01)	19700.55[a]
5.5	19716.20(0.01)	19722.02(0.02)	19700.78(0.00)
6.5	19709.55(-0.09)	19716.20(0.01)	19691.51(0.08)
7.5	19702.32(-0.03)	19709.55(-0.09)	19681.30(-0.04)
8.5	19694.30(-0.02)	19702.32(-0.03)	19670.62(0.10)
9.5	19685.49(-0.07)	19694.30(-0.02)	19658.90(-0.06)
10.5	19676.03(-0.03)	19685.49(-0.07)	19646.67(0.01)
11.5	19665.78(-0.04)	19676.03(-0.03)	19633.60(-0.03)
12.5	19654.85(0.00)	19665.78(-0.04)	19619.88(0.02)
13.5	19643.12(-0.01)	19654.85(0.00)	19605.38[0.03)
14.5	19630.68(0.01)	19643.12(-0.01)	19590.30[a]
15.5	19617.46(-0.02)	19630.68(0.01)	19574.17(0.05)
16.5	19603.60(0.06)	19617.46(-0.02)	
17.5		19603.60(0.06)	

[a]Not used in the analysis.

TABLE 7.7   Vacuum wavenumbers (in cm^{-1}) of the rotational lines of the 0-1
              band

$$^2\Pi_{1/2} - {}^2\Sigma^+$$

J	$R_{21ee}(J)$	$R_{22ff}(J)$	$Q_{21fe}(J)$
0.5		18403.10[a]	
1.5	18410.26(-0.03)	18403.19(-0.05)	18403.19[a]
2.5	18413.52[a]	18402.75(-0.03)	18403.19(-0.05)
3.5	18415.75(-0.04)	18401.69(0.01)	18402.75(-0.03)
4.5	18417.60(0.02)	18399.98(-0.04)	18401.69(0.01)
5.5	18418.78(0.05)	18397.55(-0.01)	18399.98(0.04)
6.5	18419.19(-0.04)	18394.58(0.03)	18397.55(-0.01)
7.5	18419.19[a]	18390.93(0.04)	18394.58(0.03)
8.5	18418.36(0.03)	18386.61(0.02)	18390.93(0.04)
9.5	18416.73[a]	18381.61(-0.04)	18386.61(0.02)
10.5	18414.83(-0.01)	18376.09(0.02)	18381.61(-0.04)
11.5	18412.12(-0.01)	18369.85(0.01)	18376.09(0.02)
12.5	18408.84(0.07)	18362.93(-0.04)	18369.85(0.01)
13.5		18355.47(0.02)	18362.93(-0.04)
14.5		18347.30(0.01)	18355.47(0.02)
15.5		18338.46(-0.02)	18347.30(0.01)
16.5		18329.03(0.00)	18338.46(-0.02)
17.5		18318.91(-0.01)	18329.03(0.00)
18.5		18308.16(0.00)	18318.91(-0.01)
19.5		18296.70(-0.05)	18308.16(0.00)
20.5		18284.71(0.02)	18296.70(-0.05)
21.5			18284.71(0.02)

TABLE 7.7 (continued)

$$^2\Pi_{1/2} - {}^2\Sigma^+$$

J	$Q_{22ef}(J)$	$P_{21ee}(J)$	$P_{22ff}(J)$
0.5	18398.72(0.02)	-	-
1.5	18395.94(-0.03)	18398.72(0.02)	18391.74(0.11)
2.5	18392.56(-0.04)	18395.94(-0.03)	-
3.5	18388.62(0.03)	18392.56(-0.04)	-
4.5	18383.96(0.01)	18388.62(0.03)	18370.96(0.02)
5.5	18378.66(0.00)	18383.06(0.01)	18362.93[a]
6.5	18372.71(-0.03)	18378.66(0.00)	18354.01(0.05)
7.5	18366.17(-0.01)	18372.71(-0.03)	18344.50(-0.01)
8.5	18358.98(0.00)	18366.17(-0.01)	18334.35(-0.07)
9.5	18351.12(-0.01)	18358.98(0.00)	18323.73(0.04)
10.5	18342.62(-0.03)	18351.12(-0.01)	18312.29(-0.03)
11.5	18333.51(-0.01)	18342.62(-0.03)	18300.23(-0.08)
12.5	18323.73(-0.02)	18333.51(-0.01)	18287.74(0.09)
13.5	18313.31(-0.03)	18323.73(-0.02)	18274.45(0.09)
14.5	18302.30(0.02)	18313.31(-0.03)	18260.43(0.01)
15.5	18290.55(-0.03)	18302.30(0.02)	18246.00[a]
16.5	18278.22(-0.01)	18290.55(-0.03)	18230.59(-0.03)
17.5	18265.26(0.03)	18278.22(-0.01)	18214.73(-0.02)
18.5	18251.63(0.04)	18265.26(0.03)	
19.5		18251.63(0.04)	

[a]Not used in the analysis.

TABLE 7.8   Vacuum wavenumbers (in cm^{-1}) of the rotational lines of the 0-2 band

$$^2\Pi_{1/2} - {}^2\Sigma^+$$

J	$R_{21ee}(J)$	$R_{22ff}(J)$	$Q_{21fe}(J)$
0.5	-	16347.98[a]	16347.26[a]
1.5	-	16348.29(-0.05)	16347.98[a]
2.5	16358.40(-0.05)	16347.98(0.00)	16348.29(-0.05)
3.5	16361.08(0.10)	16347.01(0.00)	16347.98(0.00)
4.5	16362.84(-0.06)	16345.42(-0.01)	16347.01(0.00)
5.5	16364.11(-0.00)	16343.23(-0.02)	16345.42(-0.01)
6.5	16364.95(0.05)	16340.46(0.00)	16343.23(-0.02)
7.5	16364.95(-0.03)	16337.07(0.01)	16340.46(0.00)
8.5	16364.53(0.08)	16333.06(0.00)	16337.07(0.01)
9.5	16363.37(0.07)	16328.42(-0.02)	16333.06(0.00)
10.5	16361.65(0.12)	16323.21(-0.01)	16328.42(-0.02)
11.5	16359.04(-0.09)	16317.39(0.01)	16323.21(-0.01)
12.5	16356.33[a]	16310.92(-0.02)	16317.39(0.01)
13.5	16352.42(-0.04)	16303.87(-0.02)	16310.92(-0.02)
14.5	16348.29[a]	16296.23(0.01)	16303.87(-0.02)
15.5	16343.23(-0.03)	16287.93(-0.02)	16296.23(0.01)
16.5	16337.74(0.04)	16279.03(-0.03)	16287.93(-0.02)
17.5	16331.48(-0.02)	16269.60(0.05)	16279.03(-0.03)
18.5		16259.47(0.03)	16269.60(0.05)
19.5		16248.66(-0.05)	16259.47(0.03)
20.5		16237.42(0.06)	16248.66(-0.05)
21.5		16225.41(0.01)	16237.42(0.06)
22.5		16212.81(-0.01)	16225.41(0.01)
23.5			16212.81(-0.01)

Table 7.8 continued

$$^2\Pi_{1/2} - {}^2\Sigma^+$$

J	$Q_{22ef}(J)$	$P_{21ee}(J)$	$P_{22ff}(J)$
0.5	16343.75(0.03)	-	-
1.5	16341.08(0.03)	16343.75(0.03)	
2.5	16337.74(-0.04)	16341.08(0.03)	16330.63(0.08)
3.5	16333.89(-0.01)	16337.74(-0.04)	16323.80(0.02)
4.5	16329.41(0.00)	16333.89(-0.01)	16316.36(-0.04)
5.5	16324.31(-0.01)	16329.41(0.00)	16308.43(0.01)
6.5	16318.62(0.00)	16324.31(-0.01)	16299.79(-0.05)
7.5	16312.31(0.00)	16318.62(0.00)	16290.67(0.02)
8.5	16305.29(-0.01)	16312.31(0.00)	16280.90(0.04)
9.5	16297.91(0.02)	16305.29(-0.01)	16270.49(0.03)
10.5	16289.77(0.01)	16297.91(0.02)	16259.47(0.03)
11.5	16280.99(-0.04)	16289.77(0.01)	16247.87(0.02)
12.5	16271.72(0.02)	16280.99(-0.04)	16235.65(0.01)
13.5	16261.75(0.00)	16271.72(0.02)	16222.84(0.01)
14.5	16251.23(0.03)	16261.75(0.00)	16209.42(0.01)
15.5	16240.05(0.01)	16251.23(0.03)	16195.37(-0.02)
16.5	16228.32(0.05)	16240.05(0.01)	16180.71(-0.05)
17.5	16215.86(-0.03)	16228.32(0.05)	
18.5	16202.90(-0.01)	16215.86(-0.03)	
19.5	16189.28(-0.03)	16202.90(-0.01)	
20.5		16189.28(-0.03)	

[a]Not used in the analysis.

expressions of their respective branches [Eq. 7.1] and the molecular constants were estimated by the method of least-squares. The $(\nu_{obs} - \nu_{calc})$ values, obtained from the least-squares fits of the vacuum wavenumbers of individual bands, are given in those tables in parentheses. However, these values are not given for a few spectral lines which are not used in the analysis. In general, the standard deviation of such a least-squares fit is ~0.04 cm^{-1}.

The molecular constants obtained from the analyses of the bands of comet-tail (A-X) and the Baldet-Johnson (B-A) systems of $^{13}C^{18}O^+$ were merged together. The $T_v' - T_v''$ values thus obtained for the comet-tail bands are listed in Table 7.1. The $T_v' - T_v''$ values given for the 0-1 and 0-2 bands in this table were obtained from the origin of the $^2\Pi_{1/2} - {}^2\Sigma^+$ sub-band and the A_0 value. The merged rotational constants B_v and D_v of the X and B states and γ_v values of the B state for various vibrational levels are listed in Table 7.9. The values of γ_v for the v=0, 1, and 2 levels of state X could not be determined in the present analysis because the spin-splitting of the rotational levels in this state is not observed. The rotational constants B_v, D_v, A_v, A_{Dv}, p_v, and q_v obtained for the $A^2\Pi_i$ state, from the same merged fit are listed separately in Table 7.10. The values obtained for the Λ-doubling parameter q_v appear to be slightly irregular, but those for all the other parameters are consistent and reasonably accurate. The values B_e and

TABLE 7.9   Rotational constants[a] (in cm^{-1}) of the $X^2\Sigma^+$ and $B^2\Sigma^+$ states of $^{13}C\ ^{18}O^+$

Vibrational Level	$X^2\Sigma^{+b}$		$B^2\Sigma^+$		
	B_v	$D_v \times 10^6$	B_v	$D_v \times 10^6$	$\gamma_v \times 10^3$
0	1.78554(8)	4.3(1)	1.6199(1)	4.4(2)	18.1(3)
1	1.7688(1)	1.5(2)	1.5943(1)	5.8(2)	17.0(5)
2	1.7543(3)	8.8(3)			

[a]The number in the parentheses indicates the uncertainty in the last digit and corresponds to one standard deviation.

[b]The γ_v values could not be estimated for the vibrational levels of the $X^2\Sigma^+$ state from the observed data.

TABLE 7.10 Rotational constants[a] (in cm^{-1}) of the A$^2\Pi_i$ state of ^{13}C ^{18}O$^+$

Vibrational Level	B$_v$	D$_v$ x 10^6	A$_v$	A$_{D_v}$ x 10^2	p$_v$ x 10^2	q$_v$ x 10^4
0	1.4340(1)	5.0(2)	-122.151(6)	-3.133(3)	-0.96(4)	-1.3(8)
1	1.4167(1)	3.4(2)	-122.062(6)	-3.089(3)	-0.65(4)	-12.3(7)
2	1.39972(9)	5.0(1)	-121.982(6)	-3.051(3)	-0.82(4)	+3.4(7)
3	1.38264(8)	3.2(1)	-121.712(6)	-3.000(3)	-1.12(5)	-0.7(2)
4	1.36566(9)	2.8(1)	-121.697(6)	-2.938(4)	-0.45(5)	-2.4(5)
5	1.34975(9)	6.4(2)	-121.618(8)	-2.865(5)	-0.52(5)	+3.8(1.5)

[a]The number in the parentheses indicates the uncertainty in the last digit and corresponds to one standard deviation.

α_e for the X and B states listed in Table 7.11 were obtained from the B_v values given in Table 7.9. For the A state, the B_e and α_e were obtained from the B_v values listed in Table 7.10, and are presented in Table 7.11. The equilibrium internuclear distance (r_e) and the corresponding moment of inertia (I_e) for states X, A, and B, calculated from their B_e values, are listed in Table 7.11.

(ii) Vibrational Analysis and Isotope Shifts

The ($T_v{}' - T_v{}''$) values of the comet-tail (A-X) bands (see Table 7.1) and the Baldet-Johnson (B-A) bands (see Table 6.1) were fitted together to Eq. [3.6] and the system origin (ν_e) of the comet-tail system and the vibrational constants of its states X and A were obtained simultaneously. The T_e value of state A, which is identical to the system origin of the A-X system, and the vibrational constants of the A and X states are listed in Table 7.11. As only the v=0 and 1 levels of state B are observed, its vibrational constants could not be obtained directly. Hence the system origin ν_e of the B-A system of $^{13}C^{18}O^+$ is assumed to be the same as that of $^{12}C^{16}O^+$ and is taken from Huber and Herzberg (1979). This system origin, the vibrational constants of $A^2\Pi_i$ (see Table 7.11) and the ($T_v{}' - T_v{}''$) values of the 1-0 and 0-0 bands of B-A system (see Table 6.1) of $^{13}C^{18}O^+$ were used in Eq. [3.6] to obtain ω_e and $\omega_e x_e$ of the B state and these estimated values are listed in Table 7.11. The T_e

TABLE 7.11 'Equilibrium molecular constants[a] (in cm^{-1}, unless stated otherwise) of the $X^2\Sigma^+$, $A^2\Pi_i$, and $B^2\Sigma^+$ states of ^{13}C $^{18}O^+$

Molecular Constant	$X^2\Sigma^+$	$A^2\Pi_i$	$B^2\Sigma^+$
T_e	0.0	$20732.6_7(3)$	45876.1
ω_e	$2110.3_0(3)$	$1488.0_8(3)$	1653.9_2
$\omega_e x_e$	$13.82_8(9)$	$12.44_5(9)$	25.6_1
$\omega_e y_e$	——	$0.026_5(9)$	——
B_e	1.79415(8)	1.44177(8)	1.63239(8)
α_e	0.01701(6)	0.01683(2)	0.02582(6)
r_e (Å)	1.1156	1.2445	1.1696
I_e (g.cm^2)	1.5603×10^{-39}	1.9416×10^{-39}	1.7149×10^{-39}

[a]The number in the parentheses indicates the uncertainty in the last digit and corresponds to one standard deviation.

value of the $B^2\Sigma^+$ state is obtained, by adding the system origin of the B-A system and the T_e value of the A state, and given in the same table. The ten $(T_v' - T_v'')$ values (see Tables 6.1 and 7.1) arising from eleven different vibrational levels of states X, A, and B could not be reduced to the vibrational term values because the corresponding system of equations is underdetermined.

In order to obtain the isotope shifts ($\Delta\nu$) of the comet-tail bands of $^{13}C^{18}O^+$ from the corresponding bands of $^{12}C^{16}O^+$, the $(T_v' - T_v'')$ values of $^{12}C^{16}O^+$ were calculated from Eq. [3.6] using the vibrational constants of the A and X states, listed by Huber and Herzberg (1979), because recent experimental values of $(T_v' - T_v'')$ are not readily available. The isotope shifts, which correspond to the differences between the calculated $(T_v' - T_v'')$ values of the bands of $^{12}C^{16}O^+$ and those of the corresponding bands of $^{13}C^{18}O^+$ obtained in the present work (see Table 7.1), are listed in Table 7.12. The isotope shifts were also calculated from Eq. [3.11] using the vibrational constants of the A and X states of $^{12}C^{16}O^+$ and the value of the ρ (see Section 6.3(ii)), and are listed in the same table. The agreement between the observed and the calculated isotope shifts is very good.

(iii) Franck-Condon Factors

According to the relative intensities of the 0-0 and 1-1 bands of the comet-tail system of $^{12}C^{16}O^+$, originally

TABLE 7.12 Isotope Shifts (in cm^{-1}) in the Comet-tail system of ^{13}C ^{18}O$^+$

Band	Observed[a]	Calculated
	Isotope Shift $\Delta\nu$ (^{12}C ^{16}O$^+$ − ^{13}C ^{18}O$^+$)	
5-0	315.85	314.92
4-0	254.60	253.77
3-0	190.98	190.19
2-0	124.66	124.16
1-1	-45.11	-45.65
0-1	-116.01	-116.61
0-2	-214.58	-215.14

[a] Relative to the $(T_v' - T_v'')$ values of ^{12}C ^{16}O$^+$ calculated from its constants listed by Huber and Herzberg (1979).

given by Baldet (1925b,c) and listed by Krupenie (1966), the 0-0 band is stronger than the 1-1 band. But in the present investigation, it is found that the 1-1 band in both $^{12}C^{16}O^+$ and $^{13}C^{18}O^+$ appears with medium intensity where as the 0-0 band is too weak to be identified precisely. In order to re-solve this controversy, the Franck-Condon factors for the bands of comet-tail system of $^{12}C^{16}O^+$ and $^{13}C^{18}O^+$ were calcu-lated using a Klein-Dunham potential, according to the theory discussed in Section 3.2. In calculating the FCFs for the bands of $^{12}C^{16}O^+$, the constants listed by Huber and Herzberg (1979) for the $A^2\Pi_i$ and $X^2\Sigma^+$ states were used. The molecular constants obtained for the A and X states of $^{13}C^{18}O^+$ in the present work (see Table 7.11) were used to calculate the FCFs for the bands of $^{13}C^{18}O^+$. These calculated FCFs are listed in Table 7.13. Earlier, Nicholls (1962) calculated the FCFs for the bands of the comet-tail system of $^{12}C^{16}O^+$ using the Morse potential. Later Krupenie and Benesch (1968) improved these values using the RKR potential. The values obtained by Krupenie and Benesch (1968) are also listed in Table 7.13 for comparison and the agreement between these values and those obtained in the present work is excellent. Hence it can be concluded that the FCFs obtained for the bands of $^{13}C^{18}O^+$ for the first time are also accurate. In the present calculations and in those of Nicholls (1962) and Krupenie and Benesch (1968) the FCF of the 0-0 band is found to be very much

TABLE 7.13   Franck-Condon factors for the bands of the Comet-tail system of
the $^{12}C^{16}O^+$ and $^{13}C^{18}O^+$ molecules

Band	$^{12}C^{16}O^+$		$^{13}C^{18}O^+$
	Present	Krupenie and Benesch (1968)	
5-0	0.122	0.122	0.128
4-0	0.159	0.158	0.160
3-0	0.180	0.180	0.175
2-0	0.167	0.167	0.156
1-0	0.113	0.113	0.102
2-1	0.099	0.099	0.110
0-0	0.042	0.042	0.036
1-1	0.193	0.193	0.190
0-1	0.152	0.152	0.137
0-2	0.251	0.251	0.239

smaller (approximately five times) than that of the 1-1 band which is in good agreement with the present observation.

FIRST NEGATIVE $(B^2\Sigma_u^+ - X^2\Sigma_g^+)$ SYSTEM OF $^{15}N_2^+$

In this chapter, the observation of fifteen bands of the first negative $(B^2\Sigma_u^+ - X^2\Sigma_g^+)$ system of $^{15}N_2^+$ and the rotational analysis of twelve of them are presented. The previous work on this system is reviewed in Section 8.1. Also given in this section is a brief description of the experimental details that are pertinent to the present investigation. In Section 8.2, the rotational structure of a $^2\Sigma^+ - ^2\Sigma^+$ transition is discussed. Finally, the results obtained from the rotational and vibrational analysis of this system are presented in Section 8.3. The perturbations observed in the v=0 level of state B are also discussed in the same section.

8.1 Introduction

Even though the first negative $(B^2\Sigma_u^+ - X^2\Sigma_g^+)$ system was first observed more than a century ago, Fassbender (1924) was the first to perform a partial rotational analysis of a few bands and list the band head positions for thirty-six bands. Merton and Pilley (1925) and Herzberg (1928) observed many bands of this system under low resolution and the latter gave the most complete vibrational analysis of this

system. Coster and Brons (1931, 1932), Parker (1933a,b), Brons (1934, 1935), Childs (1932), and Crawford and Tsai (1935) performed the rotational analysis of many bands of this system and studied the perturbations in various vibrational levels of the $B^2\Sigma_0^+$ state. Later, Douglas (1952) and Tyte (1962, 1963) studied this system extensively and found a number of new bands degraded to longer wavelengths and analyzed the rotational structure of some of these bands. Klynning and Pages (1972) analyzed the rotational structure of six bands, degraded to shorter wavelengths. The previous work done on this system has been published in the form of review articles by Tyte and Nicholls (1965) and Lofthus and Krupenie (1977).

The most recent investigations of the first negative system of $^{14}N_2^+$ began with the work of Dick et al. (1978) who photographed some bands under high resolution and reported preliminary results of their analysis. Later Gottscho et al. (1979) performed a complete deperturbation of this system and presented most precise constants for the X, A, and B states of this molecule and also reported that there is no evidence of $a^4\Sigma_u^+ - B^2\Sigma_u^+$ perturbations and $A^2\Pi_{i,u}$ is the only state causing perturbations in the $B^2\Sigma_u^+$ state. Chevaleyre and Perrot (1981) performed the rotational analysis of some bands degraded to longer wavelengths and analyzed some perturbations in the higher vibrational levels of state B. Recently, Klynning and Pages (1982) reanalyzed twenty-five bands of

this system and presented the molecular constants for the X, A, B, and $C^2\Sigma_u^+$ states obtained from the term value approach, using seventy one bands in total.

The bands of the first negative system of $^{14}N_2^+$ arising from the vibrational levels $v \leq 11$ of the upper state are strong and degraded to shorter wavelengths, whereas those arising from the vibrational levels $v \geq 11$ are very weak and degraded to longer wavelengths. The bands arising from the levels $v=8$ to 11 of state B, depending on the lower state vibrational levels to which the transitions are taking place, either belong to one of these two categories or appear without any head. In most of the excitation conditions, the bands of this system are overlapped by those of the second positive $(C^3\Pi_u - B^3\Pi_g)$ system of $^{14}N_2$. Under favorable conditions, the intensity of the second positive system may be reduced but it is very difficult to suppress it completely. Because of these reasons, the rotational analysis of the first negative system of $^{14}N_2^+$ is very complex.

Although the work done on the first negative system of $^{14}N_2^+$ is very extensive, the work done on this system of the isotopically substituted nitrogen ions $(^{14}N^{15}N)^+$ and $^{15}N_2^+$, is very fragmentary. The work done by Wood and Dieke on this system of $(^{14}N^{15}N)^+$ (1938) and $^{15}N_2^+$ (1940) confirmed the vibrational numbering of the bands of this system. Wood and Dieke (1940) measured the rotational structure of 1-0, 0-0, 1-2, 0-1, and 0-2 bands of $^{15}N_2^+$ and estimated the

nuclear spin of ^{15}N, but did not report the molecular constants
of the B and X states from their analysis. Colbourn and
Douglas (1977) reported the observation of the 0-0 band of
this system of $^{15}N_2^+$ without giving the rotational analysis.
The molecular constants of the B and X states of $^{15}N_2^+$ have
not yet been estimated from the experimental data and the
perturbations occurring in its B state have also not been
analyzed. The main objective of the present study of this
system of $^{15}N_2^+$ is to obtain accurate molecular constants
for the B and X states and understand the perturbations
occurring in the rotational structure of the bands of this
system.

The first negative system of $^{15}N_2^+$ was excited in the
cathode glow of the hollow-cathode discharge tube. Fifteen
bands of this system were photographed under medium dispersion
in the first order of a 600 grooves/mm grating on a Bausch
and Lomb spectrograph. Except for the very weak 3-5 and
3-6 bands, the rest were photographed under high resolution.
The 0-2, 1-3, and 2-4 bands were photographed in the third
order of a 1200 grooves/mm grating on the Bausch and Lomb
spectrograph. Of the remaining ten bands (2-1, 1-0, 1-1,
0-0, 2-3, 1-2, 0-1, 2-5, 1-4, and 0-3) which were photographed
on the Jarrell-Ash spectrograph, the 0-3, 1-4, and 2-5 bands
were recorded in the second order and the rest were recorded
in the third order of a 1200 grooves/mm grating. The exposure
times for the high resolution spectra photographed on the

Bausch and Lomb spectrograph are about 5 minutes, and those photographed on the Jarrell-Ash spectrograph vary from 5 seconds (for the strong lines of the 0-0 band) to five hours (for the 0-3, 1-4, and 2-5 bands). Kodak Spectrum Analysis No. 1, 103 a-O, and 103-F plates were used to photograph the spectra. The slit width was maintained at 20 μm on the Bausch and Lomb spectrograph but it was varied from 15 μm to 30 μm on the Jarrell-Ash spectrograph, depending on the intensity of the band. The reciprocal dispersions of the spectra vary from 0.51 Å/mm at 4200 Å in third order to 0.95 Å/mm at 5100 Å in the second order. The measurements of the spectral lines are accurate up to ~0.002 Å.

8.2 Rotational Structure of a $^2\Sigma^+$ – $^2\Sigma^+$ System

In most of the situations, a $^2\Sigma^+$ state belongs to Hund's case (b) and hence, a $^2\Sigma^+$ – $^2\Sigma^+$ system represents pure case (b) transition. In this case, the quantum number N of the total angular momentum, apart from spin, is defined. The rotational structure of a band belonging to this system contains four main branches R_1, R_2, P_1, and P_2 and two satellite branches $^RQ_{21}$ and $^PQ_{12}$. A schematic energy level diagram showing all these six branches is given in Figure 24. The selection rules to be satisfied for the main branches (indicated by the solid lines in this figure) of this transition are
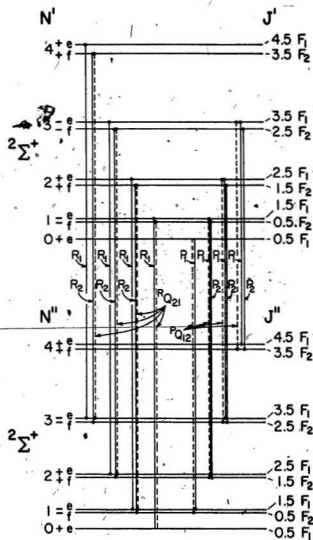
Figure 24. A schematic energy level diagram showing the first few rotational transitions in a band of a $^2\Sigma^+ - {}^2\Sigma^+$ system.

$$\Delta N = \pm 1, \quad e \longleftrightarrow e, \quad f \longleftrightarrow f$$

$$+ \longleftrightarrow -, \quad + \longleftrightarrow +, \quad - \longleftrightarrow -$$

The selection rules for the satellite branches (shown in dashed lines in Figure 24) are

$$\Delta J = 0 \text{ and } e \longleftrightarrow f.$$

The labelling of these satellite branches, $^RQ_{21}$ and $^PQ_{12}$, is dependent upon their proximity to the R and P branches, respectively. The intensity of these satellite branches is always small compared to that of the main branches and falls off very rapidly with increasing N. In some instances, the satellite branches may be too weak to be observed.

The rotational levels of a $^2\Sigma^+$ state in Hund's case (b) are given by Eqs. [6.1] and [6.2]. The expressions for the six branches of a $^2\Sigma^+ - {}^2\Sigma^+$ can be obtained from Eqs. [6.1] and [6.2], according to the general expression,

$$\nu = \nu_0 + F_\Sigma{}'(N') - F_\Sigma{}''(N''), \qquad [8.1]$$

with $N'' = N$. Here ν_0 is the band origin and F_Σ are the expressions for the rotational levels of a $^2\Sigma$ state. The quantum number N' takes values N+1 and N-1 for R and P branches, respectively, in accordance with the selection rules given above. The expressions for all the six branches are explicitly given by Herzberg (1950).

8.3 Analysis of the Spectra

The first negative $(B^2\Sigma_u^+ - X^2\Sigma_g^+)$ system of $^{15}N_2^+$, photographed under medium dispersion, is shown in Figure 25. In all, fifteen bands degraded to shorter wavelengths are identified here. In addition, some bands of the second positive $(C^3\Pi_u - B^3\Pi_g)$ system of $^{15}N_2$ can also be seen. The 3-5 and 3-6 bands of the first negative system, which are very weak, were neither measured under medium dispersion nor photographed under high resolution. The vacuum wavenumbers of the band heads of all the remaining thirteen bands measured on plates photographed under high resolution, their relative intensities, and the vibrational quantum numbers are given in Table 8.1.

(i) Rotational Analysis

The rotational structure of the 1-3 band of the first negative system of $^{15}N_2^+$ photographed under high resolution on the Bausch and Lomb spectrograph is shown in Figure 26. It is clearly seen in this figure that the rotational lines with the odd N values are stronger than those with the even N values, giving alternation of intensity in the band. The alternation of the intensity, which is observed for all the bands of this system, can be understood on the basis of the nuclear spin of 1/2 for the ^{15}N nucleus (see Herzberg, 1950; p. 135, 209). Similar alternation of intensity is expected in the rotational structure of the bands of the neutral $^{15}N_2$

Figure 25. The emission band systems produced in the cathode glow of the hollow-cathode discharge tube by the excitation of the $^{15}N_2$ molecules in the region 3475 – 5206 Å. (a) First negative $(B^2\Sigma_u^+ - X^2\Sigma_g^+)$ system of $^{15}N_2^+$ and (b) Second positive $(C^3\Pi_u - B^3\Pi_g)$ system of $^{15}N_2$. Dot (.) represents the band head of the second positive system of $^{14}N^{15}N$ and dagger (†) represents the band head of the first negative system of $(^{14}N^{15}N)^+$. This spectrum is photographed on Bausch and Lomb spectrograph in the first order of a 600 grooves/mm grating.

- 192 -
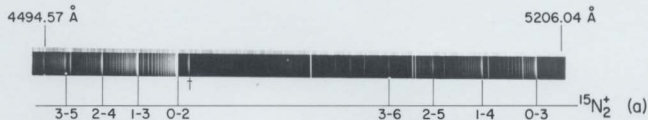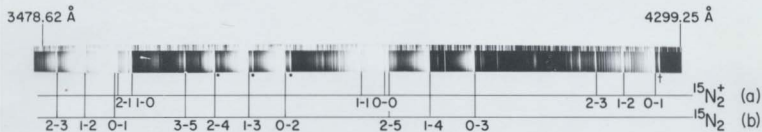
TABLE 8.1 First negative (B $^2\Sigma_u^+$ – X $^2\Sigma_g^+$) band system of the $^{15}N_2^+$ molecule

Band Head (cm^{-1})	Band Origin[a] (cm^{-1})	Relative Intensity[b]	Assignment v'–v"
27968.4	27997.49[c]	m	2-1
27827.6	27855.985(6)	m	1-0
25729.0	25753.656(6)	m	1-1
25538.4	25562.783(6)	vs	0-0
23862.4	23884.296(6)	w	2-3
23659.9	23681.709(7)	m	1-2
23438.7	23460.493(5)	s	0-1
21854.2	21873.709(6)	w	2-4
21620.9	21640.266(6)	m	1-3
21369.1	21388.491(6)	s	0-2
19876.8	19894.179(14)	vw	2-5
19612.5	19629.869(7)	w	1-4
19329.8	19347.246(6)	m	0-3

[a]The number in the parentheses indicates the uncertainty in the last digit and corresponds to one standard deviation.

[b]Abbreviations for relative intensities vs, s, m, w, and vw represent very strong, strong, medium, weak, and very weak respectively.

[c]Calculated from the term values of v'=2 and v"=1 levels.

Figure 26. Rotational structure of the 1-3 band of the first negative $(B^2\Sigma_u^+ - X^2\Sigma_g^+)$ system of $^{15}N_2^+$ photographed on the Bausch and Lomb spectrograph in the third order of a 1200 grooves/mm grating.

2-4 Band
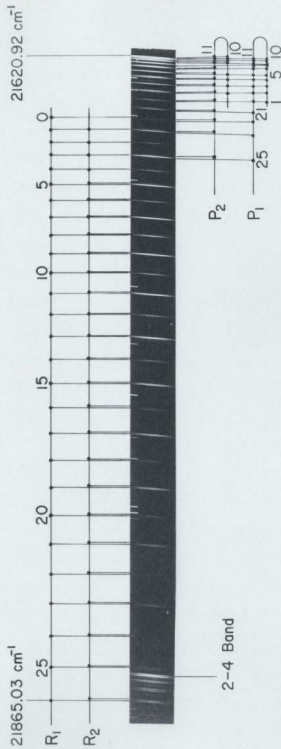
molecule. The electron spin splitting of the rotational lines can also be clearly seen in Figure 26 for the spectral lines with $N \geq 5$. Similar splitting of the rotational lines is observed in all the bands with $v' = 0$ for $N \geq 19$ and in those with $v' = 1$ for $N \geq 5$. Of all the four bands with $v' = 2$, photographed under high resolution, the rotational structure of the 2-1 band could not be analyzed because it is overlapped by the strong 0-1 band of the second positive system of $^{15}N_2$. In the remaining three bands (2-3, 2-4, and 2-5), the rotational lines are identified only up to $N = 19$ and for all these spectral lines the spin splitting is not observed. The satellite branches $^PQ_{12}$ and $^RQ_{21}$ are not observed in any of the bands of this system. In the rotational structure of the 0-0 band, the lines in the P_1 and P_2 branches with $N = 22$ to 32 could not be identified because these lines are overlapped by the strong lines of the R_1 and R_2 branches as well as the initial lines of the P_1 and P_2 branches. The rotational quantum numbers and the vacuum wavenumbers of the spectral lines of all the twelve bands analyzed in the present work are listed in Tables 8.2 to 8.13. The vacuum wavenumbers of the spectral lines of all the branches of a band were simultaneously fitted to the expressions of the R_1, R_2, P_1, and P_2 branches [Eq. 8.1] and the molecular constants were estimated by the method of least-squares. The $(\nu_{obs} - \nu_{calc})$ values, obtained from the least-squares fits of the vacuum wavenumbers of individual bands, are given in parentheses in these

TABLE 8.2   Vacuum wavenumbers (in cm^{-1}) of the rotational lines of the 1-0 band

N	R$_1$(N)	R$_2$(N)	P$_1$(N)	P$_2$(N)
0	27859.84(0.01)	-	-	-
1	27863.94(0.02)	27863.94(0.06)	27852.44(0.02)	27849.09(0.05)
2	27868.25(0.00)	27868.25(0.06)	27849.09(0.01)	27845.98(0.05)
3	27872.84(0.02)	27872.75[a]	27845.98(-0.01)	27845.98(0.05)
4	27877.58(-0.05)	27877.58(0.05)	27843.12(-0.02)	27843.12(0.06)
5	27882.54(-0.05)	27882.59(0.02)	27840.54(0.00)	27840.43(-0.01)
6	27888.00(0.01)	27887.87(0.03)	27838.16(-0.02)	27838.05(-0.01)
7	27893.49(-0.05)	27893.33(-0.04)	27836.06(0.00)	27835.86(-0.07)
8	27899.30(-0.02)	27899.10(-0.03)	27834.17(-0.02)	27833.98(-0.06)
9	27905.35(0.00)	27905.11(-0.02)	27832.60(0.04)	27832.43(0.04)
10	27911.64(0.03)	27911.37(-0.01)	27831.15(-0.02)	27831.02(0.03)
11	27918.11(-0.01)	27917.83(-0.04)	27830.01(-0.02)	27829.75(-0.08)
12	27924.89(0.02)	27924.59(0.00)	27829.17(0.04)	27828.88(-0.03)
13	27931.88(0.02)	27931.53(-0.03)	27828.54(0.06)	27828.20(-0.04)
14	27939.12(0.03)	27938.74(-0.03)	-	-
15	27946.60(0.04)	27946.20(-0.02)	27827.85(-0.05)	27827.58(-0.05)
16	27954.29(0.02)	27953.91(0.00)	27827.95(-0.03)	27827.65(-0.04)
17	27962.20(-0.02)	27961.81(-0.01)	-	27827.95(-0.04)
18	27970.40(-0.01)	27970.03(0.03)	27828.88(0.02)	27828.54(0.00)
19	27978.83(-0.01)	27978.43(0.03)	27829.75(0.08)	27829.30(-0.03)
20	27987.48(-0.02)	27987.06(0.02)	27830.76(0.04)	27830.35(-0.01)
21	27996.38(-0.02)	27995.94(0.02)	27832.03(0.02)	27831.61(-0.02)
22			27833.60(0.06)	27833.12(-0.03)
23			27835.32(0.00)	27834.92(0.01)
24			27837.30(-0.03)	27836.91(0.01)
25			27839.61(0.02)	27839.17(0.03)
26			27842.08(-0.01)	27841.61(-0.02)
27			27844.84(0.01)	27844.30(0.04)
28			27847.81(0.00)	27847.22(-0.09)
29			27851.02(-0.01)	27850.55(0.04)
30			-	-
31			27858.20(0.01)	27857.72(0.09)
32			-	-
33			27866.24(-0.06)	27865.71(0.00)
34			-	-
35			27875.30(-0.06)	27874.77(0.04)

[a] Not used in the analysis.

TABLE 8.3   Vacuum wavenumbers (in cm^{-1}) of the rotational lines of the
band

N	$R_1(N)$	$R_2(N)$	$P_1(N)$	$P_2(N)$
0	25757.48(-0.02)			
1	25761.62(0.00)	25761.62(0.03)	25750.11(-0.01)	
2	25766.00(-0.02)	25766.00(0.03)	25746.84(-0.01)	25746.84(0.04)
3	25770.67(-0.03)	25770.67(0.05)	25743.82(-0.04)	25743.82(0.03)
4	25775.56^a	25775.56(0.01)	25741.10(-0.04)	25741.10(0.04)
5	25780.85(-0.03)	25780.77(0.01)	25738.66(-0.05)	25738.61(0.00)
6	25786.37(-0.01)	25786.25(0.00)	25736.52(-0.03)	
7	25792.18(0.01)	25791.98(-0.03)	25734.63(-0.04)	
8	25798.26(0.03)	25798.06(0.01)	25733.02(-0.05)	
9	25804.58(0.02)	25804.33(-0.03)	25731.76(0.01)	25731.60(0.03)
10	25811.22(0.05)	25810.93(-0.02)		
11	25818.09(0.03)	25817.75(-0.07)	25729.96(0.02)	25729.69(-0.04)
12	25825.27(-0.05)	25824.94(-0.02)		25729.27(0.05)
13	25832.69(0.04)	25832.35(-0.02)	25729.27(0.03)	25728.99(-0.01)
14	25840.40(0.04)	25840.09(0.03)	25729.27(-0.04)	25728.99(-0.06)
15	25848.39(0.05)	25847.99(-0.03)	25729.69(0.03)	
16	25856.64(0.04)	25856.23(-0.02)	25730.31(0.03)	25729.96(-0.02)
17	25865.15(0.02)	25864.74(-0.01)	25731.21(0.03)	25730.84(-0.03)
18	25873.93(0.00)	25873.53(-0.01)	25732.41(0.05)	25732.05(0.02)
19	25883.03(0.03)	25882.57(-0.02)	25733.88(0.06)	25733.51(0.04)
20	25892.30(-0.04)	25891.87(-0.04)	25735.58(0.02)	25735.16(-0.03)
21	25901.96(0.00)	25901.52(0.01)		
22	25911.78(-0.06)	25911.35(-0.02)	25739.81(-0.05)	25739.43(-0.02)
23	25921.99(0.00)	25921.50(0.00)	25742.41(-0.01)	25741.98(-0.02)
24	25932.37(-0.05)	25931.91(0.00)		25744.80(-0.02)
25	25943.11(0.00)	25942.61(0.00)	25748.35(-0.03)	25747.91(-0.01)
26	25954.05(-0.02)	25953.55(0.03)		25751.33(0.03)
27	25965.26(-0.03)	25964.79(0.07)		25754.96(0.01)
28			25759.46(0.07)	25758.81(-0.06)
29	25988.53(-0.02)	25987.95(0.02)	25763.57(-0.04)	25763.09(0.02)
30				
31			25772.81(-0.06)	25772.36(0.06)

^{a}Not used in the analysis.

TABLE 8.4 . Vacuum wavenumbers[a] (in cm^{-1}) of the rotational lines of the 0-0 band

N	$R_1(N)$	$R_2(N)$	$P_1(N)$[b]	$P_2(N)$[b]
1	25570.77(-0.03)	25570.77(-0.03)	25559.21(0.03)	
2	25575.25(0.00)	25575.25(0.00)	25555.85(-0.02)	25555.85(-0.02)
3	25579.99(0.02)	25579.99(0.02)	25552.87(0.02)	25552.87(0.02)
4	25584.96(-0.02)	25584.96(-0.02)	25550.16(0.04)	25550.16(0.04)
5	25590.29(0.01)	25590.29(0.01)	25547.67(0.00)	25547.67(0.00)
6	25595.84(-0.01)	25595.84(-0.01)	25545.53(0.03)	25545.53(0.03)
7	25601.71(0.00)	25601.71(0.00)	25543.62(0.00)	25543.62(0.00)
8	25607.87(0.01)	25607.87(0.01)	25542.05(0.03)	25542.05(0.03)
9	25614.29(0.01)	25614.29(0.01)	25540.68(-0.03)	25540.68(-0.03)
10	25620.95(-0.04)	25620.95(-0.04)	25539.66(-0.02)	25539.66(-0.02)
11	25627.97(0.00)	25627.97(0.00)	25538.90(-0.04)	25538.90(-0.04)
12	25635.25(0.01)	25635.25(0.01)	25538.37(-0.11)	25538.37(-0.11)
13	25642.78(-0.01)	25642.78(-0.01)	25538.37(0.07)	25538.37(0.07)
14	25650.65(0.03)	25650.65(0.03)	25538.37(-0.04)	25538.37(-0.04)
15	25658.73(0.01)	25658.73(0.01)	25538.90(0.10)	25538.90(0.10)
16	25667.09(-0.02)	25667.09(-0.02)		
17	25675.77(0.00)	25675.77(0.00)	25540.45(0.01)	25540.45(0.01)
18	-	-	25541.69(0.01)	25541.69(0.01)
19	25693.98	25693.75	25543.18(-0.02)	25543.18(-0.02)
20	25703.37	25701.80	25544.98(-0.02)	25544.98(-0.02)
21	25712.98	25713.43	25547.09(0.00)	25547.09(0.00)
22	25722.40	25723.34		
23	25737.33	25733.51		
24	25745.42	25743.20		
25	25755.78	25755.63		
26	25766.74	25766.74		
27	25777.15	25778.06		
28	25791.02	25789.81		
29	25802.60	25801.80		
30	25814.80	25814.13		
31	25827.33	25826.66		
32	25840.09	25839.53		
33	25853.22	25852.65	25595.40	25594.81
34	25866.63	25866.06	25601.17	25600.58
35	25880.31	25879.72	25607.26	25606.66
36	25894.19	25893.68	25613.70	25613.06
37	25908.50	25907.89	25620.28	25619.70
38	25922.93	25922.30	25627.24	25626.62
39	25937.76	25937.20	25634.42	25633.88
40	25952.70	25952.36	25641.98	25641.38

TABLE 8.4 (continued)

N	$R_1(N)$	$R_2(N)$	$P_1(N)$[b]	$P_2(N)$[b]
41	25968.11	25967.53	25649.75	25649.23
42			25657.93	25657.41
43	25999.54	25998.98	25666.14	25665.57

[a] The $(\nu_{obs} - \nu_{calc})$ values are given in parentheses only for the unperturbed lines which are used in the analysis.

[b] The lines in the $P_1(N)$ and $P_2(N)$ branches with N=22 to 32 which fall in the returning branch could not be identified correctly.

TABLE 8.5   Vacuum wavenumbers (in cm^{-1}) of the rotational lines of the 2-3 band

N	$R_1(N)$	$R_2(N)$	$P_1(N)$	$P_2(N)$
1	23892.20(-0.03)	23892.20(-0.03)		
2	23896.55(-0.07)	23896.55(-0.07)		
3	23901.30(0.00)	23901.30(0.00)	23874.80(0.01)	23874.80(0.01)
4	23906.36(0.07)	23906.36(0.07)	23872.22(0.01)	23872.22(0.01)
5	23911.56(-0.01)	23911.56(-0.01)	23869.92(0.00)	23869.92(0.00)
6	23917.15(0.00)	23917.15(0.00)	23867.94(0.01)	23867.94(0.01)
7	23923.06(0.03)	23923.06(0.03)	23866.26(0.01)	23866.26(0.01)
8	23929.20(-0.01)	23929.20(-0.01)	23864.88(0.02)	23864.88(0.02)
9	23935.69(0.01)	23935.69(0.01)	23863.81(0.03)	23863.81(0.03)
10	23942.44(-0.01)	23942.44(-0.01)	23862.97(-0.02)	23862.97(-0.02)
11	23949.52(0.01)	23949.52(0.01)	23862.46(-0.04)	23862.46(-0.04)
12	23956.86(-0.01)	23956.86(-0.01)		
13	23964.48(-0.04)	23964.48(-0.04)	23862.46(0.03)	23862.46(0.03)
14	23972.49(0.03)	23972.49(0.03)	23862.81(-0.03)	23862.81(-0.03)
15	23980.70(0.00)	23980.70(0.00)	23863.53(-0.02)	23863.53(-0.02)
16			23864.57(0.01)	23864.57(0.01)
17			23865.88(0.01)	23865.88(0.01)

TABLE 8.6   Vacuum wavenumbers (in cm^{-1}) of the rotational lines of the 1-2 band

N	$R_1(N)$	$R_2(N)$	$P_1(N)$	$P_2(N)$
0	23685.52(-0.01)	-	-	-
1	23689.62(-0.07)	23689.62(-0.03)	23678.19(0.01)	-
2	23694.18(0.03)	23694.18(0.08)	23674.97(-0.01)	23674.97(0.03)
3	23698.86(-0.07)	23698.86(0.00)	23672.08(-0.01)	23672.08(0.05)
4	23703.98(-0.04)	23703.98(0.05)	23669.51(0.00)	23669.51(0.07)
5	23709.44(0.02)	23709.29(-0.02)	23667.20(-0.05)	23667.20(0.04)
6	23715.11(-0.02)		23665.26(-0.03)	23665.26(0.07)
7	23721.19(0.03)	23720.99(-0.04)	23663.69(0.04)	23663.52(-0.01)
8	23727.56(0.07)	23727.30(-0.03)	23662.36(-0.03)	23662.16(-0.03)
9	23734.13(0.00)	23733.86(-0.09)	23661.89(-0.02)	23661.06(-0.10)
10	23741.17(0.00)	23740.88(0.00)	23660.56(-0.05)	23660.40(-0.04)
11	23748.33(-0.02)	23748.05(-0.08)	23660.20(-0.02)	23660.08(0.05)
12	23755.98(0.06)	23755.69(0.01)	23660.20(0.05)	23659.92(-0.02)
13	23763.88(0.08)	23763.53(-0.01)	23660.33(-0.05)	23660.11(-0.05)
14	23772.04(0.05)	23771.69(-0.02)	23661.06	23660.71(0.02)
15	23780.55(0.06)	23780.17(-0.02)	23661.76(-0.03)	23661.51(-0.03)
16	23789.27(-0.03)	23788.98(0.00)	23663.04(0.07)	23662.71(0.01)
17	23798.39(-0.02)	23798.00(-0.08)	23664.49(0.04)	23664.16(-0.01)
18	23807.90(0.07)	23807.49(0.01)	23666.32(0.07)	23665.98(0.03)
19	23817.52(-0.04)	23817.14(-0.05)	23668.42(0.05)	23668.05(0.00)
20	23827.63(0.04)	23827.21(0.01)	23670.82(0.03)	23670.42(-0.03)
21	23837.88(-0.05)	23837.45(-0.07)	23673.54(0.02)	23673.13(-0.04)
22	23848.59(0.01)	23848.16(0.01)	23676.54(-0.03)	
23	23859.55(0.02)	23859.10(0.01)	23679.91(-0.02)	23679.48(-0.07)
24	23870.80(0.02)	23870.32(0.01)	23683.63(0.03)	23683.22(0.02)
25	23882.35(0.01)	23881.89(0.04)	23687.57(-0.01)	23687.11(-0.06)
26	23894.17(-0.03)	23893.70(0.01)	23691.91(0.03)	
27	23906.36(-0.01)	23905.89(0.05)	23696.47(-0.01)	23696.01(-0.02)
28	23918.82(-0.01)	23918.25(-0.03)	23701.41(0.02)	23700.96(0.03)
29	23931.57(-0.03)	23931.09(0.06)	23706.65(0.03)	23706.16(0.03)
30	23944.60(-0.07)	23944.07(-0.01)	23712.07(-0.08)	
31	23958.01(-0.03)	23957.51(0.03)	23717.99(0.00)	23717.52(0.04)
32				
33		23985.03(0.00)	23730.54(-0.07)	23730.11(0.05)

[a]Not used in the analysis.

TABLE 8.7   Vacuum wavenumbers (in cm^{-1}) of the rotational lines of the 0-1 band

N	$R_1(N)$	$R_2(N)$	$P_1(N)$	$P_2(N)$
1	23468.58(0.02)	23468.58(0.02)	23456.94(0.01)	-
2	23473.01(-0.06)	23473.01(-0.06)	23453.64(-0.05)	23453.64(-0.05)
3	23477.91(0.01)	23477.91(0.01)	23450.80(0.03)	23450.80(0.03)
4	23483.05(0.00)	23483.05(0.00)	23448.17(0.00)	23448.17(0.00)
5	23488.51(0.00)	23488.51(0.00)	23445.90(0.01)	23445.90(0.01)
6	23494.30(0.01)	23494.30(0.01)	23443.95(0.03)	23443.95(0.03)
7	23500.40(0.01)	23500.40(0.01)	23442.29(0.02)	23442.29(0.02)
8	23506.81(0.00)	23506.81(0.00)	23440.95(0.00)	23440.95(0.00)
9	23513.55(0.02)	23513.55(0.02)	23439.94(0.00)	23439.94(0.00)
10	23520.55(-0.03)	23520.55(-0.03)	23439.26(0.01)	23439.26(0.01)
11	23527.94(0.00)	23527.94(0.00)	23438.86(-0.02)	23438.86(-0.02)
12	23535.63(0.01)	23535.63(0.01)	23438.86(0.04)	23438.86(0.04)
13	23543.60(-0.01)	23543.60(-0.01)	23439.06(-0.03)	23439.06(-0.03)
14	23551.94(0.03)	23551.94(0.03)	23439.61(-0.07)	23439.61(-0.07)
15	23560.54(0.01)	23560.54(0.01)	23440.62(0.04)	23440.62(0.04)
16	23569.45(-0.01)	23569.45(-0.01)	23441.79(-0.01)	23441.79(-0.01)
17	23578.70(0.00)	23578.70(0.00)	23443.38(0.04)	23443.38(0.04)
18	23588.24(-0.02)	23588.24(-0.02)	23445.14(-0.06)	23445.14(-0.06)
19	23598.14(0.01)	23598.14(0.01)	23447.41(0.03)	23447.41(0.03)
20			23449.89(0.01)	23449.89(0.01)
21			23452.69(0.00)	23452.69(0.00)

TABLE 8.8   Vacuum wavenumbers (in cm^{-1}) of the rotational lines of the 2-4 band

N	$R_1(N)$	$R_2(N)$	$P_1(N)$	$P_2(N)$
1	21881.65(0.04)	21881.65(0.04)	21870.24(0.00)	-
2	21886.12(0.04)	21886.12(0.04)	21867.13(0.00)	21867.13(0.00)
3	21890.90(0.01)	21890.90(0.01)	21864.39(0.03)	21864.39(0.03)
4	21896.02(-0.01)	21896.02(-0.01)	21861.93(0.00)	21861.93(0.00)
5	21901.48(-0.02)	21901.48(-0.02)	21859.83(0.00)	21859.83(0.00)
6	21907.29(-0.02)	21907.29(-0.02)	21858.07(0.00)	21858.07(0.00)
7	21913.42(-0.03)	21913.42(-0.03)	21856.65(0.00)	21856.65(0.00)
8	21919.88(-0.03)	21919.88(-0.03)	21855.53(-0.03)	21855.53(-0.03)
9	21926.67(-0.04)	21926.67(-0.04)	21854.77(-0.03)	21854.77(-0.03)
10	21933.81(-0.01)	21933.81(-0.01)	21854.39(0.02)	21854.39(0.02)
11	21941.23(-0.02)	21941.23(-0.02)	21854.25(-0.02)	21854.25(-0.02)
12	21949.04(0.03)	21949.04(0.03)	-	-
13	21957.11(0.04)	21957.11(0.04)	21855.02(-0.02)	21855.02(-0.02)
14	21965.50(0.06)	21965.50(0.06)	21855.92(0.01)	21855.92(0.01)
15	21974.12(0.00)	21974.12(0.00)	21857.08(-0.01)	21857.08(-0.01)
16	21983.09(0.00)	21983.09(0.00)	21858.63(0.05)	21858.63(0.05)
17	21992.32(-0.04)	21992.32(-0.04)	21860.30(0.01)	21860.30(0.01)
18			21862.48(0.00)	21862.48(0.00)
19			21864.86(-0.02)	21864.86(-0.02)

TABLE 8.9   Vacuum wavenumbers (in cm^{-1}) of the rotational lines of the 1-3 band f

N	$R_1(N)$	$R_2(N)$	$P_1(N)$	$P_2(N)$
0	21644.09(-0.01)			
1	21648.24(-0.05)	21648.24(-0.01)	21636.78(-0.01)	
2	21652.81(-0.02)	21652.81(0.04)	21633.63(-0.03)	21633.63(0.02)
3	21657.63(-0.09)	21657.63(0.00)	21630.87(0.00)	21630.87(0.07)
4	21662.90(-0.05)	21662.90(0.06)	21628.40(-0.04)	21628.40(0.05)
5	21668.54(0.01)	21668.42(0.02)	21626.32(-0.03)	21626.32(0.08)
6	21674.46(0.01)	21674.30(0.00)	21624.61(0.00)	
7	21680.73(0.01)	21680.55(0.04)	21623.17(-0.05)	
8	21687.37(0.03)	21687.14(-0.01)	21622.20(0.03)	21621.92(-0.09)
9	21694.33(0.03)	21694.06(-0.04)	21621.49(0.02)	21621.21(-0.08)
10	21701.62(0.01)	21701.30(-0.01)	21621.21(0.08)	21620.92(0.00)
11	21709.25(-0.01)	21708.98(-0.02)	21621.21(0.08)	21620.92(0.02)
12	21717.32(0.07)	21716.96(-0.01)	21621.49(0.02)	21621.21(0.02)
13	21725.60(0.01)	21725.28(0.00)	21622.20(0.03)	21621.92(0.01)
14	21734.27(0.00)	21733.93(-0.01)	21623.17(-0.04)	
15	21743.26(0.00)	21742.91(-0.04)	21624.61(0.01)	21624.26(-0.01)
16	21752.65(-0.01)	21752.28(-0.01)	21626.32(-0.02)	21626.02(0.00)
17	21762.36(-0.01)	21761.96(-0.01)	21628.40(-0.02)	21628.07(-0.01)
18	21772.40(-0.02)	21772.00(0.00)	21630.87(0.02)	21630.51(0.01)
19	21782.78(-0.03)	21782.38(0.01)	21633.63(0.00)	21633.23(-0.02)
20	21793.53(-0.01)	21793.13(0.05)	21636.78(0.02)	21636.34(-0.02)
21	21804.58(-0.03)	21804.14(-0.01)	21640.19(-0.04)	21639.80(-0.01)
22	21816.03(0.01)	21815.55(0.04)	21644.09(0.04)	21643.53(-0.08)
23	21827.74(-0.03)	21827.31(0.07)	21648.24(0.03)	21647.74(-0.01)
24	21839.79(-0.06)	21839.35(0.05)		
25	21852.23(-0.05)	21851.77(0.07)	21657.63(0.06)	21657.07(-0.01)
26	21865.03(-0.01)	21864.40(-0.04)		

TABLE 8.10   Vacuum wavenumbers[a] (in cm^{-1}) of the rotational lines of the 0-2 band

N	R₁(N)	R₂(N)	P₁(N)	P₂(N)
0	21392.43(0.06)	-	-	-
1	21406.57(-0.02)	21396.57(-0.02)	21384.97(0.00)	-
2	21401.17(0.00)	21401.17(-0.00)	21381.82(0.02)	21381.82(-0.02)
3	21406.11(0.01)	21406.11(0.01)	21378.95(-0.03)	21378.95(-0.03)
4	21411.37(-0.02)	21411.37(-0.02)	21376.49(-0.03)	21376.49(-0.03)
5	21417.01(-0.01)	21417.01(-0.01)	21374.39(-0.02)	21374.39(-0.02)
6	21423.01(0.00)	21423.01(0.00)	21372.71(0.06)	21372.71(0.06)
7	21429.34(-0.01)	21429.34(-0.01)	21371.22(-0.02)	21371.22(-0.02)
8	21436.06(0.02)	21436.06(0.02)	21370.22(0.03)	21370.22(0.03)
9	21443.07(-0.01)	21443.07(-0.01)	21369.48(0.00)	21369.48(0.00)
10	21450.48(0.01)	21450.48(0.01)	21369.12(-0.01)	21369.12(-0.01)
11	21458.22(0.00)	21458.22(0.00)	21369.12(-0.01)	21369.12(-0.01)
12	21466.37(0.06)	21466.27(-0.04)	21369.48(-0.01)	21369.48(-0.01)
13	21474.83(0.07)	21474.69(-0.07)	21370.22(0.03)	21370.22(-0.03)
14	21483.62(0.07)	21483.47(-0.08)	21371.22(-0.03)	21371.22(-0.03)
15	21492.74(0.04)	21492.62(-0.08)	21372.71(0.06)	21372.71(0.06)
16	21502.25(0.06)	21502.13(-0.04)	21374.39(-0.02)	21374.39(-0.02)
17	21512.06(0.03)	21511.90	21376.49(-0.03)	21376.49(-0.03)
18	21522.24(0.02)	21522.06	21378.95(-0.03)	21378.95(-0.03)
19	21532.74(-0.02)	21532.50	21381.82(0.03)	21381.82(0.03)
20	21543.55	21541.97	21384.92(-0.02)	21384.92(0.03)
21	21554.59	21555.03	21388.47(0.02)	21388.47(0.02)
22	21565.55	21566.48		
23	21582.02	21578.25		
24	21591.80	21589.55		
25	21603.99	21603.85		
26	21616.63	21616.63		

[a]The $(\nu_{obs} - \nu_{calc})$ values are given in parentheses only for the unperturbed lines which are used in the analysis.

TABLE 8.11 Vacuum wavenumbers (in cm^{-1}) of the rotational lines of the 2-5 band

N	R$_1$(N)	R$_2$(N)	P$_1$(N)	P$_2$(N)
3	19911.62(0.04)	19911.62(0.04)	19885.02(-0.04)	19885.02(-0.04)
4	-	-	19882.77(0.00)	19882.77(0.00)
5	19922.50(-0.02)	19922.50(-0.02)	19880.94(0.08)	19880.94(0.08)
6	-	-	-	-
7	19934.92(-0.01)	19934.92(-0.01)	19878.15(0.00)	19878.15(0.00)
8	19941.65(-0.03)	19941.65(-0.03)	-	-
9	19948.81(0.01)	19948.81(0.01)	19876.93(0.01)	19876.93(0.01)
10	19956.20(-0.07)	19956.20(-0.07)	19876.79(-0.06)	19876.79(-0.06)
11	19964.11(0.01)	19964.11(0.01)	19877.12(-0.03)	19877.12(-0.03)
12	19972.31(0.03)	19972.31(0.03)	19877.87(0.06)	19877.87(0.06)
13	19980.86(0.06)	19980.86(0.06)	19878.80(-0.02)	19878.80(-0.02)
14	-	-	-	-
15	19999.04[a]	19999.04[a]	19881.91(0.01)	19881.91(0.01)
16	-	-	-	-
17	20018.26(-0.02)	20018.26(-0.02)	19886.35(-0.02)	19886.35(-0.02)
18			-	-
19			19892.19(0.01)	19892.19(0.01)

[a]Not used in the analysis.

TABLE 8.12   Vacuum Wavenumbers (in cm^{-1}) of the rotational lines of the 1-4 band

N	R$_1$(N)	R$_2$(N)	P$_1$(N)	P$_2$(N)
0	19633.66(-0.03)	-	-	~
1	19637.87(-0.05)	19637.87(-0.02)	19626.39(-0.03)	-
2	19642.52(0.00)	19642.52(0.05)	19623.35(-0.02)	19623.35(0.04)
3	19647.44(-0.07)	19647.44(0.00)	19620.65(-0.03)	19620.65(0.04)
4	19652.83(-0.05)	19652.83(0.05)	19618.37(-0.01)	19618.37(0.07)
5	19658.62(-0.01)	19658.55(0.04)	19616.44(-0.03)	19616.44(0.08)
6	19664.80(0.05)	19664.65(0.03)	19614.93(-0.01)	19614.71(-0.10)
7	19671.27(0.01)	19671.17(0.07)	19613.76(-0.03)	19613.68(0.04)
8	19678.13(-0.02)	19677.98(0.01)	19613.00(-0.02)	19612.86(0.00)
9	19685.43(0.01)	19685.20(-0.02)	19612.63(0.00)	19612.46(0.01)
10	19693.02(-0.05)	19692.81(-0.04)	19612.63(0.00)	19612.46(0.01)
11	19701.10(0.01)	19700.82(-0.03)	19613.00(-0.01)	19612.76(-0.03)
12	19709.52(0.02)	19709.18(-0.06)	19613.76(-0.01)	19613.60(0.06)
13	19718.34(0.05)	19718.01(0.01)	19614.93(0.01)	19614.71(0.04)
14	19727.43(-0.02)	19727.03^a	19616.44(-0.01)	-
15	19737.05(0.06)	19736.69(0.02)	19618.37(0.01)	19618.07(0.00)
16	19746.93(0.02)	19746.54(-0.03)	19620.65(0.00)	19620.35(0.01)
17	19757.21(0.00)	19756.87(0.03)	19623.35(0.02)	19623.01(0.01)
18	19767.79(-0.09)	19767.48(-0.02)	19626.39(0.00)	19626.00(-0.04)
19	19778.98(0.04)	19778.54(0.01)	19629.81(-0.03)	19629.46(-0.01)
20			19633.66(0.00)	19633.23(-0.05)
21			19637.87(0.00)	19637.48(0.01)
22			19642.52(0.00)	19642.04(0.00)
23			19647.44(0.00)	19646.99(-0.01)

^{a}Not used in the analysis.

TABLE 8.13   Vacuum wavenumbers (in cm^{-1}) of the rotational lines of the 0-3 band

N	$R_1(N)$	$R_2(N)$	$P_1(N)$	$P_2(N)$
0	19351.17(0.03)	-	-	
1	19355.37(-0.03)	19355.37(-0.03)	19343.79(0.01)	-
2	19360.02(-0.03)	19360.02(-0.03)	19340.73(0.05)	19340.73(0.05)
3	19365.01(-0.07)	19365.01(-0.07)	19337.97(0.00)	19337.97(0.00)
4	19370.57(0.07)	19370.57(0.07)	19335.66(0.02)	19335.66(0.02)
5	19376.32(0.01)	19376.32(0.01)	19333.69(-0.02)	19333.69(-0.02)
6	19382.49(-0.02)	19382.49(-0.02)	19332.18(0.02)	19332.18(0.02)
7	19389.07(-0.02)	19389.07(-0.02)	19331.00(0.00)	19331.00(0.00)
8	19396.04(-0.01)	19396.04(-0.01)	19330.23(0.00)	19330.23(0.00)
9	19403.40(-0.01)	19403.40(-0.01)	19329.84(0.00)	19329.84(0.00)
10	19411.15(0.01)	19411.15(0.01)	19329.84(0.00)	19329.84(0.00)
11	19419.27(0.00)	19419.27(0.00)	19330.23(0.00)	19330.23(0.00)
12	19427.81(0.04)	19427.81(0.04)	19331.00(-0.01)	19331.00(-0.01)
13	19436.72(0.05)	19436.61(-0.06)	19332.18(0.01)	19332.18(0.01)
14	19445.94(0.00)	19445.94(0.00)	19333.69(-0.04)	19333.69(-0.04)
15	19455.67(0.07)	19455.53(-0.07)	19335.66(0.00)	19335.66(0.00)
16	19465.69(0.04)	19465.52^a	19337.97(-0.02)	19337.97(-0.02)
17	19476.14(0.07)	19475.99(-0.08)	19340.73(0.03)	19340.73(0.03)
18	19486.86(-0.02)	19486.86(-0.02)	19343.79(-0.01)	19343.79(-0.01)
19	19498.00(0.02)	19497.83^a	19347.32(0.04)	19347.32(0.04)
20	19509.57^a	19507.98^a	19351.17(0.02)	19351.17(0.02)
21	19521.35^a	19521.83^a	19355.37(-0.03)	19355.37(-0.03)

^{a}Not used in the analysis.

tables. However, these values are not given for the perturbed lines and a very few unperturbed lines which are excluded from the analysis. In general, the standard deviation of such a least-squares fit is ~ 0.03 cm^{-1}.

The molecular constants obtained from the analysis of the individual bands were merged together to obtain a unique set of molecular constants for the X and B states (see Section 3.3). The band origins obtained from the merged least-squares fit are given in Table 8.1. The uncertainty in the origin of the 2-5 band appears to be high because the number of spectral lines used in the analysis is limited. The band origin of the 2-1 band quoted in this table was obtained from the term values of the levels v = 2 and 1 of states B and X, respectively. The B_v, D_v, and γ_v values of states X and B obtained from the merged least-squares fit are listed in Table 8.14. The uncertainties in the B_v and D_v values of the $X^2\Sigma_g^+$, v = 5 and the $B^2\Sigma_u^+$, v = 2 are rather large compared to those of the other levels because these values were obtained from limited wavenumber data. The γ_0 value of the B state was estimated exclusively from the wavenumber data of N = 33 to 43 in the 0-0 band and was not included in the merged fit. The value of γ_2 of state B could not be estimated because the spin splitting was not observed in any of the bands with v' = 2. Similarly, γ_5 of state X could not be obtained because the v" = 5 level was observed only in the 2-5 band. The B_e

TABLE 8.14   Rotational constants[a] (in cm^{-1}) of the X $^2\Sigma_g^+$ and B $^2\Sigma_u^+$ states of $^{15}N_2^+$

Vibrational Level	X $^2\Sigma_g^+$			B $^2\Sigma_u^+$		
	B_v	$D_v \times 10^6$	$-\gamma_v \times 10^3$	B_v	$D_v \times 10^6$	$\gamma_v \times 10^3$
0	1.79520(8)	5.5(1)	18.3(4)	1.93731(9)	6.6(2)	1.1(9)
1	1.77817(8)	5.6(1)	18.8(4)	1.91709(7)	6.4(1)	1.2(4)
2	1.76114(8)	5.8(1)	17.2(5)	1.89548(12)	16.0(3)	-
3	1.74342(8)	5.6(1)	19.1(5)			
4	1.72639(10)	6.2(2)	19.1(6)			
5	1.70783(23)	4.0(6)	-			

[a]The number in the parentheses indicates the uncertainty in the last digit and corresponds to one standard deviation.

and α_e values of states X and B were obtained according to
Eq. [3.13a], from the B_v values given in Table 8.14. The
B_e and α_e values thus obtained are listed in Table 8.15.
The equilibrium internuclear distance r_e and the correspnding
moment of inertia I_e of states X and B, obtained from their
respective B_e values, are also presented in the same table.

(ii) Vibrational Analysis and Isotope Shifts

All the band origins of the bands of the first negative
(B-X) system of $^{15}N_2^+$, except that of the 2-1 band (see
Table 8.1), were fitted to Eq. [3.6], and the system origin
ν_e and the vibrational constants obtained simultaneously
from this fit are listed in Table 8.15. In this table, the
T_e value of state B is identical to the ν_e value of the B-X
system. The twelve band origins given in Table 8.1, except
that of the 2-1 band, were also used to obtain the vibrational
term values of the X and B states. These term values,
which are relative to that of the v = 0 level of the X state
are presented in Table 8.16. Using the vibrational constants
of the X state (see Table 8.15), the actual position of the
v = 0 level from the minimum of its potential energy curve
is calculated to be 1062.522 cm^{-1}.

The isotope shifts of the bands of the first negative
system of $^{15}N_2^+$ are obtained as the differences of the origins
of the $^{14}N_2^+$ bands of this system and those of the corresponding
bands of $^{15}N_2^+$, i.e., $\nu_0(^{14}N_2^+) - \nu_0(^{15}N_2^+)$. The values of

TABLE 8.15   Equilibrium molecular constants[a] (in cm^{-1}, unless stated otherwise) of the X $^2\Sigma_g^+$ and B $^2\Sigma_u^+$ states of $^{15}N_2^+$

Molecular Constant	X $^2\Sigma_g^+$	B $^2\Sigma_u^+$
T_e	0.0	25460.258(9)
ω_e	2132.584(9)	2342.811(9)
$\omega_e x_e$	15.063(4)	24.656(3)
$\omega_e y_e$	-0.0324(4)	-
B_e	1.80392(8)	1.94775(10)
α_e	0.01720(1)	0.02046(4)
r_e (Å)	1.1162	1.0742
I_e (g.cm^2)	1.5518×10^{-39}	1.4372×10^{-39}

[a]The number in the parentheses indicates the uncertainty in the last digit and corresponds to one standard deviation.

TABLE 8.16 Vibrational term values[a] (in cm^{-1}) of the X $^2\Sigma_g^+$ and B $^2\Sigma_u^+$ states of $^{15}N_2^+$

Vibrational Level	X $^2\Sigma_g^+$	B $^2\Sigma_u^+$
	G(v) – G(0)	T_e – (G(0))$_X$
0	0.0	25562.803(5)
1	2102.329(4)	27855.974(5)
2	4174.328(5)	30099.822(7)
3	6215.579(6)	
4	8226.135(7)	
5	10205.614(11)	

[a]The term values are expressed relative to the v=0 level of the X $^2\Sigma_g^+$ state, which is at a height of 1062.522 cm^{-1} from the minimum of its potential energy curve.

$\nu_0(^{14}N_2^+)$ for the bands of this system were either directly taken from Gottscho et al. (1979) or calculated from the vibrational constants reported by them. The values of $\nu_0(^{15}N_2^+)$ are the experimental values obtained from the present work. The isotope shifts thus obtained are listed in Table 8.17. The isotope shifts were also calculated from Eq. [3.11] using the vibrational constants of the X and B states of $^{14}N_2^+$ taken from Gottscho et al. (1979) and the value of $\rho = [\mu^{\frac{1}{2}}(^{14}N_2^+) / \mu^{\frac{1}{2}}(^{15}N_2^+) = 0.9662]$ and are listed in the same table. The agreement between columns 2 and 3 of this table is very good.

(iii) Perturbations in the $B^2\Sigma_u^+$ State of $^{15}N_2^+$

According to Kronig's selection rules (see Section 3.4) a $^2\Sigma_u^+$ state can be perturbed by either doublet or quartet Σ_u^+ or Π_u states. In this section, the perturbations caused by a $^2\Pi_u$ state in a $^2\Sigma_u^+$ state are of particular interest. As both the perturbing and perturbed states are doublet states, the maximum perturbations are expected at four different positions in the rotational structure of a band. Hence, when a $^2\Sigma^+$ state is perturbed, the maximum perturbations are expected twice in the F_1 levels and twice in the F_2 levels. Ittmann (1931) has given a general theoretical description of the perturbations between $^2\Sigma$ and $^2\Pi$ states. In general, when a $^2\Sigma_u^+$ state is perturbed by a $^2\Pi_u$ state, the four maximum perturbations expected are in

TABLE 8.17 Isotope shifts (in cm^{-1}) in the first negative system of $^{15}N_2^+$

| Band | Isotope Shift $\Delta\nu$ ($^{14}N_2^+$ - $^{15}N_2^+$) | |
	Present work	Calculated
2-1	84.37	84.33
1-0	81.70	81.99
1-1	9.26	9.53
0-0	3.24	3.48
2-3	-54.16	-54.05
1-2	-61.01	-60.76
0-1	-69.21	-68.98
2-4	-120.06	-119.93
1-3	-129.03	-128.85
0-2	-139.44	-139.27
2-5	-183.79	-183.56
1-4	-195.14	-194.72
0-3	-207.68	-207.36

the following order: first, a perturbation at low N affecting only one spin component (either F_1 or F_2); then, two close perturbations affecting both the spin components; and finally, a fourth one affecting only one spin component at higher N. In some instances, the perturbations caused by a $^2\Pi_u$ state in a $^2\Sigma_u^+$ state may affect both the spin components (F_1 and F_2) twice in rapid succession.

Among the twelve bands of the first negative system of $^{15}N_2^+$, for which the rotational structure is analyzed, some irregularities are observed only in the 0-0, 0-1, 0-2, and 0-3 bands. This indicates that the v = 0 level of the $B^2\Sigma_u^+$ state of $^{15}N_2^+$ is perturbed. In the 0-1 and 0-3 bands, the rotational lines are identified only up to N = 21 and it is difficult to make any conclusions from their structure regarding the perturbations. In the 0-0 and 0-2 bands the spectral lines are identified up to N = 43 and 26, respectively, and the perturbations in the v = 0 level are confirmed with the help of similar irregularities in the structure of these two bands. From Table 8.4, it can be noticed that the spectral lines belonging to $R_1(N)$ and $R_2(N)$ branches are completely identified whereas the lines of $P_1(N)$ and $P_2(N)$ branches with N = 22 to 32 are not identified. Hence, only the lines of $R_1(N)$ and $R_2(N)$ branches were used in the subsequent analysis. Using the appropriate molecular constants listed in Tables 8.1 and 8.14, the wavenumbers of $R_1(N)$ and $R_2(N)$ branches of the 0-0 band were calculated.

The deviations of the observed wavenumbers of these spectral lines from the calculated ones are plotted against N' in Figure 27. From this figure, it can be found that the maximum perturbations are observed at $N' = 24$ and 29 of the F_1 levels and at $N' = 21$ and 26 of the F_2 levels. Two extra lines are observed at the maximum perturbations for $R_1(23)$ ($N' = 24$) and $R_2(20)$ ($N' = 21$) corresponding to F_1 and F_2 levels respectively. Comparing the perturbation curves shown in Figure 27 with those given in Figure 11, it can be concluded that this is a heterogeneous perturbation, for which $\Delta \Lambda \neq 0$. In such a situation, Σ_u^+ state can be perturbed only by a Π_u state. As the maximum perturbations are occurring at four different N values and the perturbed state is the $^2\Sigma_u^+$ state, this perturbing Π_u state is obviously a $^2\Pi_u$ state. In the $^{15}N_2^+$ molecule a $^2\Pi_u$ state which is lying close to the $B^2\Sigma_u^+$ state is the $A^2\Pi_{i,u}$ state. Thus it is concluded that the $A^2\Pi_{i,u}$ state is causing perturbations in the $v = 0$ level of the $B^2\Sigma_u^+$ state.

The molecular constants listed by Gottscho et al. (1979) for the $A^2\Pi_{i,u}$ state of $^{14}N_2^+$ and the value of ρ (=0.9662) were used to obtain the corresponding constants of $^{15}N_2^+$. Using these constants of state A of $^{15}N_2^+$, the $(T_e + G(v))$ and B_v values of the vibrational levels of state A were calculated. As the B_v values of state A are smaller than the B_0 value of state B, only the vibrational levels of state A which are slightly above the $v = 0$ level of state B

Figure 27. Plot of deviations ($\nu_{obs} - \nu_{calc}$) of the rotational lines of R_1 and R_2 branches versus the rotational quantum number of the upper state N' in the 0-0 band. The lines joining the dots (.) represent R_1 branch and those joining the crosses (x) represent R_2 branch.
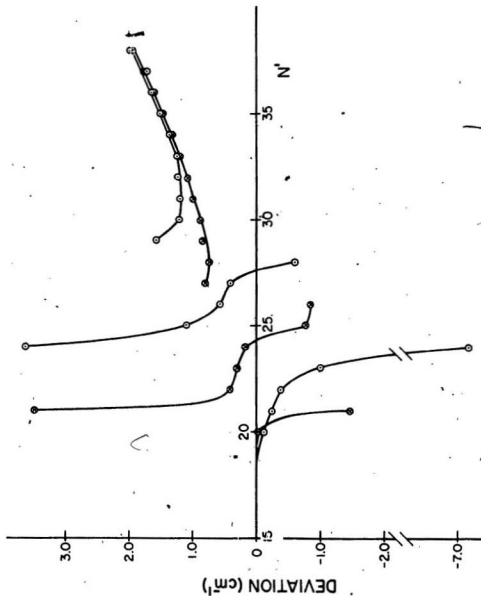
can perturb the latter. The $v = 0$ level of state B is at 26625.33 cm^{-1} with respect to the minimum of the potential energy curve of state X. Only the levels with $v \geq 24$ are lying above the $v = 0$ level of state B. According to Kronig (1928), at the points of maximum perturbation, both the perturbed and the perturbing levels have equal energy and the same J value. Using this principle, the B_v value of the perturbing level was calculated from the corresponding $F(J)$ value which is the difference between the total energy of the perturbed rotational level $(T_e + G(v) + F(J)$ of state B) and the sum of the electronic and vibrational terms of the perturbing level $(T_e + G(v)$ of state A). The values of B_v for $v = 24$, 25 and 26 of state A thus obtained and the corresponding values calculated from the known values of B_e and α_e are listed below:

$$^{15}N_2{}^+ : A^2\Pi_{i,u}$$
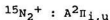
v	Value of B_v from Observed Perturbations (cm^{-1})	Value of B_v from B_e and α_e (cm^{-1})
24	1.891	1.249
25	1.197	1.237
26	0.557	1.226

A glance at the values listed above indicates that those obtained for $v = 25$ from both methods are closer than the corresponding pairs of values. It is thus concluded that

the level $v = 25$ of state A is perturbing the level $v = 0$ of state B of $^{15}N_2^+$. The calculated position of this perturbing vibrational level is 27017.58 cm^{-1} and its B_v value, obtained from the observed perturbations, is 1.197 cm^{-1}, which is only an approximate value. In the levels $v = 1$ and 2 of state B, the rotational levels are observed up to N = 34 and 18, respectively, and no perturbations are observed within these rotational levels.

CHAPTER 9

CONCLUSIONS

The conclusions arrived at from the study of various bands systems, discussed at length in the previous chapters, are briefly summarized in this chapter. The hollow-cathode discharge tube, of special design used in the present work, is a very useful device to excite the spectra of neutral molecules and molecular ions. The feasibility of producing the spectra of neutral molecules and their ions without the overlap of each other greatly reduces the complexity of the spectra and this, in turn, helps to unambiguously assign the quantum numbers for the vibrational and rotational structure of the bands. A classic example of exciting the second positive system of neutral $^{14}N_2$ and the first negative system of $^{14}N_2{}^+$ in the anode and cathode glows, respectively, is clearly demonstrated in Figure 5.

In the present work on the third positive ($b^3\Sigma^+ - a^3\Pi_r$) system of both $^{12}C^{16}O$ and $^{13}C^{18}O$ the $v = 2$ level of state b is identified for the first time (Chapter 5). This work has contributed to the spectroscopic knowledge of the carbon monoxide molecule in the following three aspects. First of all, the three Kaplan bands first observed in 1930 have not been fully understood for the last fifty-seven years. With the observation of additional bands in

$^{12}C^{16}O$ and new bands in $^{13}C^{18}O$, these Kaplan bands have now been consistently interpreted as a part of the third positive system of CO. Secondly, prior to the present work, a variety of values ranging from 55822 to 89608 cm^{-1} were proposed for the dissociation limit of the CO molecule. Generally, a "high" value (89460 cm^{-1}) has been recognized as the dissociation limit, but the lack of v = 2 level of state b favored a "low" value (≤ 88262 cm^{-1}). Now with the identification of the v = 2 level of state b, the arguments in favor of a "low" value are no longer valid and the present work strongly favors a "high" value for the dissociation limit. Thus the longstanding controversy regarding the dissociation energy of the CO molecule has now been resolved. Finally, the $\omega_e x_e$ value for the $b^3\Sigma^+$ state of $^{12}C^{16}O$ is reported for the first time in the present work. All the data of the third positive system of $^{13}C^{18}O$ is, of course, completely new.

The Herzberg ($C^1\Sigma^+ - A^1\Pi$) system of $^{13}C^{18}O$ (Chapter 4), the Baldet-Johnson ($B^2\Sigma^+ - A^2\Pi_i$) system (Chapter 6), and the comet-tail ($A^2\Pi_i - X^2\Sigma^+$) system (Chapter 7) of $^{13}C^{18}O^+$ have been observed and their molecular constants are reported for the first time in the present work. These molecular constants are useful in theoretical calculations, such as Franck-Condon factors, estimation of new vibrational levels and the RKR potential energy curves, etc. The observed perturbations in the Herzberg band system have been interpreted and the nature of the perturbing state is inferred. Similarly, the first

negative ($B^2\Sigma_u^+ - X^2\Sigma_g^+$) system of $^{15}N_2^+$ molecule is observed and twelve bands of this system have been rotationally analyzed for the first time. Just as for $^{13}C^{18}O$ and $^{13}C^{18}O^+$, the derived molecular constants of the B and X states of $^{15}N_2^+$ are useful in calculation of several molecular properties of these two states. The analysis of the perturbations observed in the v = 0 level of state B indicated that the $A^2\Pi_{i,u}$ (v = 25) is the perturbing state. The experimental data obtained on these three molecules in the present work are useful in identifying their spectra in the celestial objects, like aurorae, comets, and stars, etc., which in turn, may help in evaluating the abundance ratios of isotopes such as $^{12}C/^{13}C$, $^{14}N/^{15}N$, and $^{16}O/^{18}O$ in these objects.

As a part of the research work in the immediate future, plans are currently underway to investigate the fourth positive ($A^1\Pi - X^1\Sigma^+$) system of $^{13}C^{18}O$, the first negative ($B^2\Sigma^+ - X^2\Sigma^+$) system of $^{13}C^{18}O^+$ and the Meinel ($A^2\Pi_{i,u} - X^2\Sigma_g^+$) band system of $^{15}N_2^+$. The $B^2\Sigma_u^+$ state of $^{14}N_2^+$ is known to be predissociating in a rather peculiar way (see Douglas, 1952). In order to understand the behavior of this state of $^{15}N_2^+$, the first negative ($B^2\Sigma_u^+ - X^2\Sigma_g^+$) system of $^{15}N_2^+$ has been investigated in the present work. However only the bands with v' = 0 to 2, all degraded to shorter wavelengths, are observed. If the bands arising from the higher vibrational levels which are expected to degrade to longer wavelengths are observed and analyzed, then the nature of the $B^2\Sigma_u^+$ state of

$^{15}N_2^+$ can be understood better. It is also planned to investigate these bands in the near future.

REFERENCES

Albritton, D. L., Harrop, W.J., Schmeltekopf, A. L., Zare, R. N., and Crow, E. L., 1973, J. Mol. Spectrosc., _46_, 67-88.

Albritton, D. L., Schmeltekopf, A. L., and Zare, R. N., 1976, in "Molecular spectroscopy: Modern Research," Vol. II, edited by K. Narahari Rao, Academic Press, New York.

Albritton, D. L., Schmeltekopf, A. L., and Zare, R. N., 1977, J. Mol. Spectrosc., _67_, 132-156.

Åslund, N., 1965, Ark. Fys., _30_, 377-396.

Asundi, R. K., 1929, Nature (London), _123_, 47-48L.

Asundi, R. K., Dhumwad, R. K., and Patwardhan, A. B., 1970, J. Mol. Spectrosc., _34_, 528-532.

Audouze, J., 1977, "CNO Isotopes in Astrophysics," D. Reidel Publishing Company, Boston, U.S.A.

Baldet, F., 1924, Compt. Rend., _178_, 1525-1527.

Baldet, F., 1925a, Nature, _116_, 360.

Baldet, F., 1925b, Compt. Rend. _180_, 271-273.

Baldet, F., 1925c, Compt. Rend. _180_, 820-822.

Barrow, R. F., Gratzer, W. B., and Malherbe, J. F., 1956, Proc. Phys. Soc. (London), _A69_, 574-576.

Birge, R. T., 1925, Nature, _116_, 170-171L.

Birge, R. T., 1926, Phys. Rev., _28_, 1157-1181.

Born, M., and Oppenheimer, J. R., 1927, Ann. Physik, _84_, 457.

Brewer, L., and Searcy, A. W., 1956, Ann. Rev. Phys. Chem., _7_, 259-286.

Brons, H. H., 1934, Physica, _1_, 739-744.

Brons, H. H., 1935, Proc. K. Akad. Wet. Amsterdam, _38_, 271-280.

Brown, J. M., Hougen, J. T., Huber, K. P., Johns, J. W. C.,
    Kopp, I., Lefebvre-Brion, H., Merer, A. J., Ramsay, D.
    A., Rostas, J., and Zare, R. N., 1975, J. Mol. Spectrosc.,
    55, 500-503.

Brown, R. D., Dittman, R. G., and McGilvery, D. C., 1984,
    J. Mol. Spectrosc., 104, 337-342.

Brown, R. D., Dittman, R. G., McGilvery, D. C., and Godfrey,
    P. D., 1983, J. Mol. Spectrosc., 101, 61-70.

Bulthuis, H., 1934, Physica, 1, 873-880.

Bulthuis, H., 1935, Proc. Acad. Sci. Amsterdam, 38, 604-617.

Cameron, W. H. B., 1926, Phil. Mag., 1, 405-417.

Chevaleyre, J., and Perrot, J. P., 1981, J. Mol. Spectrosc.,
    85, 85-96.

Childs, W. H. J., 1932, Proc. Roy. Soc. (London), A137,
    641-661.

Colburn, E. A., and Douglas, A. E., 1977, J. Mol. Spectrosc.,
    65, 332-333.

Čonkić, L., Janjić, J. D., Pešić, D. S., Rakotoarijimy, D.,
    Vujisić, B. R., and Weniger, S., 1978, Astrophys. J., 226,
    1162-1170.

Coster, D., and Brons, F., 1934, Physica 1, 634-648.

Coster, D., and Brons, H. H., 1931, Z. Physik, 70, 492-497.

Coster, D., and Brons, H. H., 1932, Z. Physik, 73, 747-774.

Coster, D., Brons, H. H., and Bulthuis, H., 1932, Z. Physik,
    79, 787-822.

Coxon, J. A., 1978, J. Mol. Spectrosc., 72, 252-263.

Coxon, J. A., and Foster, S. C., 1982, J. Mol. Spectrosc.,
    93, 117-130.

Crawford, F. H., and Tsai, P. M., 1935, Proc. Amer. Acad.
    Arts. Sci., 69, 407-437.

Crosswhite, H. M., 1958, John Hopkins Spectroscopic Report
    No. 13

Crosswhite, H. M., 1975, J. Res. Natl. Bur. Stds., A Phys.
    and Chem., 79A, 17-69.

Damany, H., Roncin, J. Y., and Damany-Astoin, N., 1966, Appl. Opt., 5, 297-299.

Dhumwad, R. K., Patwardhan, A. B., and Kulkarni, V. T., 1979, J. Mol. Spectrosc., 78, 341-343.

Dick, K. A., Benesch, W., Crosswhite, H. M., Tilford, S. G., Gottscho, R. A., and Field, R. W., 1978, J. Mol. Spectrosc., 69, 95-108.

Dieke, G. H., 1941, Phys. Rev. 60, 523-529.

Dieke, G. H., and Mauchly, J. W., 1932, Nature (London), 129, 546.

Dieke, G. H., and Mauchly, J. W., 1933, Phys. Rev., 43, 12-30.

Douglas, A. E., 1952, Canad. J. Phys., 30, 302-313.

Douglas, A. E., and Møller, C. K., 1955, Canad. J. Phys., 33, 125-132.

Duffendack, O. S., and Fox, G. W., 1927, Astrophys. J., 65, 214-237.

Edlen, B., 1953, J. Opt. Soc. Amer., 43, 339-344.

Eidelsberg, M., Roncin, J. Y., LeFloch, A., Launay, F., Letzelter, C., and Rostas, J., 1987, J. Mol. Spectrosc., 121, 309-336.

Fassbender, M., 1924, Z. Physik, 30, 73-92.

Field, R. W., Tilford, S. G., Howard, R. A., and Simmons, J. D., 1972, J. Mol. Spectrosc., 44, 347-382.

Fowler, A., 1909, Monthly Notices Roy. Astron. Soc., 70, 176-182.

Fowler, A., 1910, Monthly Notices Roy. Astron. Soc., 70, 484-496.

Gagnaire, H., and Goure, J. P., 1976, Canad. J. Phys., 54, 2111-2117.

Gaydon, A. G., 1968, "Dissociation Energies and Spectra of Diatomic Molecules," 3rd ed., Chapman and Hall, London.

Gottscho, R. A., Field, R. W., Dick, K. A., and Benesch, W., 1979, J. Mol. Spectrosc., 74, 435-455.

Herzberg, G., 1928, Ann. Phys. (Leipzig), 86, 189-213.

Herzberg, G., 1929, Z. Physik, 52, 815-845.

Herzberg, G., 1950, "Molecular Spectra and Molecular Structure," Vol. I, "Spectra of Diatomic Molecules," 2nd ed., D. Van Nostrand Company, Inc., New York.

Herzberg, G., 1971, "The Spectra and Structures of Simple Free Radicals," Cornell University Press, Ithaca.

Herzberg, G., Lew, H., Sloan, J. J., and Watson, J. K. G., 1981, Canad. J. Phys., 59, 428-440.

Huber, K. P., and Herzberg, G., 1979, "Molecular Spectra and Molecular Structure," Vol. IV, "Constants of Diatomic Molecules," Van Nostrand Reinhold Company, New York.

Ittmann, G. P., 1931, Z. Physik, 71, 616-626.

Jakubek, Z., Kepa, R., Para, R., and Rytel, M., 1987, Canad. J. Phys., 65, 94-100.

Jakubek, Z., Kepa, R., Rzeszut, Z., and Rytel, M., 1986, J. Mol. Spectrosc., 119, 280-290.

Janjić, J. D., Čonkić, L. J. U., Pešić, D. S., Kepa, R., and Rytel, M., 1978, J. Mol. Spectrosc., 72, 297-300.

Jarmain, W. R., 1960, Canad. J. Phys., 38, 217-230.

Jarmain, W. R., 1971, J. Quant. Spectrosc. Radiat. Transfer, 11, 421-426.

Jarmain, W. R., and McCallum, J. C., 1970, TRAPRB (A Computer Program for Molecular Transitions), Univ. of Western Ontario, Canada.

Johnson, R. C., 1925, Proc. Roy. Soc. (London), Ser. A, 108, 343-355.

Johnson, R. C., 1926, Nature, 117, 376-377L.

Johnson, R. C., and Asundi, R. K., 1929, Proc. R. Soc. (London) Ser. A 123, 560-574.

Kaplan, J., 1930, Phys. Rev., 35, 1298L.

Katayama, D. H., and Welsh, J. A., 1981, J. Chem. Phys., 75, 4224-4230.

Katayama, D. H., and Welsh, J. A., 1982, J. Chem. Phys., 76, 3848.

Kepa, R., 1969, Acta Phys. Pol., A36, 1109-1110.

Kepa, R., 1978, Acta Phys. Acad. Sci. Hungar., 45, 133-147.

Kepa, R., 1982, Acta Phys. Pol., A62, 467-472.

Klynning, L., and Pages, P., 1972, Physica Scripta, 6, 195-199.

Klynning, L., and Pages, P., 1982, Physica Scripta, 25, 543-560.

Kopp, I., and Hougen, J. T., 1967, Canad. J. Phys. 45, 2581-2596.

Kovács, I., 1969, "Rotational Structure in the Spectra of Diatomic Molecules," American Elsevier Publishing Company, Inc., New York.

Kronig, R. de L., 1928, Z. Physik, 50, 347.

Krupenie, P. H., 1966, "The Band Spectrum of Carbon Monoxide," National Standard Reference Data Series, Natl. Bur. Stand., Vol. 5.

Krupenie, P. H., and Benesch, W., 1968, J. Res. Natl. Bur. Stds., A. Phys. and Chem., 72A, 495-503.

Lefebvre-Brion, H., and Field, R. W., 1986, "Perturbations in the Spectra of Diatomic Molecules," Academic Press, New York.

Lefebvre-Brion, H., Moser, C. M., and Nesbet, R. K., 1964, J. Mol. Spectrosc., 13, 418-429.

LeFloch, A. C., Launay, F., Rostas, J., Field, R. W., Brown, C. M., and Yoshino, K., 1987, J. Mol. Spectrosc., 121, 337-379.

Lofthus, A., and Krupenie, P. H., 1977, J. Phys. Chem. Ref. Data, 6, 113-307.

Marchand, J., D'Incan, J., and Janin, J., 1969, Spectrochim. Acta, 25A, 605-609.

Merton, T. R., and Pilley, J. G., 1925, Phil. Mag., 50, 195-199.

Mulliken, R. S., 1930, Rev. Mod. Phys., 2, 60-115.

Mulliken, R. S., 1931, Rev. Mod. Phys., 3, 89-155.

Mulliken, R. S., 1932, Rev. Mod. Phys., 4, 1-86.

Mulliken, R. S., 1937, J. Phys. Chem., 41, 5-45.

Mulliken, R. S., and Christy, A., 1931, Phys. Rev., 38, 87-119.

Nicholls, R. W., 1962, Canad. J. Phys., 40, 1772-1783.

Ortenberg, F. S., 1964, Opt. Spectrosc., 16, 398-400.

Parker, A. E., 1933a, Phys. Rev., 44, 84-89.

Parker, A. E., 1933b, Phys. Rev., 44, 90-91.

Pluvinel, A. B., and Baldet, F., 1909, Compt. Rend., 148, 759-762.

Pluvinel, A. B., and Baldet, F., 1911, Astrophys. J., 34, 89-104.

Prasad, C. V. V., 1983, M.Sc. Thesis, Memorial University of Newfoundland.

Prasad, C. V. V., Bhale, G. L., and Reddy, S. P., 1984, J. Mol. Spectrosc., 104, 165-173.

Prasad, C. V. V., Bhale, G. L., and Reddy, S. P., 1987, J. Mol. Spectrosc., 121, 261-269.

Prasad, C. V. V., Reddy, S. P., and Sandys-Wunsch, M., 1985, J. Mol. Spectrosc., 114, 436-444.

Rao, K. N., 1950a, Astrophys. J., 111, 306-313.

Rao, K. N., 1950b, Astrophys. J., 111, 50-59.

Rao, K. N., and Sarma, K. S., 1953, Mem. Soc. Roy. Sci. Liege Collect., 13, 181-186.

Schmid, R., and Gerö, L., 1933, Z. Physik, 86, 297-313.

Schmid, R., and Gerö, L., 1935a, Z. Physik, 93, 656-668.

Schmid, R., and Gerö, L., 1935b, Z. Physik, 96, 546-550.

Simmons, J. D., Bass, A. M., and Tilford, S. G., 1969, Astrophys. J., 155, 345-358.

Skerbele, A., Meyer, V. D., and Lassetre, E. N., 1966, J. Chem. Phys., 44, 4069-4072.

Tilford, S. G., and Simmons, J. D., 1972, J. Phy. Chem. Ref. Data, 1, 147-187.

Tilford, S. G., and Vanderslice, J. T., 1968, J. Mol. Spectrosc., 26, 419-431.

Tyte, D. C., 1962, Proc. Phys. Soc. (London), 80, 1364-1369.

Tyte, D. C., 1963, Proc. Phys. Soc. (London), 81, 163-170.

Tyte, D. C., and Nicholls, R. W., 1965, Identification Atlas of Molecular Spectra, No. 3, "The First Negative System of N_2^+".

Verma, K. K., 1977, Ph.D. Thesis, Memorial University of Newfoundland.

Vujisić, B. R., Pešić, D. S., Weniger, S., and Rakotoarijimy, D., 1980, Indian J. Pure and Appl. Phys., 18, 370-372.

Wood, R. W., and Dieke, G. H., 1938, J. Chem. Phys., 6, 734-739.

Wood, R. W., and Dieke, G. H., 1940, J. Chem. Phys., 8, 351-361.

PUBLICATIONS

C. V. V. Prasad, G. L. Bhale, and S. P. Reddy, "The Third Positive ($b^3\Sigma^+ - a^3\Pi_r$) System of CO: Observation of the v=2 level of $b^3\Sigma^+$ state," J. Mol. Spectrosc., **121**, 261-269. (1987).

C. V. V. Prasad, S. P. Reddy, and M. Sandys-Wunsch, "The Herzberg ($C^1\Sigma^+ - A^1\Pi$) Band System of $^{13}C^{18}O$," J. Mol. Spectrosc., **114**, 436-444 (1985).

C. V. V. Prasad, G. L. Bhale, and S. P. Reddy, "The Ångström ($B^1\Sigma^+ - A^1\Pi$) Band System of $^{13}C^{18}O$," J. Mol. Spectrosc., **104**, 165-173 (1984).

C. V. V. Prasad and M. Sakuntala, "Acoustic Wave Interaction with Plasma Pulse," Proc. Indian Natl. Sci. Acad., **43**, (2), 283-289 (1982).

M. Sakuntala, B. Chaturvedi, and C. V. V. Prasad, "Audio Signal Interaction with Moving Plasma Pulse," Ind. J. Phys. **56B**, 52-61 (1982).